2009

Integrated Actuation And Energy Harvesting In Prestressed Piezoelectric Synthetic Jets

Poorna Mane
Virginia Commonwealth University

School of Engineering
Virginia Commonwealth University

This is to certify that the dissertation prepared by Poorna Mane entitled INTEGRATED ACTUATION AND ENERGY HARVESTING IN PRESTRESSED PIEZOELECTRIC SYNTHETIC JETS has been approved by her committee as satisfactory completion of the dissertation requirement for the degree of Doctor of Philosophy

Dr. Karla Mossi, Committee Chair, School of Engineering

Dr. Gary Atkinson, Committee Member, School of Engineering

Dr. Robert Bryant, Committee Member, NASA Langley Research Center

Dr. Mohamed Gad-el-Hak, Committee Member, School of Engineering

Dr. Ramana Pidaparti, Committee Member, School of Engineering

Dr. Rosalyn Hobson, Associate Dean for Graduate Studies, School of Engineering

Dr. Russell D. Jamison, Dean, School of Engineering

Dr. F. Douglas Boudinot, Dean of the Graduate School

08/07/2009

INTEGRATED ACTUATION AND ENERGY HARVESTING IN PRESTRESSED PIEZOELECTRIC SYNTHETIC JETS

A Dissertation submitted in partial fulfillment of the requirements for the degree of Doctor of Philosophy at Virginia Commonwealth University.

by

POORNA MANE

M.S., Virginia Commonwealth University, 2005

Director: Dr. KARLA MOSSI

ASSOCIATE PROFESSOR, MECHANICAL ENGINEERING

Virginia Commonwealth University

Richmond, Virginia

August 2009

Acknowledgements

I would like to express my sincere thanks to my mentor and advisor Dr. Karla Mossi for her support and guidance; both academic and personal, throughout my stay at VCU. She has been an integral part of my learning process and has helped tremendously in the completion of this work. Her enthusiasm and love for students is contagious – motivating me to pursue a career in higher education. I hope you will continue to guide me with the same insight, as a scientist, mentor, teacher and friend, in my future endeavors. Thank you for welcoming me into your lab and home. My stay in VCU was brightened by the countless occasions we would spend talking "everyday stuff" in your office, numerous times that I visited your house, Steve's constant advice to "graduate and get a real job", Dante reminding me of the child in everyone of us; the list is endless.

I am grateful to Dr. Gary Atkinson, Dr. Robert Bryant, Dr. Mohammed Gad el Hak and Dr. Ramana Pidaparti for being on my committee. Thank you for your crucial input and feedback whenever it was necessary.

I am indebted to Ann Yates for her eternal sweetness and relentless support and that kept me going.

I would also like to thank Dr. Rosalyn Hobson for her constant encouragement and introducing me to the Society of Women Engineers. I will continue to treasure our association together and hope that our paths cross often.

A big thank you dedicated to my labmates and friends, including Amol, Chris Green, Ihab, Jingsi Xie, Jugal, Koyal, Matthew, Ravi, Sonya and Vivek for making the lab and life in Richmond, a fun and enjoyable place. A special thank you to Leena, for being a great friend, colleague, roommate and not to mention a splendid cook.

And, most importantly, the biggest thank you to the key component of my success-my family. Thank you Mom and Dad, Mr. P.J. Mane and Mrs. Bharati Mane, for your unconditional love and support and making me believe that I could achieve anything I set my mind to. I could not have done it without you. And finally my brother, Paresh, thank you for advising and guiding me all these years.

Table of Contents

List of Figures

List of Tables

Abstract

INTEGRATED ACTUATION AND ENERGY HARVESTING IN PRESTRESSED PIEZOELECTRIC SYNTHETIC JETS

By Poorna Mane, Ph.D.

A Dissertation submitted in partial fulfillment of the requirements for the degree of Doctor of Philosophy at Virginia Commonwealth University.

Virginia Commonwealth University, 2009

Major Director: Karla Mossi

Associate Professor, Mechanical Engineering

With the looming energy crisis compounded by the global economic downturn there is an urgent need to increase energy efficiency and to discover new energy sources. An approach to solve this problem is to improve the efficiency of aerodynamic vehicles by using active flow control tools such as synthetic jet actuators. These devices are able to reduce fuel consumption and streamlined vehicle design by reducing drag and weight, and increasing maneuverability.

Hence, the main goal of this dissertation is to study factors that affect the efficiency of synthetic jets by incorporating energy harvesting into actuator design using prestressed piezoelectric composites.

Four state-of-the-art piezoelectric composites were chosen as active diaphragms in synthetic jet actuators. These composites not only overcome the inherent brittle and fragile nature of piezoelectric materials but also enhance domain movement which in turn enhances intrinsic contributions. With these varying characteristics among different types of composites, the intricacies of the synthetic jet design and its implementation increases. In addition the electrical power requirements of piezoelectric materials make the new SJA system a coupled multiphysics problem involving electro–mechanical and structural–fluid interactions.

Due to the nature of this system, a design of experiments approach, a method of combining experiments and statistics, is utilized. Geometric and electro-mechanical factors are investigated using a fractional factorial design with peak synthetic jet velocity as a response variable. Furthermore, energy generated by the system oscillations is harvested with a prestressed composite and a piezo-polymer. Using response surface methodology the process is optimized under different temperatures and pressures to simulate harsh environmental conditions.

Results of the fractional factorial experimental design showed that cavity dimensions and type of signal used to drive the synthetic jet actuator were statistically significant factors when studying peak jet velocity. The Bimorph (~50m/s) and the prestressed metal composite (~45m/s) generated similar peak jet velocities but the later is the most robust of all tested actuators. In addition, an alternate input signal to the composite, a sawtooth waveform, leads to jets formed

with larger peak velocities at frequencies above 15Hz. The optimized factor levels for the energy harvesting process were identified as 237.6kPa, 3.7Hz, 1MΩ and 12°C and the power density measured at these conditions was 24.27μW/mm^3.

Finally, the SJA is integrated with an energy harvesting system and the power generated is stored into a large capacitor and a rechargeable battery. After approximately six hours of operation 5V of generated voltage is stored in a 330μF capacitor with the prestressed metal composite as the harvester. It is then demonstrated that energy harvested from the inherent vibrations of a SJA can be stored for later use. Then, the system proposed in this dissertation not only improves on the efficiency of aerodynamic bodies, but also harvests energy that is otherwise wasted.

1 Introduction

1.1 Motivation

Modern civilization thrives on the abundance of oil. Oil is exceptionally versatile and can power almost all machines that move. In particular and of major impact are transportation machines such as airplanes and automobiles. Figure 1–1 (a) shows oil, coal and natural gas together supplying 85 percent of the world's energy supply in 2008 as published by the Energy Information Administration (EIA).

At the current rate of production and consumption, the existing oil reserves are sufficient to last 42 years. That figure is 61 years for natural gas and 133 years for coal as shown in Figure 1–1 (b). Oil and gas wells produce less as they become depleted which makes it impossible to keep production constant. Thus it is inevitable that oil and gas will become scarce and expensive within the life time of living humans. The two possible solutions to this problem are:

1. Use existing energy supplies wisely and more efficiently to delay the problem as long as possible.
2. Identify alternate and renewable energy sources which are fairly inexpensive and can sustain the needs of mankind.

This dissertation is focused on the study of an active flow control method which can increase the fuel efficiency of aerodynamic and automotive vehicles by reducing weight and complexity of the system. Using active flow control tools such as synthetic jet actuators could lead to saving millions of dollars in fuel costs.

Another aspect of this dissertation presents an energy source which, until recently, has largely been ignored due to the very small amounts of power that is produced. Piezoelectric sensors can harvest energy from ambient sources such as vibrations and heat which are usually wasted. Although the amount of energy harvested by piezos is very small in comparison to solar or wind energy sources, piezoelectric sources can operate in any environment (day or night) and do not need complex and expensive installation procedures. Since vibrations exist in all dynamics systems can be used to harvest the kinetic energy to power small devices.

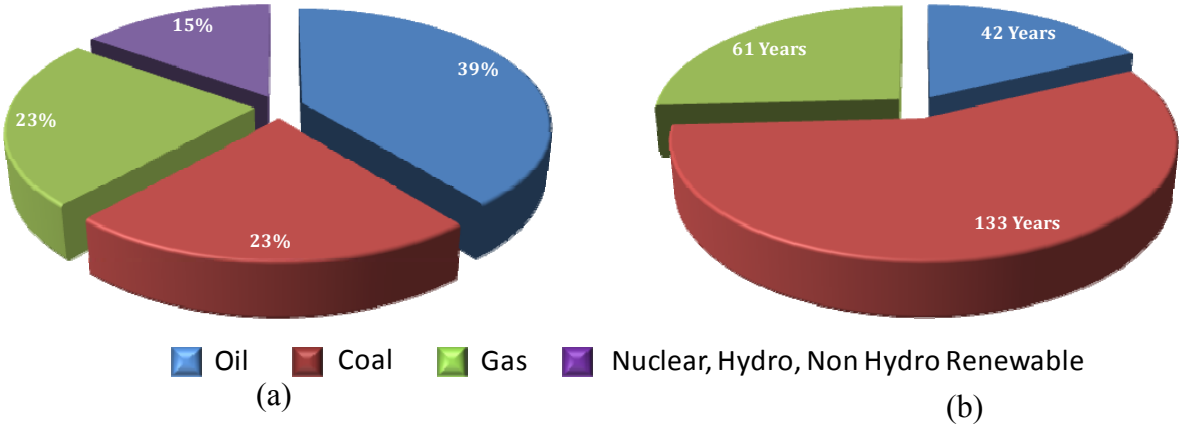

Figure 1-1 (a) World Energy Supply 2008, (b) Years of energy supply left at constant production rate (Energy Information Administration EIA)

Thus the motivation of this dissertation is to study synthetic jet active flow control actuators which can provide a potential solution towards solving the energy crisis. Further it is also shown that energy harvesting principles can be integrated into synthetic jets to generate enough energy to charge a large capacitor which in turn can be used to power other sensors

needed for optimal flow control. The following sections will provide more details about the mechanisms and advantages of using active flow control tools such as synthetic jet actuators.

1.2 Active Flow Control

Flow control refers to the idea of manipulating flow fields around and within structures in such a manner so as to improve efficiency and performance. In the case of aerodynamic vehicles the potential benefits of flow control include improved performance and maneuverability, affordability, increased range and payload, and environmental compliance. Thus flow control has become one of the leading areas of research for many scientists and engineers in industry as well as academia.

The German engineer Ludwig Prandtl first introduced the world to flow control by publishing the boundary layer theory at the beginning of the 20th century. Flow control was extensively studied and applied mainly to military related flow system all throughout the cold war and also in the period before and during World War II. The 1961 paper by Lachman gives a complete review and analysis and more recently Gad-el-Hak has published papers on flow control history and eras (Lachman, 1961, Gad-el-Hak *et al.*, 1998, Gal-el-Hak, 2000). Preceding the pioneering work of Schubauer and Skramstad in 1947, all the work on flow control used steady state passive tools and mechanisms for flow management (Schubauer and Skramstad, 1947). Such passive flow control techniques have marginal power efficiency, and therefore limit the implementation in operational applications.

Active flow control (AFC) methods however, are much more efficient. During the last decade, emphasis has been placed on the development of active control methods in which energy, or auxiliary power, is introduced into the flow. AFCs can adapt to the constantly

changing conditions by introducing small amounts of energy locally to achieve non-local changes in the flow field with large performance gains (Amitay *et al*., 1997, Amitay *et al*., 1998, Gad-el-Hak, 2000, Kral *et al*., 1997, Smith and Glezer, 1998). The feasibility of increasing the efficiency and simplifying fluid related systems is very appealing considering that one percent saving in world consumption of jet fuel is worth about 1.25 million dollars a day of direct operating costs (Collis *et al.*, 2004). Likewise, such fuel savings would lead to reduced environmental impact, although such environmental effects are difficult to quantify. McLean et al. evaluated different AFC concepts and candidate applications were considered for civil jet transports (McLean *et al.*, 1999). The simplification of conventional high lift systems by AFC was identified as a prime candidate, possibly providing 0.3% airplane cost reduction, up to 2% weight reduction and about 3% cruise drag reduction. Also, the advent of MEMS (Micro Electro Mechanical Systems) technology in the last two decades has provided a new impetus to the field of active control. The MEMS based actuators are easy to mass manufacture and they provide a unified framework for implementing flow control including actuation, power transmission, sensing and incorporation of control algorithms (Ho and Tai, 1996).

In spite of all the advantages, using active flow control devices usually adds complexity in design, increases manufacturing and operation cost, which prevents their use. For this reason, many researchers have focused on designing better active flow control devices that are easy to manufacture, are small in size, require little power to operate and are highly reliable. A promising concept that has shown much potential during the last decade is synthetic jet actuators, a form of AFC.

1.3 Synthetic Jet Actuators (SJA)

Synthetic jet actuators consist of a cavity with an oscillating diaphragm as shown in Figure 1-2. When the diaphragm oscillates air is pushed out an orifice forming a jet (Smith, 1999). The interaction of the jets with an external flow leads to the formation of closed re-circulating flow regime near the surface. This interaction can act as a "virtual surface" and consequently is an apparent modification of the flow boundary (Amitay *et al.*, 1997). An array of such fabricated devices can produce a large jet velocity if the orifices are at the correct spacing and the driving signals are in phase.

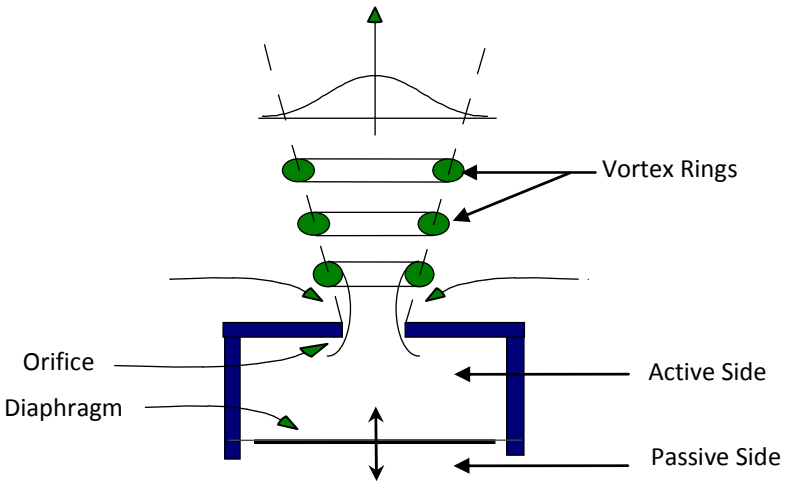

Figure 1-2 Synthetic Jet Actuator

Synthetic jets are popular flow control devices capable of causing an apparent modification to the flow boundary through periodic oscillations. Their popularity stems from the self-contained design, lack of fluid source, and the fact that no ducting is required, only an applied voltage. The design of the micro scale synthetic jet actuator proposed by Glezer and his co-workers (Coe *et al*., 1994) has been adapted widely by a number of researchers. The design is very simple consisting of a diaphragm that is driven by an electric field, set within a cavity. The

diaphragm is made up of a piezo disk glued to a metal shim, a Unimorph. An orifice in the lid of the device allows fluid to be drawn into, and forced out of the cavity. To obtain high velocities, the diaphragm has to be driven at its resonant frequency, which is in the kHz range.

Smith and Glezer performed a detailed experimental investigation into the synthetic jet created by these devices (Smith and Glezer, 1997, 1998). It is claimed, that during the outflow cycle a vortex ring is formed at the orifice. This ring then travels away from the device under its own self-induced velocity. By the time the fluid is drawn into the cavity, the vortex ring has moved sufficiently far away so as to be relatively unaffected. Consequently, a train of vortices traveling away from the orifice is generated. In their experiments, the vortices rapidly undergo transition and lose their coherence. The resulting synthetic jet is turbulent. The experimental findings of Smith and Glezer were supported by Kral *et al.* who performed a two dimensional numerical study of a laminar synthetic jet (Kral *et al.*, 1997).

Rathnasingham and Breuer drew attention away from the jet and instead focused on the physics within the cavity (Rathnasingham and Breuer, 1997 *a* and *b*). It was demonstrated, by the use of experimental and simple numerical models, that there was significant fluid structure interaction between the resonant diaphragm and the fluid pressure in the cavity. Interest in the cavity was continued by Rizzetta *et al*. who solved the three-dimensional compressible Navier-Stokes equations both inside and outside of the cavity (Rizetta *et al.*, 1999). It was shown that significant vertical disturbances could be created in the cavity during the inflow cycle of the actuator. The cavity dimensions, such as cavity depth, also influenced the velocity profile of the jet at the orifice exit.

The effectiveness of oscillatory blowing in separation control has been established experimentally and numerically (Hasan, 1998, Donovan *et al.*, 1998, Seifert *et al.*, 1993, Seifert *et al.,* 1996, Seifert and Pack, 1999). Active separation control was applied successfully for the first time at Reynolds numbers, corresponding to a jetliner at takeoff conditions. Oscillatory blowing proved to be an effective and efficient tool for the control of boundary-layer separation over a wide range of chord Reynolds numbers, representative of a micro-aerial-vehicle to commercial jetliners at takeoff. Using bench-top experiments accompanied by theoretical analysis, it was determined that for low amplitudes (velocity < 10m/s), the level of velocity fluctuations exiting the blowing slot was proportional to the cavity pressure fluctuations normalized by the density, whereas for high amplitudes it is proportional to the square root of the normalized pressure (Seifert *et al.*, 1999). Based on these results, Seifert et al. proposed that a possible approach to closed-loop control of separation is to sense the trailing edge pressure and use that as an input to adjust the oscillatory blowing momentum coefficient to achieve the desired aerodynamic behavior, while maintaining effective frequency as 1 at all times. Effective frequency, as defined by Seifert and Pack, is the oscillation of the diaphragm divided by the free stream velocity multiplied by the location of the jet on a wing.

These successful attempts in separation control encouraged the investigation of the effect of synthetic jet actuators on simple two dimensional cylinder flows. Amitay *et al*. controlled lift and drag forces successfully by installing a pair of synthetic jet actuators side by side radially on the cylinder shell (Amitay *et al.*, 1997, 1998). Mallinson *et al*. investigated similar control on a cylinder but used a circular orifice instead of a rectangular orifice as in the previous case (Mallinson *et al.*, 1999). Again, control over a cylinder was performed by Crook *et al*. and Wood *et al.*, using a spanwise array of synthetic jet actuators to delay separation (Crook *et al.*, 1999,

Wood *et al.*, 2000). Crook *et al.* constructed a device, a piezoelectric disc bonded to a brass shim, based on preliminary analysis by Rathnasingham and Breuer that modeled a thin circular plate as a piston. Results showed the model provided a good prediction of the mean value of the velocity in the developed jet though the model did not predict the peak centerline jet velocity.

The 2004 CFD validation workshop for synthetic jets and turbulent separation control held in Williamsburg, VA asked seventy five researchers representative of seven countries to attempt to model one of three cases experimentally tested at NASA Langley Research Center. These cases included: 1) synthetic jets in quiescent air, 2) synthetic jet in a turbulent boundary crossflow, and 3) flow over a hump model with no crossflow. Until this CFD workshop, most CFD validation efforts of experimental results have been and continue to be rather isolated making it difficult to accurately determine the reliability of synthetic jet CFD modeling (Rumsey *et al.*, 2004, Schaeffler and Jenkins, 2004, Yao *et al.*, 2004).

For case one, synthetic jets in quiescent air, participants at the workshop were given the experimental jet velocity as a function of time near the center of the orifice exit and were granted the choice of applying arbitrary boundary conditions, grid, and method of solution to attempt to numerically reproduce the results. Since no guidelines were given regarding particular boundary conditions, grids or methods of solution to encourage broad participation it inevitably introduced a source of uncertainty when attempting to evaluate and compare the various CFD results against one another.

For the quiescent flow case believed to be mostly laminar or transitional, there were eight participants that submitted twenty five separate numerical models that included large eddy simulation (LES), reduced order models, 2D blended RANS-LES, laminar Navier Stokes, and unsteady Reynolds Average Navier-Stokes (RANS). Most of the numerical cases were 2D with a

few 3D models that used periodicity in the direction aligned with the slot's long axis. The vast majority of participants simulated the diaphragm motion via a transpiration condition imposed on the diaphragms neutral surface. A transpiration condition is one that applies either an assumed oscillating fluid velocity profile or pressure oscillation to emulate the effects of the oscillating diaphragm within the cavity. Others participants further simplified the cavity by imposing a transpiration condition not at the neutral surface but at the bottom of the slit's neck or directly on the slit's exit, thus neglecting the effects of the cavity itself. Results of the workshop showed significant variation among the proposed CFD techniques and established that no one method in particular clearly excelled above the others.

A more recent paper by Rumsey (2009) talks about the success and challenges of flow control simulations in the past decade. The paper states that the active flow control problem is very complex. Current models have coupled CFD tools with considerable experiments and such empirical designs are extremely expensive and time consuming. Current computational tools have inherent limitations and a generalized model for synthetic jet actuators does not exist. It was also established that there are still inconsistencies not only with the numerical models but also between the different experimental time-dependent flow measurement techniques, Particle Image Velocimetry (PIV), hot-wire probes, and Laser Doppler Velocimetry (LDV) (Yao *et al.*, 2004). The greatest variation in the experimental measurements was mostly attributed to the piezoelectric diaphragms observed performance time degradation, which further complicated validation of the various CFD models.

The oscillating diaphragm used in the synthetic jet cavity is usually driven using electrical or mechanical power. In the past, researchers have used mechanical shakers, compressed air, or regulated blowers as a means of supplying steady or oscillating flow (Seifert

et al., 1993, Seifert *et al.*, 1996). This adds to the complexity and weight of the system. To overcome these drawbacks piezoelectric diaphragms are commonly used to increase efficiency. The diaphragms consist of a piezoelectric ceramic bonded to a metal shim. This arrangement reduces the number of moving parts prone to failure. Several investigators have adopted piezoelectric disks as oscillating diaphragms in synthetic jets to attempt to make the systems lighter, increase efficiency and save resources without the use of complex circuitry as compared to previously used methods (Crook *et al.*, 1999, Rathnasingham and Breuer, 1997 *a* and *b*, Smith and Glezer, 1998). Synthetic jet actuators with piezoelectric discs need to be operated at very high resonant frequencies to achieve the desired output. This is a major disadvantage since at high frequencies debonding and degradation occurs leading to the failure of the actuator.

The standard synthetic jet actuator cavity design proposed by Glezer *et al.* was further modified by Bryant et al. (Bryant *et al.*, 1999) to demonstrate the potential benefits of high displacement piezoelectric composite actuators (HGA's) such as Bimorph and Thunder® in synthetic jet actuation. These pre-stressed devices have the advantage of durability and being able to produce large deflections at non-resonant driving frequencies. Several studies conducted by Mossi (Mossi and Bryant, 2003, 2004, Mossi *et al.*, 2005 *a* and *b*) have shown that the diaphragm used in the synthetic jet cavity has a significant effect on the jet velocity, yet its performance is highly dependent on geometrical, mechanical, and electrical parameters.

An added advantage of using piezoelectric diaphragms is their sensing functionality. According to the direct piezoelectric effect, a charge develops on the surface of the material when a stress is applied. In the case of a synthetic jet actuator, the converse piezoelectric effect is in effect such that application of electric field causes a change in strain. While the jet is operational, the diaphragm is constantly vibrating, generating kinetic energy which is usually

wasted. Using the direct piezoelectric effect this energy can be harvested to charge a storage device or to run a low power device such as wireless sensors.

1.4 Energy Harvesting

Energy harvesting is a process in which energy which would otherwise be wasted is processed and stored for future use by an application. The use of harvested energy could extend the operational life of devices traditionally powered by batteries. This is particularly advantageous in systems with limited accessibility such as biomedical implants and structures with embedded micro and wireless sensors. It is feasible that such devices would have the ability to generate their own power from the ambient environment. This can either prolong the life of an existing battery or eliminate the battery. With advances in design and manufacturing as well as reduced power requirements, the use of energy harvesting methods has become practical and has gained significant popularity (Chandrakasan *et al.*, 1998, Davis *et al.*, 2002).

There are several types of ambient energy which exist in nature that can be harvested. Heat, electricity, solar, and biomass are forms of energy that are stored differently, but can be converted from one form to the other. Photocells convert light to electricity, thermocouples convert heat to electricity, and magneto-electric generators convert mechanical energy to electricity. These are all power generators and are frequently used in electricity generation. Similar to magneto-electric generators, piezoelectric materials can also convert mechanical energy from vibrations to electrical energy.

Piezoelectric power generators can be advantageous for some systems over other conversion methods. Because of their simplicity, they can be made small enough to fit inside of micro electromechanical systems (MEMS) (Roundy *et al.*, 2004). Another advantage of using

piezoelectric generators is that the life span of the system is increased if the applied force and external temperature are within the operational range of the material. The mechanical energy required for conversion can feasibly be obtained from the environment. However, because of the small electrical output, piezoelectric generators have been largely neglected for power generation. But with advances in integrated circuit technology this is no longer an issue. Other problems with piezoelectric generators are application specific so that a common solution does not exist. Hence, power requirements are different for a variety of modules, thus suitable circuitry is required to adapt to various applications. In the current study, relevant factors are identified and a process through which these parameters can be optimized is outlined.

Piezoelectric materials are versatile because vibrations occur in most dynamic systems. These materials also have a wide dynamic range and low output noise. There are many piezoelectric materials from which to choose for designing a power conversion mechanism. Roundy *et al*. have shown that a power density of 70μW/cm^3 is quite feasible from a PZT Bimorph beam mounted as a cantilever. Simulations by the same investigators show that an optimized design would be capable of 250μW/cm^3 from a vibration source with input vibrations of 2.5m/s^2 at 120Hz (Roundy, 2003, Roundy *et al.*, 2003, Roundy *et al.*, 2004). Erika *et al.* modeled and tested a Unimorph membrane consisting of PZT and brass encircled by an aluminum ring mounted on a mechanical shaker (2005). The excitation of the shaker was varied between 0–5g of acceleration. The electrical output of the membrane was connected to load resistors which varied from 100Ω to 1MΩ. It was found that a maximum power of 1.8mW was generated at an acceleration of 2g with a 56kΩ load resistance. Yoon, Washington, and Danak studied the charge generation properties of curved rectangular PZT Unimorph beams by optimizing geometric parameters such as length, width and thickness of the device (2005). A

shoe insert which was used in a previous study to harvest energy while walking, was modeled using the piezoelectric constitutive equations and the shallow, thin shell theory. An equation was derived that expressed charge generation of the PZT beam in terms of applied force, material properties and geometry. In a parametric study using the dimensions from nine samples, it was shown that geometry and material properties do affect charge production. Increasing the width, center height, and thickness of the substrate produces increased charge generations. During this study, an experiment was conducted by dropping a 5lb weight on a sample and determining its charge production. Another experiment was conducted by determining the charge production of a sample while a 100lb human stepped on it.

An additional aspect of the energy harvesting process is signal conditioning, as the electrical charge generated by a piezoelectric generator is usually insufficient to power a commercial device. By using circuitry the generated signal is processed such that a usable voltage is obtained which can be applied to the device directly or used to charge a battery (Elvin *et al.*, 2003). The type of circuitry used to harvest the energy from a piezoelectric transducer is determined by the desired output to the load which most often needs to be rectified, filtered, and regulated (Park, 2001). To that end, a piezoelectric transducer can be modeled as an AC source in parallel with a capacitor. To convert this signal into a useful one, an AC—DC converter is used to rectify the AC signal. The output from this converter is then sent to a DC—DC converter where it is regulated to the desired voltage. Roundy *et al*. explored the possibility of scavenging low level vibrations as a power source for wireless sensor nodes. In this study, the geometry of the piezoelectric device was optimized while the load resistance of the circuitry, which consisted of a series inductor with an active bridge, was varied. A piezoelectric generator was modeled as an AC source in series with a capacitor and a resistance (Roundy, 2003, Roundy *et al.*, 2003,

Roundy *et al.*, 2004). Other approaches include the use of piezoelectric composites. Sodano, Lloyd, and Inman, for instance, compared the ability of three types of composites to convert mechanical strain into electrical energy by exciting them while attached to an aluminum beam. Their study concluded that impedance matching between the transducer and the circuit is critical when optimizing for power (Sodano *et al.*, 2005, 2006).

Mossi *et al*. performed an investigation of parameters that affect actuation and energy harvesting on rectangular pre-stressed piezoelectric Unimorphs (Mossi *et al.*, 2005*c*). Parameters such as conductivity of the adhesive, composition, size, type, and thickness of the layers, were investigated using fractional factorial experimental design techniques. Statistical analyses of all the results were performed to determine the significance of the parameters tested. The study concluded that circuitry must be coupled with device geometry to optimize its performance.

The vibration energy harvesting process described in this section can be integrated into a synthetic jet actuator to achieve multi–functionality. Actuation and sensing will be integrated into one system such that additional information can be obtained about the working of the synthetic jet and concurrently the harvested energy can be used for used for other applications. Limited work exists on the integration of sensing and actuation in piezoelectric materials as described in the following section.

1.5 Integrated Energy Harvesting in Synthetic Jet Actuators

Piezoelectric materials have been widely used as sensors and actuators owing to their excellent conversion properties between the electrical and mechanical strain energies. , and independent piezoelectric devices for the sensor and actuator are generally necessary. The process of concurrent actuation and sensing by a single transducer is described as self—sensing

(Simmers *et al*., 2004, Hanson and Levesley, 2004). Using such a technique leads to an immediate reduction in the number of sensing and actuation devices. Associated costs of power, wiring and interfacing are drastically reduced also making the system simpler. A self-sensed system can also offer increased robustness if an actuator can be used without sensors; it is generally noted when a failure occurs in a sensor—actuator system, the fault is far more frequently due to sensor failure (or failure of related interfacing or wiring) than actuator failure (Lorenz , 2001).

The concept of self—sensing actuators was first developed and published by Dosch *et al.* (1992) and Anderson *et al.* (1992). The motivation behind the concept was to truly integrate sensors and actuators to have applications in active and intelligent structures. Dosch *et al.* verified the technique experimentally by mounting piezoceramic wafers to a cantilevered beam and using them to suppress the beam's vibrations. Anderson *et al.* applied self-sensing to an active strut for vibration control.

Subsequent to the work of Dosch *et al.*, self—sensing piezoelectric actuators have been widely employed in vibration and control applications. Tzou and Hollkamp investigated the use of self sensing orthogonal model actuators to effectively control vibration in beam-like structures (1994). Frampton *et al.* (1995) and Dongi *et al.* (1995) investigated the feasibility of using a self—sensing actuator for active flutter suppression. Vallone successfully applied self—sensing actuators to control vibrations in large scale structures (Vallone, 1995). In addition, self—sensing actuation has been extended to active acoustic noise control and structutal health monitoring applications. While most studies use monolithic piezoceramic material for its d_{31} coupling coefficients, Jones *et al.* applied the self-sensing actuation concept to PZT stack actuators used as

a micropositioner (1994). The authors used a nonlinear element in the self—sensing circuit to negate any nonlinear effects, thus improving the signal to noise ratio. More recently, Sodano *et al.* investigated the feasibility of Micro Fiber Composites used in self—sensing actuation for vibration reduction in flexible structures, such as inflatable space devices (2004).

A number of techniques are presently used to achieve integrated sensing and actuation with separate piezoelectric sensors and actuators. One existing method applicable to beams is to layer a piezoelectric sensor on top of a piezoelectric actuator (Cudney *et al.*, 1990). If the sensor and actuator layers are thin compared to the thickness of the beam it can be said that strain in the sensor is the same as the strain in the actuator. A major challenge in this scheme is to minimize capacitive coupling between the sensor and actuator by electrically shielding.

A second method for achieving integrated control on a beam is to place the sensor and actuator alongside each other (Fanson and Caughey, 1987). The arrangement tends to reduce the capacitive coupling between the sensor and actuator compared to the previous method. For a beam undergoing pure bending, and equal thickness sensor and actuator, the strain in the actuator will be equivalent to the strain in the sensor. A disadvantage of this method is that less area of the beam is available for the actuator, having been sacrificed to the sensor.

A third method can be found in manufactured piezoelectric alarms and buzzers. One piezoelectric material is used and the sensor and actuator are separated by discontinuous electrode areas. On one electrode area the control voltage is applied and on the other electrode area the sensor voltage is measured. Because the electrode areas are alongside each other the capacitive coupling should be minimized. As with the previous method, part of the potential actuator area is sacrificed to the sensor.

The self-sensing piezoelectric actuator operation is based on the linear system principle that states that if two signals are added into a linear system and one of the signals is known, the second input can be determined. In this case, the two signals are the voltage from the controller and the voltage produced by piezoelectric material as it strains. In summary self–sensing is an expanding field and in this dissertation it is incorporates into flow control.

1.6 Chapter Summary

This chapter gives an overview of the research that has been performed on synthetic jet actuators and energy harvesting. A synthetic jet actuator is an active flow control tool used in automotive and aerodynamic industry. Although they have been studied extensively in the past decade, they have still not been implemented commercially in airplanes. Recently Ferrari and Renault automotives have integrated them in their new prototype models to reduce drag. Implementation in the aerospace industry is hindered by the limited results obtained using computational tools. In fact, CFD tools have proven insufficient in modeling these actuators accurately. It has been suggested that a coupling of experimental data and CFD tools is required to truly describe the physics of the problem. Furthermore a generalized model does not exist. One of the hurdles in the processes has been the implementation of an effective and reliable mechanism for generating the jets. Piezoelectric discs are commonly used in the implementation but further research is required in resolving the reduced lifetime issues. In the current study a type of prestressed piezoelectric composite is suggested as a possible solution due to its robustness and enhanced performance as compared to piezoelectric discs.

Research into energy harvesting with piezoelectric materials has gained tremendous impetus in the last few years. This chapter provides a summary of the work that has been performed in the last few years. Comparisons between different piezoelectric harvesting systems

are discussed with both advantages and disadvantages of the technology. It is indicated that the circuitry used in converting the harvested AC voltage to DC is critical to preserving efficiency. The energy harvested with piezos is too small to directly power existing devices. Thus it is more feasible to collect the harvested energy in a storage device such as a battery or a large capacitor.

A section in this chapter discusses the limited work that has been done on self–sensing actuators and sensors. In self–sensing devices a single device acts as both sensor and actuator. The motivation behind the concept is that such a sensor/actuator pair will be truly integrated and has applications in active and intelligent structures. The concept of self–sensing actuator was first developed and published by Dosch *et al.* (1992) and Anderson *et al.* (1992). In the current study sensing and actuation is integrated into synthetic jet actuators using prestressed piezoelectric composites.

2 Piezoelectric Materials

Piezoelectricity is defined by Jaffe, Cook, and Jaffe as the "ability of certain crystalline materials to develop an electric charge proportional to a mechanical stress" (1971). The discovery of this phenomenon is attributed to two brothers, Jacque and Pierre Curie. In 1880, these two men presented their work, *Development by pressure of polar electricity in hemihedral crystals with inclined faces,* which stated:

> *Those crystals having one or more axes whose ends are unlike, that is to say hemihedral crystals with oblique faces, have the special physical property of giving rise to two electrical poles of opposite signs at the extremities of these axes when they are subjected to a change in temperature: this is the phenomenon known under the name of pyroelectricity…We have found a new method for the development of polar electricity in these same crystals, consisting in subjecting them to variations in pressure along their hemihedral axes.*
>
> P. & J. Curie

Not long after this discovery, a contemporary of the Curies' by the name of Wilhelm Hankel suggested the name "piezoelectricity" based on the Greek—derived *piezein*, meaning "to squeeze" (Katzir, 2003). In 1881, Nobel Prize winner Gabriel Lippmann used the fundamentals

of thermodynamics to derive mathematical expressions that helped him formulate a prediction he named the “converse piezoelectric effect”: the development of a mechanical stress in response to an electrical charge. The Curie brothers quickly confirmed this prediction and proved that the coefficients in each of the mathematical models describing the direct and converse piezoelectric effects were, in fact, one and the same (Ballato, 1996, Katzir, 2003). The efforts of Lord Kelvin, Pierre-Maurice-Marie Duhem, Frederich Pockels, and Woldemar Voigt developed the laboratory curiosity demonstrated by the Curies into an emerging field of science before the end of the 1800’s (Ballato, 1996, Katzir, 2003).

Today we know that the piezoelectric effect that Jacque and Pierre Curie were able to demonstrate using Rochelle salt results from the inherent polarity the material derives from its crystalline structure. By the end of 1940’s, scientists and engineers discovered that such a polarity need not be inherent to a material's structure but that this property could be macroscopically induced in originally isotropic polycrystalline material by application of an electric field (Boyd, 1993). The process by which this is done is analogous to the magnetization of a permanent magnet and was thus termed “poling.” Figure 2.1 provides an illustration of the direct and converse piezoelectric effects (APC International).

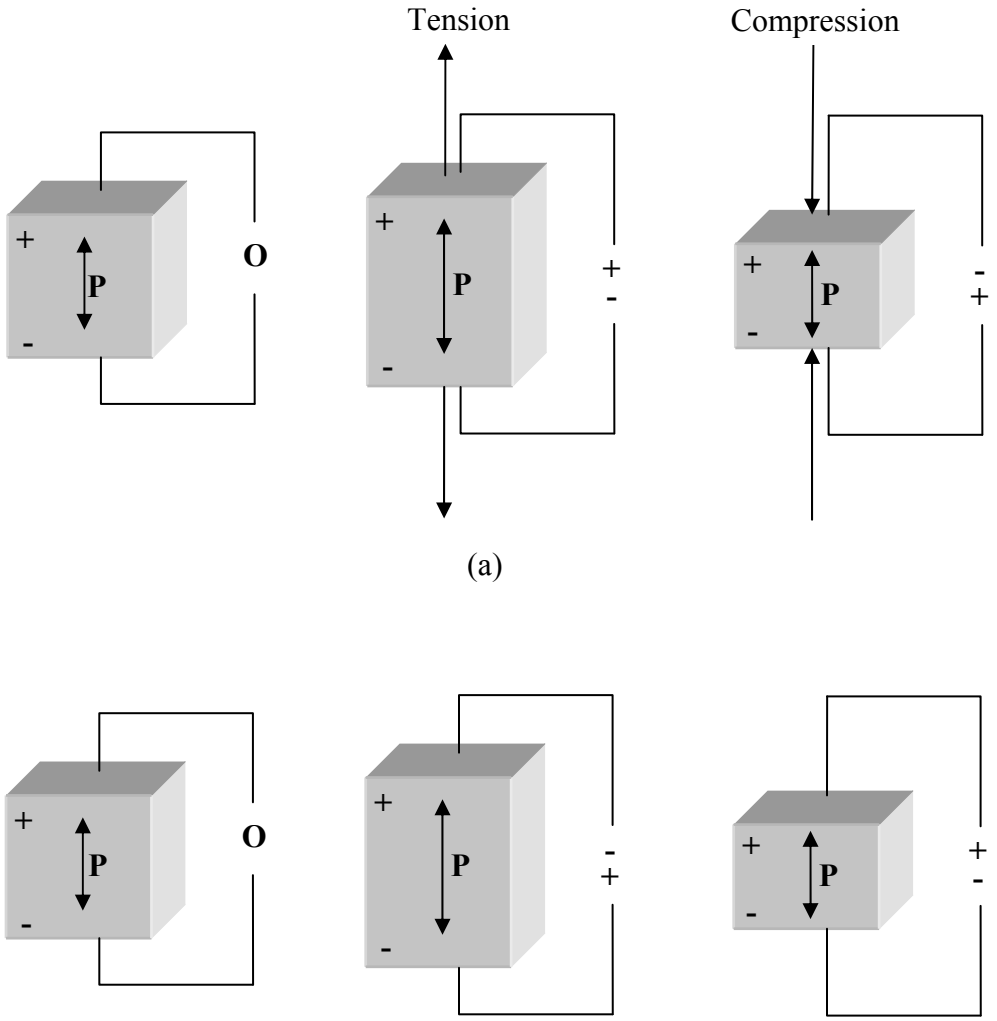

Figure 2-1 Piezoelectric effect (courtesy APC International)
(a) direct effect, (b) converse effect

Piezoelectricity is described mathematically within a material's constitutive equation, which defines how the piezoelectric material's stress (*T*), strain (*S*), charge density displacement (*D*) or dielectric displacement, and electric field (*E*) interact. *T* and *S* are tensor magnitudes (Jaffe e*t al.*, 1971). The equations can be written in matrix form as follows in Equation 2-1 and Equation 2-2:

$$\begin{bmatrix} D_1 \\ D_2 \\ D_3 \end{bmatrix} = \begin{bmatrix} \varepsilon_1 & 0 & 0 \\ 0 & \varepsilon_1 & 0 \\ 0 & 0 & \varepsilon_3 \end{bmatrix} \begin{bmatrix} E_1 \\ E_2 \\ E_3 \end{bmatrix} + \begin{bmatrix} 0 & 0 & 0 & 0 & d_{15} & 0 \\ 0 & 0 & 0 & d_{15} & 0 & 0 \\ d_{31} & d_{31} & d_{33} & 0 & 0 & 0 \end{bmatrix} \begin{bmatrix} T_1 \\ T_2 \\ T_3 \\ T_4 \\ T_5 \\ T_6 \end{bmatrix}$$

Equation 2-1

$$\begin{bmatrix} S_1 \\ S_2 \\ S_3 \\ S_4 \\ S_5 \\ S_6 \end{bmatrix} = \begin{bmatrix} 0 & 0 & d_{31} \\ 0 & 0 & d_{32} \\ 0 & 0 & d_{33} \\ 0 & d_{24} & 0 \\ d_{15} & 0 & 0 \\ 0 & 0 & 0 \end{bmatrix} \begin{bmatrix} E_1 \\ E_2 \\ E_3 \end{bmatrix} + \begin{bmatrix} s_{11} & s_{12} & s_{13} & 0 & 0 & 0 \\ s_{12} & s_{11} & s_{13} & 0 & 0 & 0 \\ s_{13} & s_{13} & s_{33} & 0 & 0 & 0 \\ 0 & 0 & 0 & s_{44} & 0 & 0 \\ 0 & 0 & 0 & 0 & s_{44} & 0 \\ 0 & 0 & 0 & 0 & 0 & s_{66} \end{bmatrix} \begin{bmatrix} T_1 \\ T_2 \\ T_3 \\ T_4 \\ T_5 \\ T_6 \end{bmatrix}$$

$$s_{66} = 2(s_{11} - s_{12})$$

Equation 2-2

Equation 2-1 describes the direct and Equation 2-2 the converse piezoelectric effect. The matrix *d* contains the piezoelectric coefficients for the material and ε is the electric permittivity matrix. The four variables can be rearranged to give an additional three forms for a piezoelectric constitutive equation. It is possible to transform piezo constitutive data in one form to another form.

While a number of naturally occurring crystalline materials possess the ability to function as active elements in piezoelectric based devices, many applications that look to exploit this

phenomena call for the higher electro—mechanical coupling coefficients found in ferroelectric ceramics. Materials such as Lead Titanate ($PbTiO_3$), Lead Zirconium Titanate (PZT), and Lead Lanthanum Zirconate Titanate (PLZT) have substantially higher piezoelectric coefficients than naturally occurring materials (Boyd, 1993).

Due to their excellent properties and easy availability the most widely used smart materials are piezoelectric ceramics. Although not as forceful as shape-memory alloys, piezoelectric ceramics respond much more quickly, making them ideal for precise, high speed actuation. Demand for these materials is being fueled largely by their application as device actuators and transducers in sonar and ultrasonic systems. They can also be used in optical tracking devices, magnetic heads, dot-matrix printers, computer keyboards, high frequency stereo speakers, accelerometers, microphones, pressure sensors, transducers, and igniters for gas grills.

The most common piezoelectric ceramics used these days is lead zirconate titanate (PZT). Advanced piezoelectric materials such as these can be obtained in several forms including disk, plates, and rings, as well as custom molded designs from commercial vendors such as Morgan Matroc Inc., Kinetic Ceramics Inc., Piezo Systems Inc., and many others. Even the advanced compositions and geometries offered by the suppliers listed, however, can fall short of meeting the force and displacement requirements called for in certain applications

For most piezoelectric actuators, the focus of research has been on an attempt to amplify the deflection of the material to cast it into a useful form. As a result, numerous novel, ingenious concepts have been created. Generally the deflection is amplified with one of three schemes; using external mechanical component, through the internal structure without the use of an

external mechanical component and on an alternating control signal to generate motion. This paper describes some of the leading actuator architectures in the following sections.

Piezoelectric sensors and actuators have been modeling extensively for various applications. While these models work fairly well for ceramics and polymers they have some inherent limitations. Most of the modeling is conducted with the assumption that the piezoelectric coefficients vary linearly with changes in stimuli. This assumption does not hold true for the entire range. Figure 2-2 shows the effect of increasing and decreasing applied stress on the d_{33} coefficient for a EC-69, EDO corporation ceramic (Yang *et al*., 2000). The coefficient is linear at low stress levels in the beginning of the cycle and becomes non linear at larger values. Another characteristic of these materials that hinders the modeling efforts is the large hysteretic effort as seen in the figure. Also these effects increase in piezoelectric composites. Owing to

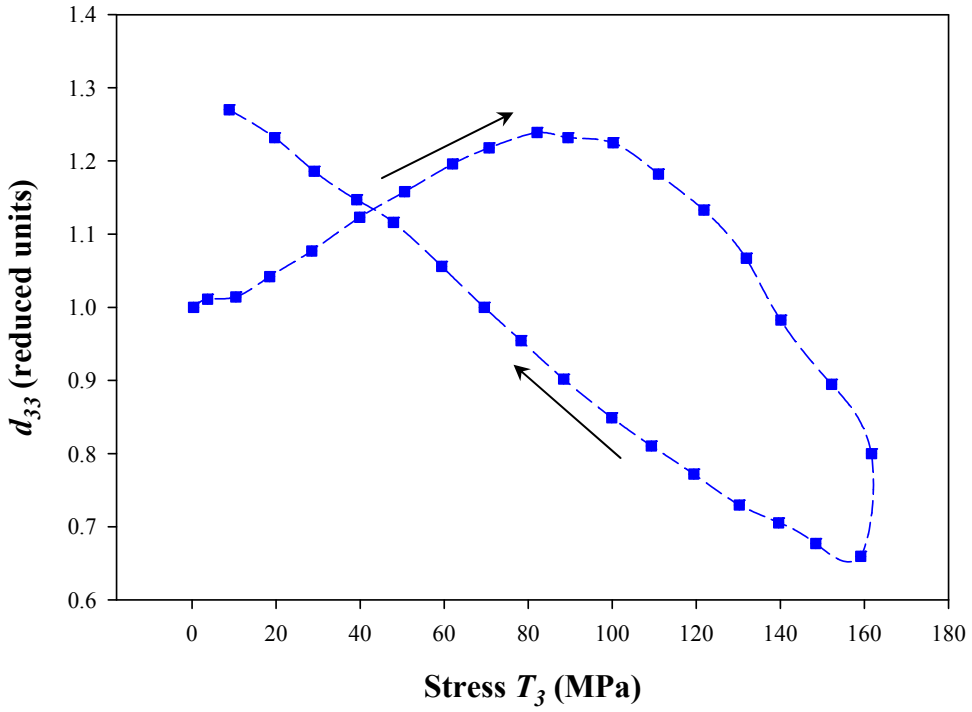

Figure 2-2 Piezoelectric charge coefficient d_{33} at a function of applied stress T (Yang *et al*., 2000)

these properties modeling of piezoelectric ceramics and composites is a very complex effort which hasn't been mastered thus far (Mukherjee *et al*., 2001).

2.1 Stacks

Stacks are the simplest form of amplification consists of thin piezoceramic layers connected in parallel. Thus their voltage requirement is low while the overall deflection is linearly increased. Figure 2-3 (a) shows a picture of a commercially sold stack actuator by Piezo systems and (b) shows a schematic of the linearly arranged piezoceramics. The displacement of a stack actuator is proportional to the high of the element and the blocking force is proportional to the cross sectional area. Ramsay and Mugridge first constructed a stack actuator in 1962 making relatively high strains feasible (Ramsay and Mugridge, 1962). Later they were studied more thoroughly by Bindal and Chandra for scientific applications (Bindal and Chandra, 1977). Some of the companies that manufacture piezoceramic patches and stacks include APC International Ltd. (Mackeyville, PA), Burleigh Instruments Inc. (Fishers, NY), EDO Corporation (Salt Lake City, UT), Etrema Products Inc. (Ames, IA), Keramos Inc. (Indianapolis, IN), Kinetic Ceramics Inc. (Hayward, CA), Morgan Matroc Inc. (Bedford, OH), Piezo Kinetics Inc. (Bellefonte, PA), Piezo Systems Inc. (Cambridge, MA), Polytec PI Inc. (Costa Mesa, CA), Sensor Technology Ltd. (Collingwood, Ontario, Canada), Staveley Sensors Inc. (East Hartford, CT), Tokin America Inc. (San Jose, CA), and TRS Ceramics Inc.

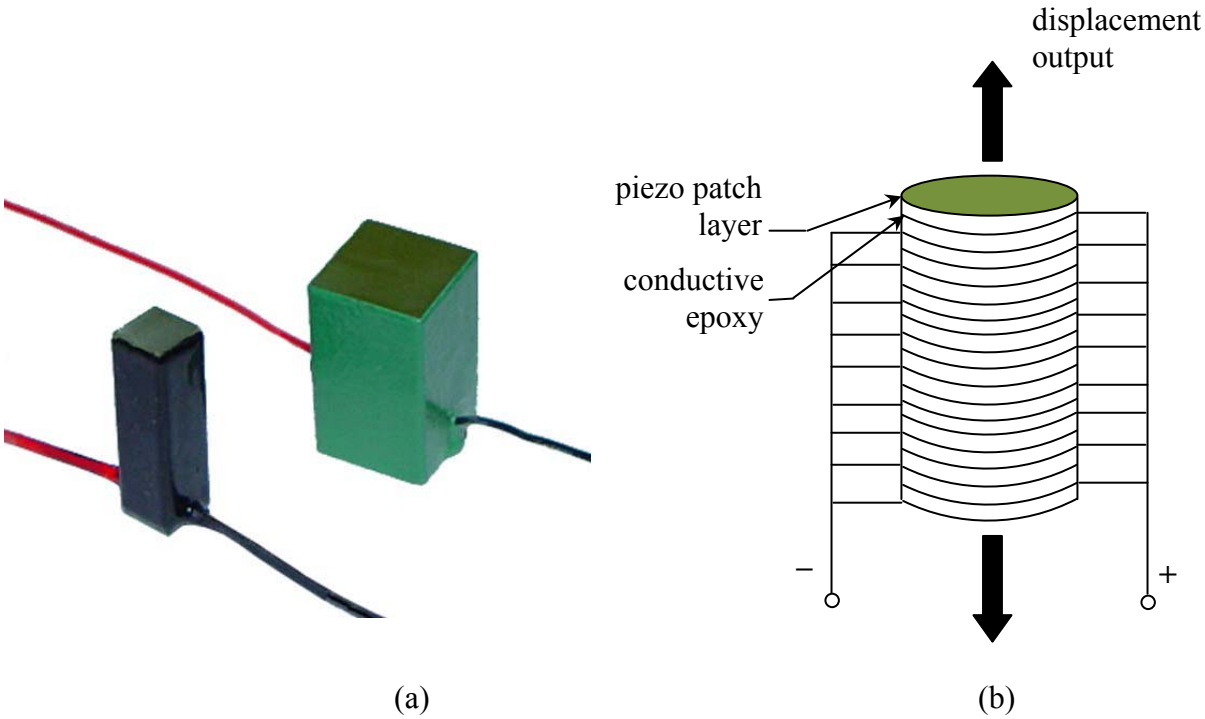

Figure 2-3 (a) Piezoceramic Stacks (courtesy of Piezo systems Inc. (b) Sketch of a Piezoceramic Stack (Niezrecki *et al*. 2001)

2.2 Bender Actuators

The other most commonly employed amplification scheme is the bender. Internal piezoelectric strains are used to indirectly induce deflections in the actuator. Layers of piezoelectric material are arranged such that the neutral axis is in the center and the layers on either side have opposing strains. While one side contracts the other side expands. Figure 2-4 shows the two commonly available bimorph bender arrangements: the two electrode serial arrangement which is commonly used in force sensor applications and the three electrode parallel arrangement.

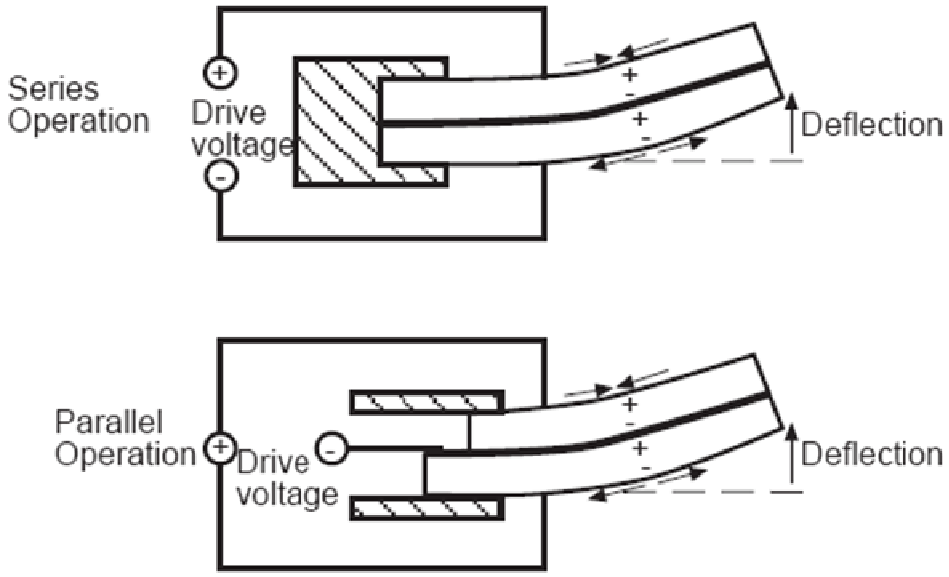

Figure 2-4 Bender Actuator (courtesy of Morgan Electro Ceramics)

Bimorph benders operate similar to a bimetallic strip in a thermostat, an internal bending moment is created by the opposing strains which cause the entire bender to flex. Some benders have inactive substrate layers in the middle for structural stability. Most benders are either circular, square or rectangular accept for one that tapered bender that staggers the thickness of the material, with the thickest portion at the root. This tapered shape increases the material bending efficiency 1996; Prechtl and Hall, 1997).

Bimorph benders were first developed in the early 1930s by Sawyer (1931) at the Brush Development Company. However, the performance of these actuators was understood only at a rudimentary level until much later, when research into smart structures became more detailed (Steel *et al*., 1978; Tzou, 1989). From a practical viewpoint, the primary difficulties with using raw piezoceramics as actuators include soldering, cracking owing to their brittle nature, and electrical isolation.

The QuickPack actuator, is another type of bender, manufactured by ACX Inc. (Cambridge, MA) (www.acx.com) that overcomes these difficulties (Figure 2-5 (a)). The QuickPack actuators contain two piezoceramic elements encapsulated in a protective polymide insulation material. The actuators can be used as patches (to induce in—plane strain, d_{31}) or operated out of phase to act like a bimorph bending actuator. The construction of the QuickPack actuators eliminates the requirement of soldering leads to the piezoelectric material, significantly improves the durability of the actuator, and electrically isolates the actuator from the attached surface.

Forming active fiber composites (AFCs) is another technique to improve the robustness of the actuator. AFCs consist of unidirectional piezoelectric fibers (*CeraNova Corporation, Franklin, MA*) embedded in a resin matrix with embedded interdigital electrodes as shown in Figure 2-5 (b) and (c). AFC actuators are extremely flexible and have a high in-plane deflection. The high in-plane actuation is attributed to the use of the fiber's d_{33} (electromechanical strain coefficient) component instead of the d_{31} coefficient (Bent, 1999; Bent and Hagood, 1993, 1997). Similar actuation can be produced using a monolithic ceramic actuator, as shown in Figure 2-5 (b) and (c). Interdigital electrode actuators are currently manufactured by MIDE Technology Corporation (Cambridge, MA) (*www.mide.com*) and ACX Inc.).

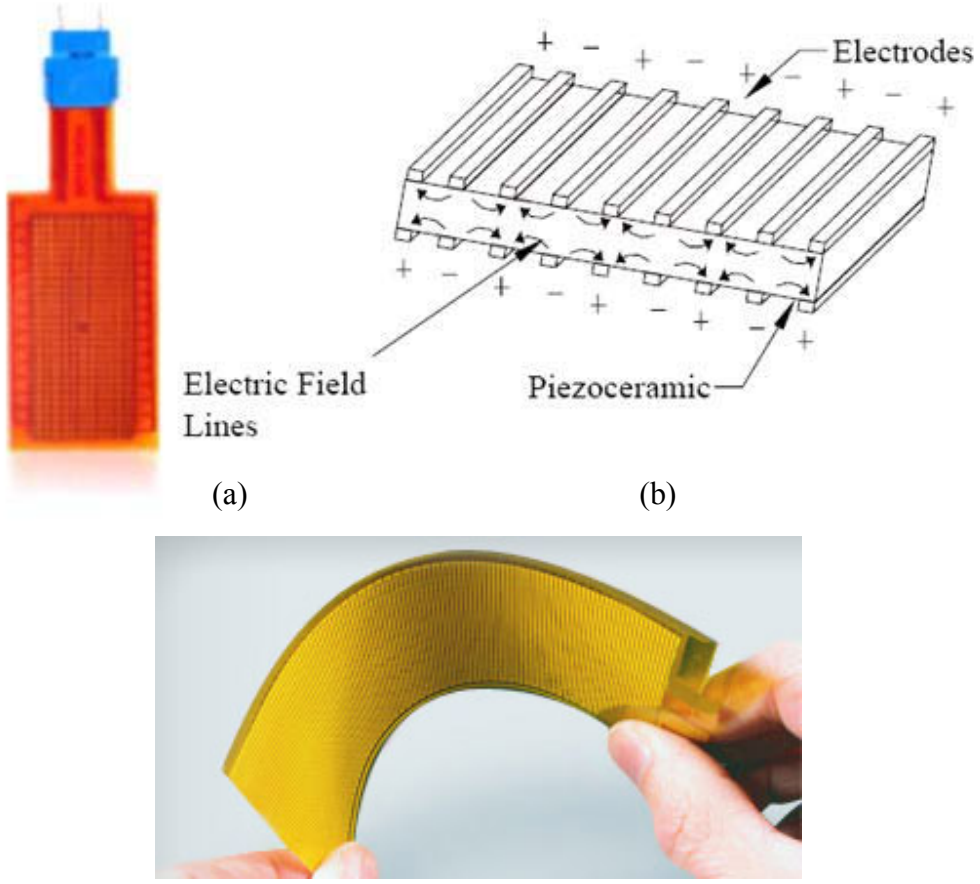

Figure 2-5 (a) Quickpack, (b) Interdigital Electrode Actuator, (c) Active Fiber Composite (Courtesy of MIDE Technology Corporation)

2.3 Flextensional Actuators

Flextensional actuators typically use a piezoceramic stack and an external amplification mechanism to convert the motion generated by the stack to a usable output motion in the transverse direction. Flextensional devices were first developed in the late 1960s ("Flexural-Extensional," 1967) and were used primarily in acoustic applications (Royster, 1970). Flextensional devices have been redesigned for enhanced deflection (Boucher, 1987). One flextensional actuator of this type is called the Moonie (Sugawara *et al*., 1992). This actuator sandwiches a piezoceramic stack between two end caps having shallow cavities. Displacement of the stack flexes the end caps, producing an increased deflection. The displacement output of the

actuator greatly increases with cavity diameter and depth. Multiple Moonie actuators can be stacked in series as shown in Figure 2-6 (Onitsuka *et al.*, 1995; Dogan *et al.*, 1994). Similar in operation to a Moonie actuator is the Cymbal actuator (Dogan *et al.*, 1996).

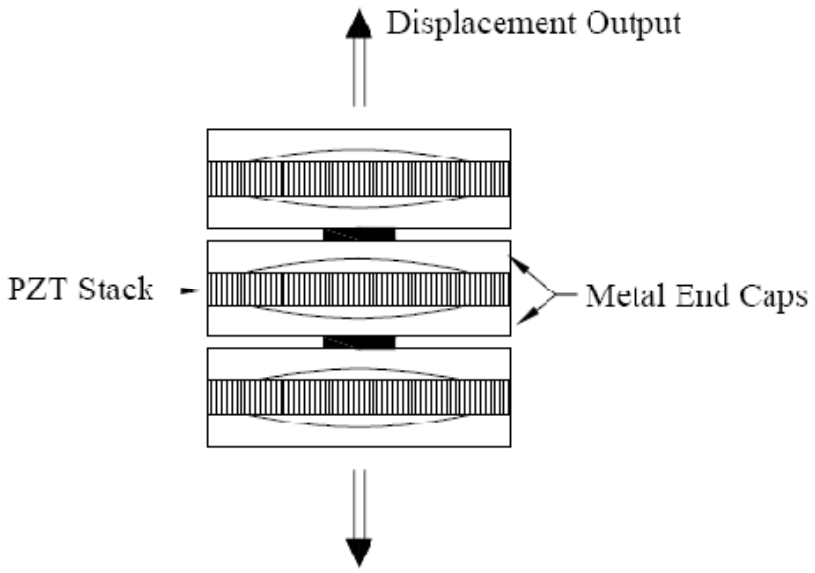

Figure 2-6 Three Moonie actuators stacked in series (Onitsuka *et al.*, 1995)

The Cymbal consists of an external piezoceramic stack with an external mechanism that generates a combination of flexural and rotational motion, as shown in Figure 2-7. The advantage of this actuator over a Moonie is that the displacement can be increased by a factor of two whereas the force output is increased by a factor of five (Dogan *et al*., 1997). In addition, the Cymbal is easier to manufacture than the Moonie. A variety of flextensional actuator designs have been created and are currently being used for proof mass actuation (Dosch *et al*., 1995), micropositioning (Pokines and Garcia, 1998; Le Letty *et al*., 1997), and active/passive vibration control (Bruneau *et al*., 1999). Flextensional actuators are currently being manufactured by Dynamic Structures and Materials LLC (*http://www.dynamicstructures. com*), EDO Corporation (*http://www.edoceramic.com*), and Cedrat (Meylan, France) (*http://www.cedrat.com*).

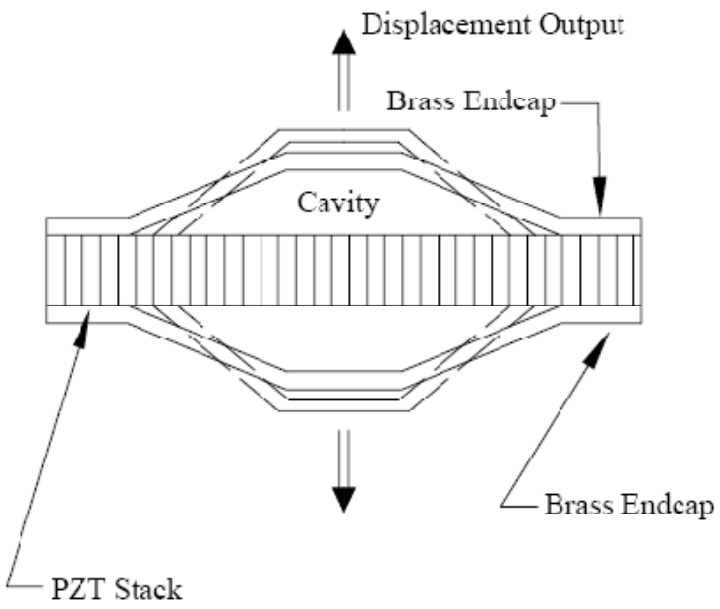

Figure 2-7 Cymbal actuator in original and deformed states (Dogan *et al.*, 1996)

2.4 Piezoelectric Polymers

The existence of piezoelectric polymers was already known since 1924. However, the early known piezoelectric polymers did not receive much attention until the work by Fukada in the fifties and sixties (Fukada and Yasuda, 1964). Fukada and his co—workers discovered that rolled films of polypeptides and numerous other polymers induce surface charges when stressed. A major milestone in this field was recorded with the Kawai's discovery of the strong piezoelectric effect in polyvinylidene fluoride (PVDF or PVF2) in 1969 (Kawai, 1969). Later, other PVDF co—polymers were also reported, including P(VDF-TrFE) and P(VDF-TeFE) (Tasaka and Miyata, 1985) and others.

Ferroelectric polymers are produced by a variety of techniques, where in the case of PVDF the material is mechanically drawn and polarized in order to form a useful transducer material. The drawing techniques include extrusion and stretching and while processing the film material is subjected to a strong electrical polarization field. Without drawing, PVDF shows a

very weak piezoelectric behavior and the higher the molecular orientation the stronger the resultant response of the polarized film.

After polarization, PVDF exhibits considerably stronger piezoelectric response than most other known polymers (Kawai, 1969). The discovery of the piezoelectric and later of the pyroelectric properties of PVDF and the growing applications of this polymer (Tamura *et al.*, 1975) sparked extensive research and development activities. Some of the piezoelectric polymers that are known today include: polyparaxylene, poly-bischloromethyuloxetane (Penton), aromatic polyamides, polysulfone, polyvinyl fluoride, synthetic polypeptide and cyanoethul cellulose (Wang *et al.*, 1988).

2.5 Prestressed Piezoelectric Composites

Two methods that have proven successful in enhancing the actuation and energy harvesting capabilities of elemental piezoelectric material are the inclusion of a substrate and the application of a prestress (Schwartz *et al*., 2000, Schwartz and Narayanan, 2002). Both of these methods are utilized in Reduced And INternally Biased Oxide Wafers or, RAINBOW^{TM}. Introduced in 1997, RAINBOW^{TM} style actuators use a thermal processing documented in the literature to render one side of a lanthanum zirconium titanate (PLZT) ceramic inactive. The resulting inactive portion of the wafer functions much like the metal shim utilized in Unimorph devices. However, due to a mismatch in the coefficients of thermal expansion found in the two sections of the wafer, the device develops internal thermal stresses which result in a domed form. This domed from produces a compressive prestress within the ceramic which enhances piezoelectric performance and protects the ceramic from developing excessive tensile stress during operation (Schwartz *et al*., 2000, Schwartz and Moon, 2001, Hyer and Jilani, 2002).

RAINBOW™ actuators were produced by Aura Ceramics Inc.; however, production of the devices has been discontinued (Niezrecki *et al.*, 2001).

While the development of a compressive thermal stress in RAINBOW™ style actuators offers great improvements over traditional composites, it was not the first actuator to incorporate this feature. THin layer Unimorph DrivER and sensor, or Thunder® actuators were developed at NASA Langley Research Center 1994 and are currently distributed by FACE International. Like RAINBOW™, these devices rely on a mismatch between the thermal properties of the constitutive layers of the composite to produce an out of plane displacement resulting from the internal thermal stresses introduced in the device during processing. Thunder® devices consist of an elastic substrate, piezoelectric ceramic, and often a protective layer of knurled aluminum adhered with a soluble polyimide developed at NASA Langley Research Center (Bryant, 1996). A schematic of a typical Thunder® configuration is shown in Figure 2-8.

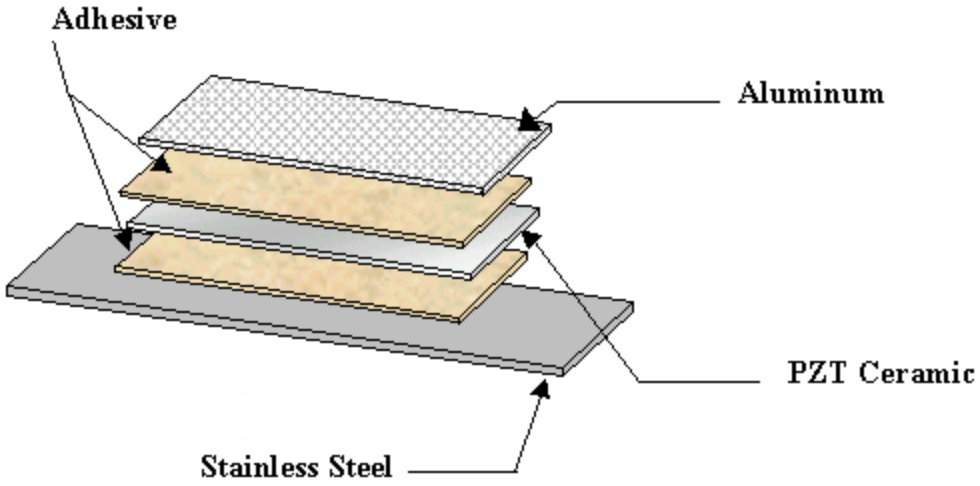

Figure 2-8 Thunder layering sequence

The manufacturing process and performance characteristics of Thunder® have been well documented in the literature by a number of research groups (Mossi, 1998, Schwartz *et al.*, 2000, Bryant, 1996, Fox *et al.*, 1997, Usher and Sim, 2005, Ounaies *et al.*, 2001). Thunder® devices

have been investigated for applications such as structural control, energy harvesting, water propulsion, robotics, flow control, and acoustical control, to name a few. Extensive analysis has been conducted regarding the thermal forces introduced in the device as a result of consolidating constitutive layers with various coefficients of thermal expansion at elevated temperatures (Schwartz *et al*., 2000, Aimmanee and Hyer, 2004). The effect these thermally induced forces have on device performance has been presented (Webber *et al*., 2006, Mossi *et al*., 2006). While these devices have been found to produce displacements on the order of several millimeters and forces greater than 4.5 N, there are inherent limitations on optimization of the design due to the coupling that exists between geometrical parameters such as layer thickness and post-manufacturing form, e.g. radius of curvature (Mossi *et al*., 2005, Balakrishnan and Nierecki, 2002).

Given the wealth of information compiled on prestressed actuators following the introduction of Thunder®, a natural progression of the technology was sure to lead to refinements of concept. One such follow up to the Thunder® concept comes from a research group at Konkuk University in Seoul South Korea. Utilizing the same concepts on which Thunder® is based; researchers at Konkuk have developed a device which replaces the metallic and soluble polyimide layers found in the Thunder® device with prepreg fiber composites. The resulting device is referred to as a LIght weight Piezoelectric Composite Actuator or, LIPCA. Several configurations of LIPCA have been presented, and a detailed account of these devices, and their manufacturing process, has been presented in the literature (Mossi *et al*., 2005). A schematic of a typical LIPCA device is shown in Figure 2-9.

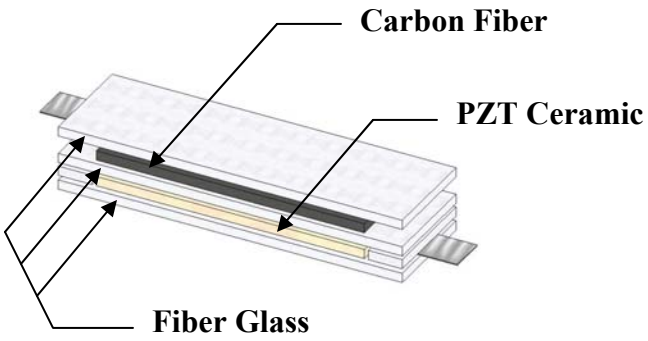

Figure 2-9 Lipca layering sequence

By utilizing fiber composites rather than a metal substrate, LIPCA devices are lighter and capable of producing greater displacements than Thunder® devices (Mossi *et al.*, 2005). Work by Aimmanee has shown that, by utilizing various fiber materials and layering configurations, the neutral axis in LIPCA can be shifted (Aimmanee, 2004). This quality allows the device to be optimized for use in various applications.

While LIPCA has been investigated by many of the same research groups that have evaluated Thunder® devices, LIPCA still lacks the commercial manufacturing methods that have been developed for the Thunder® devices. Other deterrents to widespread use arise from the materials used in LIPCA device. When compared with the stainless steel elements typically used to construct Thunder® devices, the carbon and Kevlar fibers found in typical LIPCA devices result in a dramatic increase in material cost.

2.6 Chapter Summary

This chapter discusses the discovery and emergence of piezoelectric materials and their applications. An overview of their operating mechanism and constitutive equations is given. Piezoelectric materials have been studied extensively for their properties as sensors and actuators. The chapter talks about the most commonly used piezos such as PZT, $BaTiO_3$.

Methods are discussed which can enhance the properties of piezoelectric ceramics such as PZT. Amplification schemes such as stacks, benders, flextensional actuators and prestressed composites are discussed. Widely studied piezoelectric polymer PVDF is also discussed.

3 Objectives and Approach

The goal of this dissertation is to increase fuel efficiency. Fuel efficiency is increased by integrating energy harvesting into an active flow control device using prestressed piezoelectric composites. Prestressed piezoelectric composites are used due to their robust nature and enhanced properties. The challenge on using these devices include, weight, fragility, power consumption, and size. These challenges are addressed as described in the objectives and the approach to fulfill these objectives is also discussed.

3.1 Objectives

The objectives of this work can be better understood by looking at Figure 3-1. The flow control device of choice is the synthetic jet actuator. Synthetic jet actuators consist of a cavity with an oscillating diaphragm and an orifice. As the diaphragm oscillates, a jet is formed through the orifice introducing small amounts of energy into the flow field to achieve non-local changes in the flow field with large performance gains.

Synthetic jet actuators increase the efficiency and simplify fluid related systems by reducing the number of moving parts and making it lighter. This could lead to reduced fuel consumption, increased payload, noise reduction and shorter takeoff and landing. In spite of all

the advantages, using synthetic jet actuators usually adds complexity in design and increases manufacturing and operating cost, which prevents their use.

Several parameters have been identified for this study that could affect operation of the synthetic jet. The main component of the actuator is the oscillating diaphragm. Selecting a suitable diaphragm can overcome of the problems faced in designing efficient synthetic jet actuators. The weight of the actuator can be reduced by using piezoelectric materials as active diaphragms. Piezoelectric materials are light weight and have a very fast response time making them suitable for synthetic jet actuators.

Piezoelectric ceramics exhibit micro scale displacements and have low force properties. Although using piezoelectric ceramics will lead to a decrease in weight of the actuator their properties need to be amplified to generate synthetic jets with large velocities. This is achieved by prestressing piezoelectric ceramics into composites such that they have a dome shape in the resting position. Due to the shape the ceramic is under a constant stress enhancing the displacement and force of the device. With amplified properties the prestressed diaphragm will exhibit enhanced momentum injection leading to larger peak velocities.

Another advantage of using prestressed composites is the increase in durability of the diaphragm. Due to the sandwich design of prestressed composites the ceramic is more robust and thus simpler to integrate into applications. They also exhibit larger force and have enhanced piezoelectric coefficients.

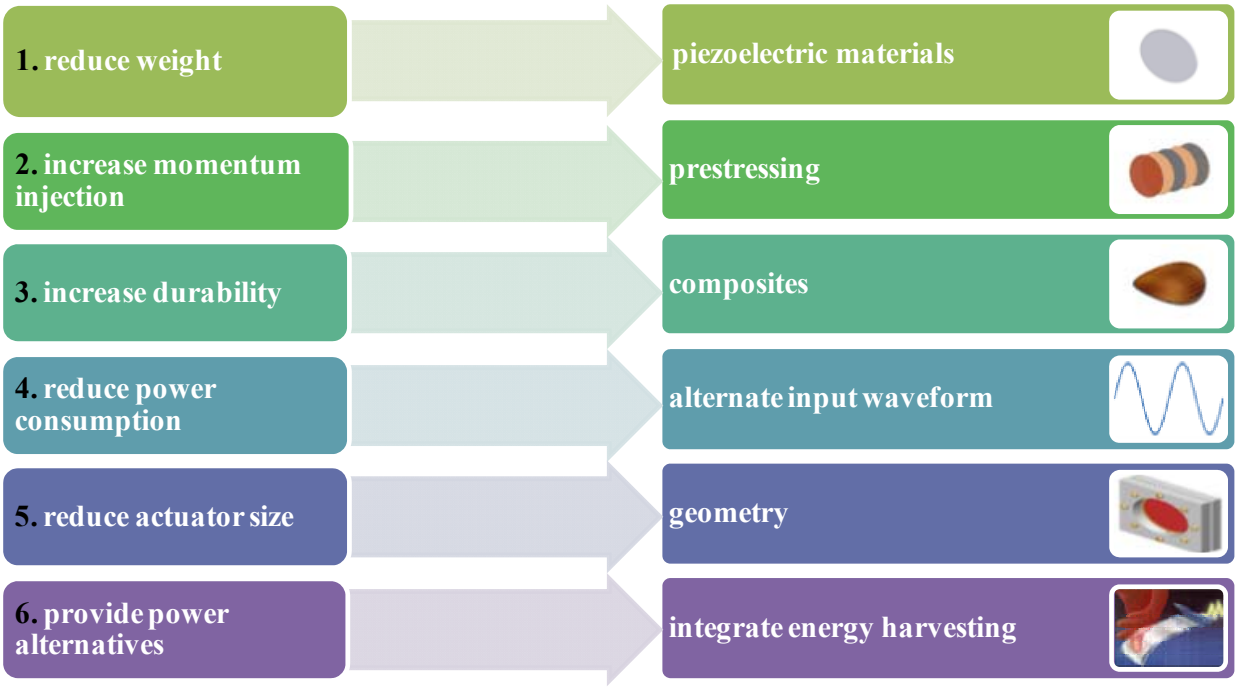

Figure 3-1 Dissertation objectives

The piezoelectric diaphragms is driven using electrical power. Typically bench top power supplies are poorly suited for driving piezoelectric actuators. Due to their high impedance, complex circuitry is required to provide adequate power for the desired functionality. This adds weight to the system thus reducing efficiency. A possible solution to this problem could be the use of alternate driving signals. Signal such as the sawtooth waveform, require considerable smaller electronics to create, compared to traditional sine waves. In the past, researchers have used sinusoid driving signals at very high frequencies leading to actuator damage. With alternate signals the same performance can be achieved at low frequencies thus requiring lower power consumption and increasing the life time of the actuator.

Another objective of this study is to study the effects of actuator geometry on the synthetic jet performance. Parameters such as cavity height and orifice diameter are studied. By

optimizing these parameters the geometry can be designed such that the actuator size and weight is reduced.

State of the art composites are selected for the study; Bimorph, Lipca, RFD and a prestressed piezoelectric metal composite. They are different in construction and have varying properties which are applied in synthetic jet actuators. Peak velocity magnitude is identified as the response variable. Large velocity values are required to have significant effects on the drag and SJA efficiency.

The final objective of the study is to provide a power alternative by harvesting energy from synthetic jet actuators. With the recent surge of micro scale devices, piezoelectric power generation can provide a convenient alternative to traditional power sources used to operate certain types of sensors and actuators, telemetry, and MEMS devices. Piezoelectric materials can transform ambient vibrations into electrical energy. Since vibrations exist in most dynamic systems and with the larger goal of integrating energy harvesting in synthetic jet actuators piezoelectric energy harvesting from vibrations is studied. Vibrations are inducted into the diaphragm by pulsing pressure inside a cavity similar to the operation of a synthetic jet. The parameters that affect energy generation such as environmental temperature, pressure magnitude, driving frequency and circuitry parameters such as frequency are studied. The diaphragms selected for the study are a piezoelectric polymer PVDF and a prestressed metal composite. Using design of experiments theory, response surface models are developed that help in determining the optimal levels of the tested parameters.

Energy is harvested from synthetic jet actuators by integrating a piezoelectric sensor into the synthetic jet actuator design. While the synthetic jet actuator is operational, vibration energy

is generated which is usually wasted. Piezoelectric sensors can be used to generate energy from the vibrations by using the direct piezoelectric effect. Two piezoelectric sensors are tested, polyvinylidene fluoride (PVDF) and a square shaped prestressed composite. PVDF is a piezoelectric polymer with the higher electromechanical conversion coefficient, making it an excellent sensor. However, the energy produced by piezoelectric materials is in many cases far too small to directly power an electrical device. Therefore, the research into energy harvesting is focused on methods of accumulating the energy until a sufficient amount is present, allowing the intended device to be powered. Since piezoelectric sensors are easy to integrate into devices, such methods could lead to self–powered systems that can operate in remote locations where regular maintenance is not feasible.

3.2 Approach

This dissertation uses a coupled approach which combines experiments and design of experiments theory. The block diagram in Figure 3-2 summarizes the approach used in the dissertation. Design of experiments theory is used in planning the experiments. Statistical design of experiments refers to the process of planning the experiment such that valid and objective conclusions can be drawn. An experimental study, which involves many parameters is time consuming and expensive. Using design of experiments, conclusions can be drawn by conducting a smaller number of experiments, saving resources and time.

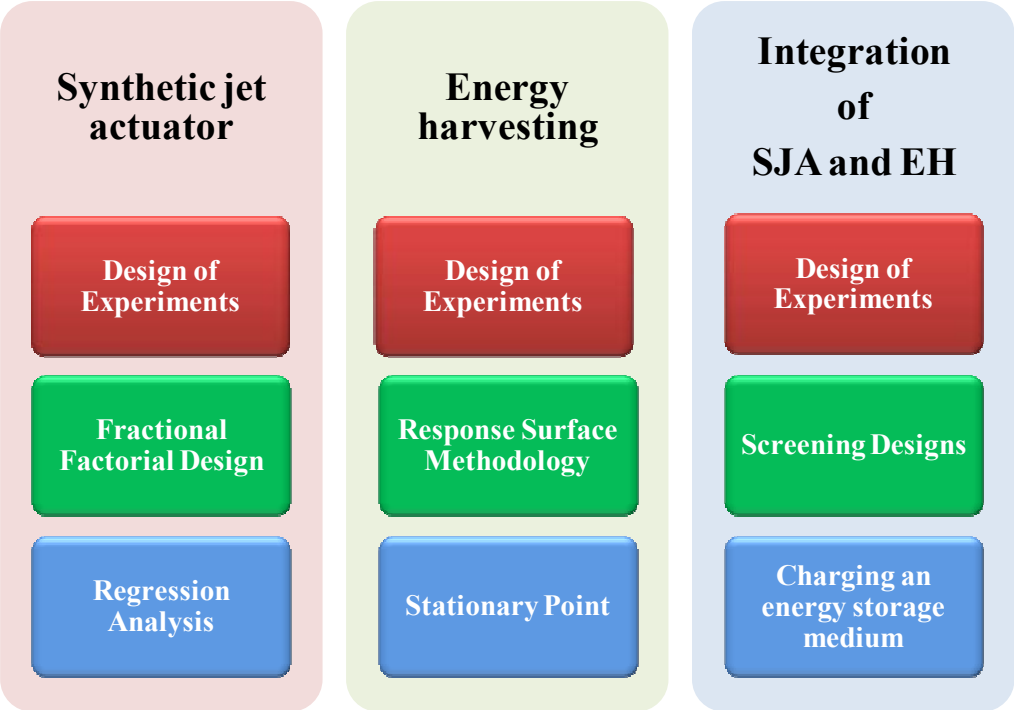

Figure 3-2 Approach of study

A literature review of synthetic jet actuator studies has shown that computational fluid dynamic (CFD) tools are not sufficient to develop a generalized model for the complex active flow control mechanism. It is suggested by many researchers that a coupling with experiments is necessary. Design of experiments methods help in identifying factors which have a significant effect on the desired response. Once these factors are identified, further experiments can be conducted focusing on the selected factors while ignoring the remaining factors. Furthermore, using these methods optimization of the significant parameters can be conducted. Models can be developed which give the optimal levels of the factors to achieve a desired response.

Within design of experiments, several theories exist and are used appropriately in the dissertation. For the synthetic jet actuator study a fractional factorial design is used to develop an experimental plan for the selected factors. Similarly for the integration part of the dissertation

when sensing and actuation are integrated another fractional factorial design is adopted for the sensor parameters. These designs reduce the number of experiments required to make conclusions by half. Data obtained from the design is analyzed using regression analysis to identify the important factors.

In the energy harvesting study, response surface methodology is used to optimize the power generation. A statistical model is developed relating the factors and a using this model the response surface is mapped for power generation. The stagnation point of the surface is the optimal response of the system. The factor levels at this point are the optimized parameters.

The following chapters describe the design of experiments theory in detail. The design tables used in each part of the dissertation are shown and the steps involved in the design and analysis process are discussed.

4 Design of Experiments Theory

Statistical design of experiments refers to the process of efficiently planning experiments which lead to valid and objective conclusions. The data obtained from design of experiments is analyzed using statistical tools. Depending on the size, nature of the dataset and the desired response, the type of experimental design to be used is determined. When the problem involves data that are subject to experimental errors, statistical methods are the only objective approach to analysis.

Figure 4-1 shows a typical process which is affected by a number of factors indicated by x_i.. The effect of varying the factors is seen on the desired response of the process. Using design of experiments an experimental plan can be developed such that

- a small number of experiments are conducted to determine the significance of each factor (screening designs)
- a model is developed relating the factors to the response (factorial designs)
- individual factors are optimized to maximize the response (response surface methodology)

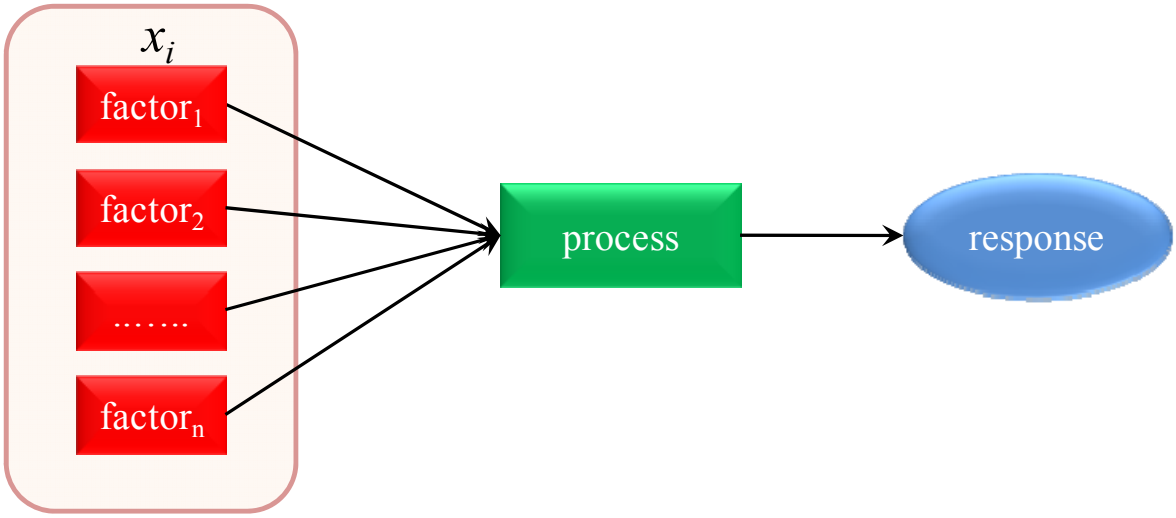

Figure 4-1 A system of experiments

4.1 Screening Designs and Factorial Designs

In an experiment, one or more variables or factors are deliberately changed in order to observe the effect the changes have on one or more response variables. Experimental data are used to derive an empirical (approximation) model linking the outputs and inputs. These empirical models generally contain first and second-order terms. This is called screening experiments. Screening designs are used to identify the few significant factors from a list of many potential ones. In short, screening designs are economical experimental plans that focus on determining the relative significance of many main effects (Montgomery, 2005).

Factorial designs are formed following screening designs to economically investigate cause-and-effect relationships of significance in a given experimental setting and to develop a relationship between the variables. By using a full factorial design, each complete trial or

replication of the experiment for all possible combinations of the levels of the factors are investigated. The effect of a factor is defined to be the change in response produced by a change in the level of the factor. This is called a main effect as it refers to the primary factors or interest in the experiment. For some experiments, it is seen that the difference in response between the levels of one factor is not the same at all levels of the other factors. When this occurs, there is an interaction between the factors.

As the number of factors in a 2^k factorial design increases, the number of runs required for a complete replicate of the design rapidly outgrows the resources of most experimenters. If the experimenter can reasonably assume that certain high-order interactions are negligible, information on the main effects and low-order interactions may be obtained by running only a fraction of the complete factorial experiment. Since we are able to choose fractions of a full design, the whole experimental research process is made more economical and efficient. These fractional factorial designs are among the most widely used types of designs for product and process design and for process improvement.

Screening experiments are usually performed in the early stages of a project when many of the factors initially considered may have little or no effect on the response. The factors identified as important are then investigated more thoroughly in subsequent experiments. It is common to begin with several discrete or continuous input factors that can be controlled, that is, varied when desired by the experimenter and one or more measured output response variables which always are assumed to be continuous.

A typical design of experiments table is shown in Table 4-1. The table represents a full factorial, two level design with three factors, x_1, x_2, x_3 and the response is indicated by the

variable y. Since this is a full factorial design the total number of runs is $2^3 = 8$. Each row represents an experiment with the factors set at the indicated levels. Each factor is assigned a low and high level indicated by '1' and '-1' respectively. To reduce error the levels have to be far apart in the lower and upper halves of the factor operational range. Column one in the table shows the patterns of each run with a '+' for '1' or 'high' level and a '-' for '-1' or 'low' level.

Table 4-1 A typical 2^3 full factorial design table

Pattern	x_1	x_2	x_3	y
+−−	1	-1	-1	$y1$
+−−	1	-1	-1	y_2
−+−	-1	1	-1	y_3
−+−	-1	1	-1	y_4
−−+	-1	-1	1	y_7
−−+	-1	-1	1	y_8
+++	1	1	1	y_9
+++	1	1	1	y_{10}

The most common empirical models fit to the experimental data take either a linear form or a quadratic form. A linear model will contain the main effect terms and interaction effect terms. The model is of the form shown in Equation 4-1.

$$Y = \mu + \sum_{i=0}^{n} \beta_i \cdot X_i + \sum_{\substack{i=0 \\ k=0}}^{n} \beta_{ik} \cdot X_i X_k + \sum_{\substack{i=0 \\ k=0 \\ z=0}}^{n} \beta_{ikz} \cdot X_i X_k X_z + \cdots + \varepsilon$$

Equation 4-1

$i = 1,2,\ldots,n$; $k = 1,2,\ldots,n$; $z = 1,2,\ldots,n$; n is the number of factors

Here, Y is the response for given levels of the main effects X_i and the X_iX_k term is included to account for a possible interaction effect between X_i and X_k. Depending on the number of factors considered, the interaction term could contain more than two factors. The constant μ represents the sample mean of the response; β's are parameters whose values are determined represent the coefficients for the considered factors and ε is the experimental error. Statistical results are used to assess the validity and influence of the particular effect on the response.

4.2 Response Surface Methodology

The Response Surface Methodology (RSM) is a collection of mathematical and statistical techniques useful for analysis and modeling. A response of interest is influenced by several variables and the objective of this methodology is to optimize this response. Given a response variable Y and n continuous factors, x_1, x_2,…, x_n, the main purpose of Response Surface Methodology (RSM), is to find the combination of factor levels to achieve the optimal response.

The typical RSM procedure is described here as in many books such as Montgomery (Montgomery, 2005, Box and Graper, 1987). For computational convenience, the natural variables or factors are usually converted to coded or design variables, X_1, X_2, …, X_n,

standardized so that the design center is at the point 0.

The first step in RSM is to find a suitable approximation for the true functional relationship between *Y* and the set of independent variables as indicated by Equation 4-2.

$$y = f(x_1, x_2, x_3, ...)$$

Equation 4-2

The relation is usually approximated by a polynomial of first or second degree in the confined region *R*. When a first order model does not yield a model the order is increased in an iterative process. A second order polynomial is used in particular when the interest is focused on the location of the stationary point or the point of inflection of the response function. The method of least squares is used to estimate the parameters in the approximating polynomials. With the aim of finding the maximum stationary point of the desired response surface function, a second order polynomial model of the form shown in Equation 4-3 is used in the analysis. Models are developed using computer softwares such as *JMP IN 7* and *SigmaStat 3.1*.

$$y = \beta_0 + \sum_{i=1}^{n} \beta_i x_i + \sum_{i=1}^{n} \beta_{ii} x_i^2 + \sum_{i<j} \sum \beta_{ij} x_i x_j + \varepsilon$$

Equation 4-3

$i = 1, 2, \ldots, n$ and $j = 1, 2, \ldots, n$

Here y is the response variable, $x_1, x_2, \ldots, x_n$ are the dependent factors, n is the number of factors, β_0 is the intercept term and β_i are the regression coefficients. ε is the random error which is assumed to be distributed as a normal distribution with zero mean and unknown variance. As the fitted surface is an adequate approximation of the true response surface, analysis of the fitted surface is approximately equivalent to analysis of the actual system. The surface represented by

Equation 4-3 is called the response surface. Response Surface plots and contour plots play a very important role in the study of the response surface. By generating these plots using computer software for response surface analysis, the shape of the surface can be characterized. Also, location of the optimum can be determined with reasonable precision. The dome shape of the response surface is result of the second order model fit. The optimal point is the peak of the dome; it can also be called the stationary point, saddle point or the maximum point.

A stationary point represents the point of maximum response, to find the optimal levels of the independent variable for the predicted response. To obtain a mathematical solution for the location of the stationary point the fitted second order model is compactly written as shown in Equation 4-4.

$$y = \beta_0 + x^T b + x^T Bx + \varepsilon$$

Equation 4-4

Where x is a n x 1 vector of factor levels, b is a n x 1 vector of regression coefficients β_i and B is a n x n symmetric matrix of regression coefficients with ith diagonal element equal to β_{ii} and the (ij)th off-diagonal element equal to $(1/2)\beta_{ij}$. For the stationary point to exist the partial derivative $\delta y/\delta x=0$. Thus from the fitted model, the estimated stationary point is computed using Equation 4-5 where x_s is a n x 1 matrix which gives the optimal levels for the factors.

$$x_s = -\frac{1}{2} B^{-1} b$$

Equation 4-5

By substituting Equation 4-5 into Equation 4-4 the predicted response at the stationary point can be found as shown in Equation 4-6.

$$y_s = \beta_0 + \frac{1}{2} x_s^T b$$

Equation 4-6

In this manner optimal parameters can be precisely identified.

5 Materials and Method

5.1 Synthetic Jet Actuator Study

From the point of view of actuator design, it is of interest to know how the geometry of the actuator can be improved so as to improve the performance of the jet. Synthetic jet flows are produced by the advection and interactions of trains of discrete vortical structures. However, a unique feature of synthetic jets is that they are formed entirely from the working fluid of the flow system in which they are deployed and, thus, can transfer linear momentum to the flow system without net mass injection across the flow boundary. The fluid that is necessary to synthesize the jet is typically supplied by intermittent suction through the same flow orifice between consecutive ejections. The impulse that is imparted to each vortex has to be large enough to overcome the influence of forces associated with the (reversed) suction flow such that time-periodic roll-up and subsequent advection of discrete vortices occurs. Thus, the key performance parameter selected for this study which measures the strength of a synthetic jet may include the jet peak velocity. Optimizing the jet peak velocity in turn enhances the strength of the vortex rollup. Therefore a study of the behavior of synthetic jets in quiescent conditions is undertaken. A parametric study of synthetic jet actuators is conducted based on the electrical parameters of the piezoelectric diaphragm and the geometric parameters of the synthetic jet cavity.

5.1.1 Experimental Setup

The synthetic jet velocity is characterized by studying several geometry and diaphragm properties. Geometric properties include the orifice diameter, D_o and cavity height, C_H, which controls the cavity volume. Oscillating diaphragm properties include the driving frequency, f, and displacement, δ_c. Another parameter of interest is the type of AC signal used to drive the actuator. This variable is also included in the study and is indicated by F_z. The standard driving signal used for synthetic jet actuators is sinusoidal. Synthetic jet actuators driven with a sinusoidal signal are operated at the resonant frequency of the diaphragm. At these high frequencies the diaphragm is prone to failure and power consumption is higher at these frequencies. Thus using an alternative, sawtooth signal could provide a solution to these problems leading to an improvement in performance. The synthetic jet study is conducted using four types of piezoelectric composites, Bimorph, Prestressed Metal Composite, Lipca and RFD. These diaphragms vary in their construction and properties. Each of these diaphragms is described in the following section.

5.1.2 Materials

5.1.2.1 Bimorph

Bimorphs consist of two thin ceramic sheets bonded together with their poling directions opposed and normal to the interface as shown in Figure 5-1 (a). When an electric field is applied to a bimorph, one of the plates expands while the other contracts. This mechanism creates a bending mode that mimics piston like displacement. Bimorphs are capable of generating large bending displacements of several hundred micrometers on center or edge, but the response time (1ms) and the generative force (1.0N) are low (Dogan *et al*., 2001). In the current study, the Bimorph used is model *T216-A4NO-573X* manufactured by Piezoelectric Systems Inc. It consists

of two nickel electroded PZT 5A discs with diameters of 63.5mm and a total thickness of 0.41mm. They have a capacitance of 130nF at 1kHz and have been shown to produce displacements up to 0.3 mm at low frequencies (Mossi *et al.*, 2005*a*). A schematic of the disc alignment along with the final shape is shown in Figure 5-1 *a* and *b*.

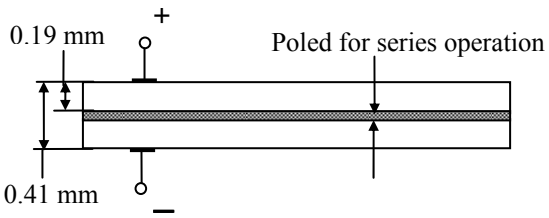

(a)

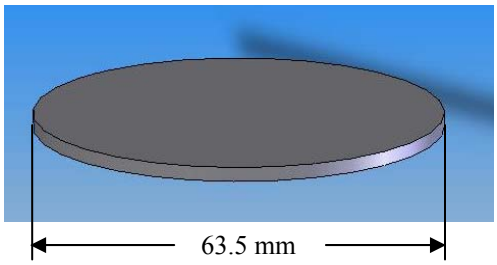

(b)

Figure 5-1 Bimorph (a) layer arrangement, (b) final shape

5.1.2.2 Prestressed PZT Metal Composite Actuator

The Prestressed PZT Metal Composite is similar in construction and properties to Thunder. THin layer composite UNimorph ferroelectric DrivER and Sensor (Thunder®) was developed at NASA Langley Research Center. It is an actuator that exploits the coefficients of thermal expansion mismatch between materials (Dausch and Wise 1998, Haertling 1994 *a* and *b*, Mossi *et al.,* 1998, Wise 1998). The significant advantage that Thunder® actuators have over other Unimorph benders is their extremely rugged construction. This allows them to be more

readily used in commercial applications, such as synthetic jets (Smith *et al.*, 1999). The mechanical advantage of the Thunder® design is due to the increased flexibility of the device and the radial expansion created by the pairing of preselected thermally mismatched materials (Hellbaum *et al.*, 1997). The Prestressed PZT Metal Composites used in the current study consist of an integrated sandwich of layers similar to Thunder® transducers. Prestressed metal layers make up the top and bottom and the piezoelectric layer is sandwich between them with a hot melt adhesive forming a thin bondline between the ceramic and metal layers. A schematic of the metal composite is shown in Figure 5-2.

Prestressed PZT Metal Composite® actuators can be fabricated in virtually any size and thickness (Mossi *et al.*, 1998). A circular device manufactured by Face International Inc. is used in the present study. It is composed of three main layers, with two additional being the thin bondline; a top chemically etched copper layer 0.0254mm thick, a middle piezoelectric layer of thickness 0.254mm, and a bottom 0.254mm thick layer of stainless steel. The copper and ceramic layers have diameters of 63.5mm and the steel layer, 68.58mm leaving a circular tab along the edge of 2.54mm. This additional tab is included in the design to facilitate clamping of the device. The layers are laminated with a high temperature polyimide adhesive (Bryant, 1996) through a layering high—temperature bonding process (Mossi *et al.*, 1998). The resulting actuator is saddle shaped with a capacitance of 110nF as shown in Figure 5-2. The piezoelectric ceramic used in both these diaphragms is a soft PZT type 5A. The composite exhibits its highest displacement at the center of the dome, and displacement decreases drastically towards the edge of the actuator (Mossi and Bryant, 2004a). The maximum center displacement measured is approximately 0.06mm with a sawtooth signal at 5Hz (Mossi *et al.*, 2005*a*).

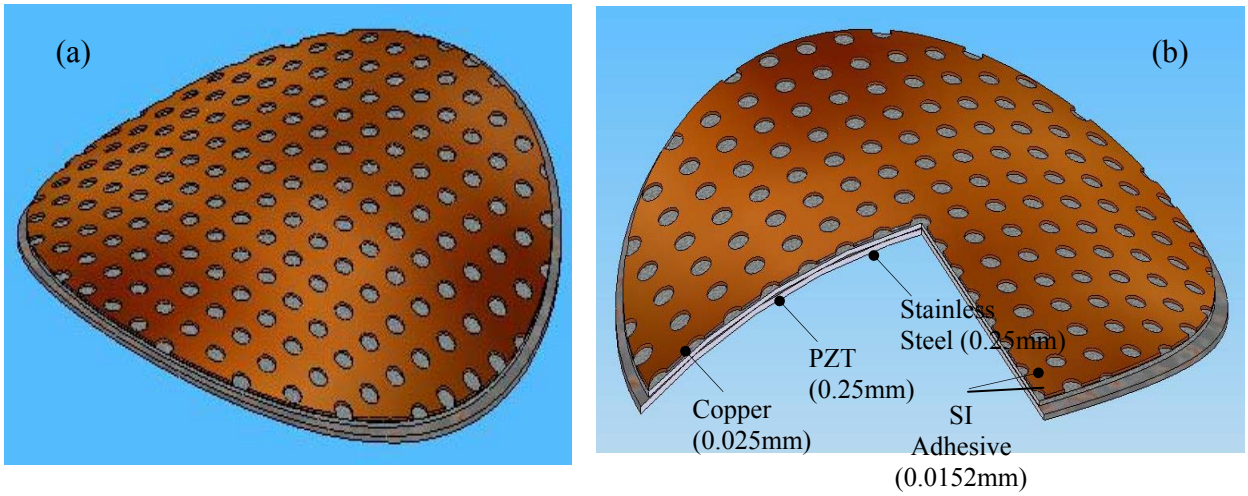

Figure 5-2 Metal Composite (a) final shape (b) layer arrangement (T_t *refers to the active layer thickness only*)

5.1.2.3 Lipca

Lightweight Piezo-composite Curved Actuator (LIPCA) is a powerful actuator that can be used for adaptive structure applications. LIPCA is manufactured by co-curing layers at an elevated temperature: glass/epoxy layer, unidirectional carbon/epoxy layer, and ceramic layer (Park *et al.*, 2001, Yoon *et al.*, 2002, Yoon *et al.*, 2003 *a* and *b*). Differences in coefficient of thermal expansion (CTE) of the layers result in the LIPCA's post cure curvature. Based on the arrangement of the layers, the curvature and the displacement vary (Yoon *et al.*, 2003*a*). The LIPCA shown in Figure 5-3(a) is made by Konkuk University, South Korea. It has a high CTE top layer of glass/epoxy with diameter 66.0mm and thickness 0.09 mm, a near zero CTE unidirectional carbon/epoxy layer with 66.0 X 1.0mm dimensions, a layer of PZT 5A ceramic 50.0 X 0.18mm, and another glass/epoxy layer with the same dimensions in the bottom as shown by Figure 5-3(b).

The circular LIPCA is not as curved as the circular prestressed metal composite but produces higher center displacement of approximately 0.075mm with a sawtooth driving signal

at 25Hz (Mane 2005). The difference in curvature is due to the fact that the processing temperature used for the LIPCA is much lower (Yoon *et al.*, 2003*b*). The capacitance is approximately the same as the metal composite, 100nF.

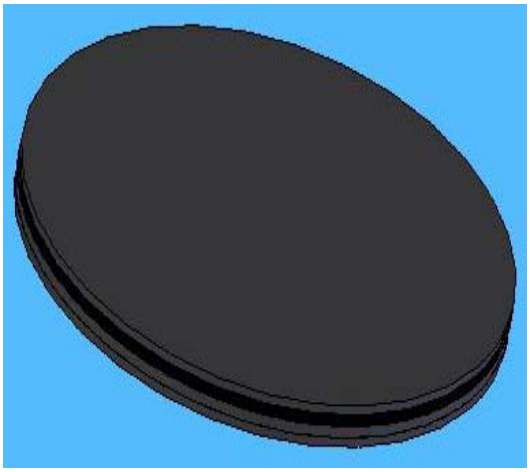

(a)

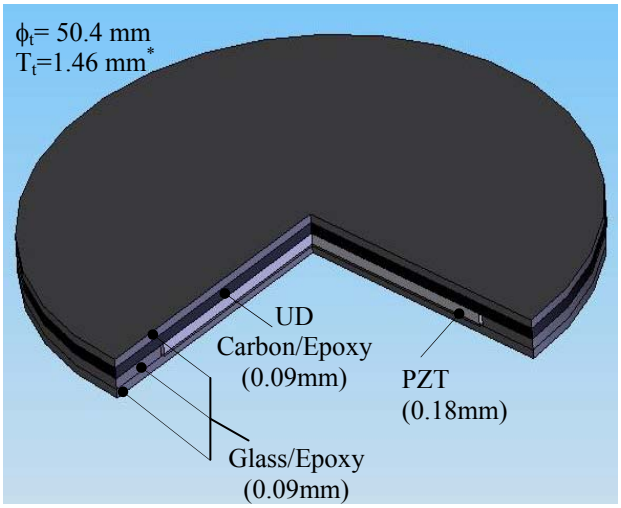

(b)

Figure 5-3 Lipca (a) final shape, (b) layer arrangement
(*T_t refers to the active layer thickness only*)

5.1.2.4 Radial Field Diaphragm (RFD)

The Radial Field Diaphragm (RFD) was developed by NASA Langley Research Center. It is comprised of a thin circular piezoelectric ceramic disk sandwiched between two polyimide "*PI*" dielectric films with either copper-etched dual intercirculating spiral or circular interdigitated ring electrodes (Bryant *et al*., 2004). For the spiraled electrode pattern, positive and negative electrodes spiral inward to the center of the disk in a serpentine manner called Inter—Circulating Electrodes (ICE). As seen in Figure 5-4 this electrode pattern induces an electric field into the piezo ceramic that extends out radially from the center of the wafer (Bryant *et al.*, 2004). The dielectric film serves as the electrode carrier and insulator. Because of its radial electric field, the ICE—RFD exhibit out of plane movement, when electrically stimulated, and does not transmit any substantial mechanical strain beyond the boundary of the ceramic element. This behavior is distinct from all other bender type actuators. The RFD in the current study has a diameter of 63.5mm and is based in the PZT 5A ceramic. It has a very low capacitance of approximately 4nF at 1kHz and can produce displacements up to 0.4mm (Mossi *et al.*, 2005*a*).

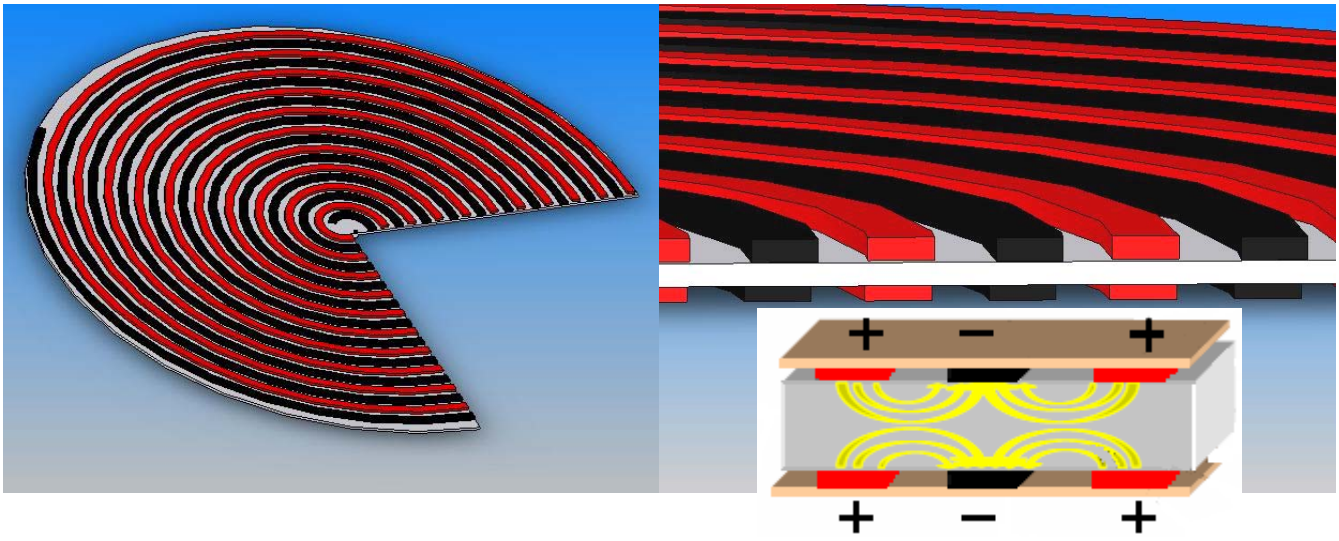

Figure 5-4 RFD Inter-Circulating Electrodes (ICE) (Bryant *et al.* 2004)

5.1.3 Synthetic Jet Cavity

The synthetic jet cavity is constructed of two 88mm x 88mm Plexiglas™ pieces. The plastic pieces have a 60.5mm circular aperture in the center. A 5mm wide and 1mm deep groove is machined along the perimeter of the aperture. The actuators are placed between the two grooves reinforced with neoprene rubber on both sides to provide both a cushion and a seal as shown in Figure 5-5(a). The plastic pieces are sealed together along with a 1.6mm thick covering plate that provides an axisymmetric orifice in the center. Seven 4 mm screws with washers are used to clamp the cavity, while one screw hole is left empty to serve as a port for the actuator electrical leads and additional attachments to the cavity. Equal torque of 424Nmm is applied on each screw using a torque screwdriver to ensure constant pressure along the perimeter of the actuator. Once the assembled cavity is in place, the sealed synthetic jet cavity is mounted on a height gauge as shown in Figure 5-5(b).

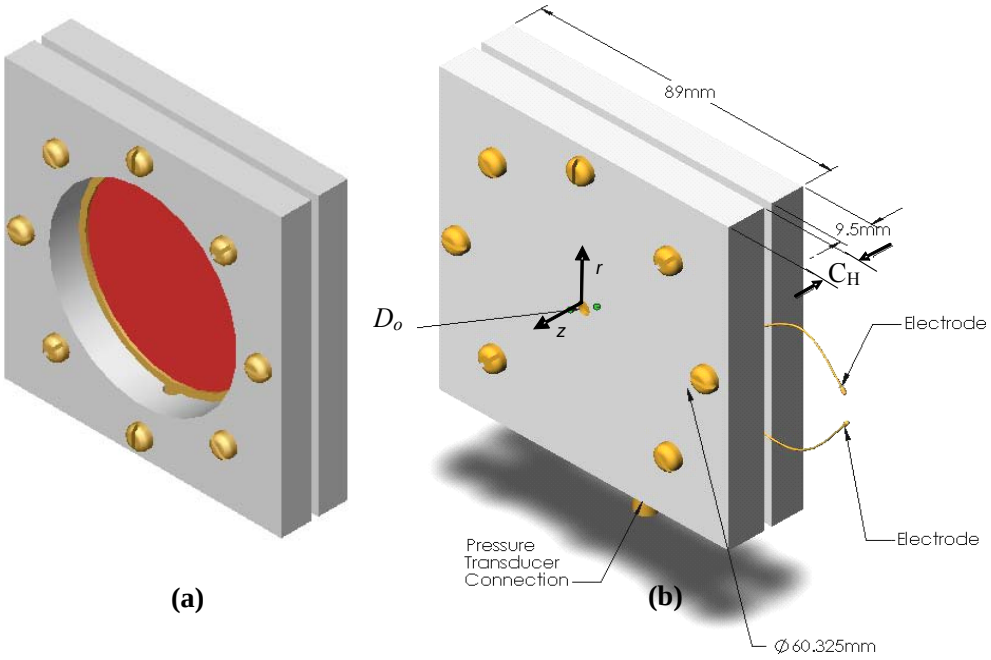

Figure 5-5 Synthetic Jet Cavity (a) clamped actuator, (b) final assembly

The cavity setup utilized allows variations in cavity height and orifice dimensions. The two cavities have overall dimensions of 88.0 x 88.0 x 19.1mm and 88.0 x 88.0 x 11.0mm, which correspond to cavity heights of 9.55mm and 5.5mm respectively. This cavity height, C_H, is measured from the diaphragm to the orifice exit. Two cover plates with circular orifices have approximate diameters, D_o, of 2.0mm (small) and 3.67 mm(large) are used. The cavity configurations are shown in Table 5-1.

Table 5-1 Cavity Parameters

		C_H (mm)	
		5.50	9.55
D_o (mm)	2.00	*cavity I*	*cavity II*
	3.67	*cavity III*	*cavity IV*

5.1.4 Instrumentation and Measurements

The driving signal is applied at high voltages and varying frequencies for each device. This signal is applied using a signal generator, a Hewlett Packard model *HP33120*, connected to an amplifier, TREK model *PZD700*. The velocity and voltage signals are monitored and recorded using an oscilloscope, LeCroy model *350L*, and a National Instruments data acquisition system as shown in Figure 5-6. The amplitude and frequency of the applied signal were kept below their allowable maximums in order to prevent electrical and mechanical failure of the diaphragms. Specifically, the field for each diaphragm was kept at a maximum of 750V/mm. Two driving signals, sine and sawtooth, are used with all experiments.

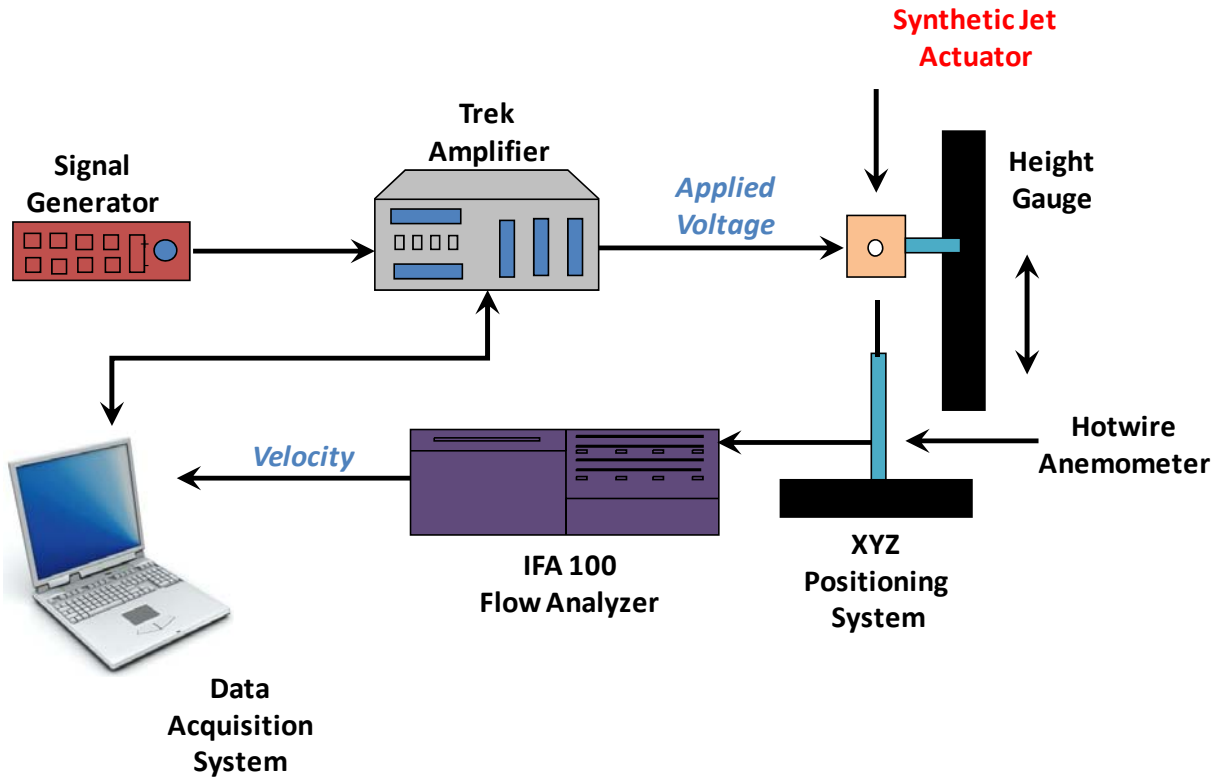

Figure 5-6 Synthetic Jet Actuator Experimental Setup

Velocity is measured in quiescent air at a fixed distance of 1mm perpendicular to the orifice exit (*z* direction) for each actuator. All velocity measurements are performed using a hotwire anemometer. It is a single cylinder sensor used for one dimensional flow measurements. It has a diameter of 4 μm and a length of 3.2 mm. With the help of the IFA 100 flow analyzer the hotwire anemometer measures the flow in terms of voltage. Using a calibration this voltage is converted to velocity. The Mathcad program used for the velocity conversion is given in APPENDIX A.

To obtain profiles along the length of the orifice, velocity is measured at various locations along the orifice. To study the effects of frequency on the jet, the velocity is measured at several frequencies up to 100Hz. These experiments are conducted on four synthetic jet cavity configurations. The differences in the cavities are the cavity height and the orifice diameter.

5.1.5 Experimental Plan

The jet peak velocity in quiescent flow is a function of these four variables and also a function of the driving signal as shown in Equation 5-1, where U_{peak} is the peak jet velocity.

$$U_{peak} = g(F_z, D_o, C_H, f, \delta_c)$$

Equation 5-1

Screening designs are used to identify the few significant factors from a list of many potential ones. Alternatively, a design is referred to as a screening design if its primary purpose is to identify significant main effects, rather than interaction effects, the latter being assumed an order of magnitude less important. Screening designs are economical experimental plans that focus on determining the relative significance of many main effects. This can be achieved using factorial designs (Montgomery, 2005). In the current study, five factors were considered for each actuator, driving waveform, voltage, frequency, cavity height, and orifice size. The peak velocity of the jet is used as the response variable. The diaphragms used in the study are Bimorph, Prestressed Metal Composite, Lipca and RFD. Each of these diaphragms is described in detail in the following section.

Screening experiments are usually performed in the early stages of a project when many of the factors initially considered may have little or no effect on the response. The factors identified as important are then investigated more thoroughly in subsequent experiments. It is common to begin with several discrete or continuous input factors that can be controlled, that is, varied when desired by the experimenter and one or more measured output response variables which always are assumed to be continuous. In the current study, five factors were considered for each actuator, driving waveform, voltage, frequency, cavity height, and orifice size. The peak velocity of the jet is used as the response variable. A two level design is chosen due to the large

number of factors involved. In a two factor experimental design each factor has two levels. These levels "low" and "high" are denoted by "–" and "+" respectively. Experiments are conducted to measure the responses at the selected factor levels. The screening experimental plan is shown in the flowing sections. The factor levels are selected based on the properties of each diaphragm used in the study.

The factor distribution showing the levels and the types of each factor is given in Table 4-1. A full factorial design requires $2^5 = 32$ runs without center points or repetitions. Instead, a fractional factorial design, 2^{5-1}, was utilized requiring a total of *16* observations. The resolution of this design is *V*, which indicates that no main effects are confounded with any *2*-factor interactions or *3*-factor interactions; main effects are confounded with four-factor interactions.

The most common models utilized to fit experimental data take either a linear form or a quadratic form. In this case only linear models are considered and interactions are neglected. In order to consider higher order interactions, replications and a higher resolution experimental design is needed. The empirical model is of the form shown in Equation 5-2.

$$Y = \mu + \sum_{i=0}^{n} \beta_i \cdot X_i + \cdots + \varepsilon$$

Equation 5-2

where $i=1, 2... n$, n is the number of factors. Here, Y is the response for given levels of the main effects X_i. The constant μ represents the sample mean of the response; β's are parameters whose values are determined represent the coefficients for the considered factors and ε is the experimental error. Statistical results are used to assess the validity and influence of the particular effect on the response.

Factor distributions for the devices are shown in Table 5-2. As stated earlier all factors have same levels except the voltage which varies due to the properties of the devices. However the electric field is approximately 750V/mm for each device. Electric field is determined by dividing the magnitude of the applied voltage by the thickness of the piezoelectric layer.

Table 5-2 Factor Distribution

Factors	Symbols	Low Level (-1)	High Level (+1)	Units	Types
Driving Waveform	F_z	Sawtooth (-1)	Sine (+1)	None	Discrete
		125 (-1)	150 (+1)	V_{pp} (Bimorph)	
Applied Voltage	E	250 (-1)	400 (+1)	V_{pp} (Thunder)	Continuous
		200 (-1)	350 (+1)	V_{pp} (Lipca)	
Frequency	f	25 (-1)	50 (+1)	Hz	Continuous
Orifice Size	D_o	2 (-1)	3.67 (+1)	mm	Continuous
Cavity Height	C_H	5.5 (-1)	9.5 (+1)	mm	Continuous

The experiments table is made based on the factorial design theory. A full factorial design requires $2^5 = 32$ runs without center points or repetitions. Instead, a fractional factorial design, 2^{5-1}, was utilized requiring a total of 16 observations. The factors, shown in Table 5-2, have a resolution V which indicates that no main effects are confounded with any *2*-factor interactions or 3-factor interactions; main effects are confounded with four-factor interactions. A *Fractional Factorial Design Matrix* (design of experiments table) with *5* factors and *16* runs is shown in Table 5-3.

Table 5-3 Fractional Factorial Experimental Design

Run No.	Factors (X_i)					Response$_j$
j	F_z	E	f	D_o	C_H	Y_j
1	-1	-1	-1	-1	+1	y_1
2	1	-1	-1	-1	-1	y_2
3	-1	+1	-1	-1	-1	y_3
4	+1	+1	-1	-1	+1	y_4
5	-1	-1	1	-1	-1	y_5
6	+1	-1	+1	-1	+1	y_6
7	-1	+1	+1	-1	+1	y_7
8	+1	+1	+1	-1	-1	y_8
9	-1	-1	-1	+1	-1	y_9
10	+1	-1	-1	+1	+1	y_{10}
11	-1	+1	-1	+1	+1	y_{11}
12	+1	+1	-1	+1	-1	y_{12}
13	-1	-1	+1	+1	+1	y_{13}
14	+1	-1	+1	+1	-1	y_{14}
15	-1	+1	+1	+1	-1	y_{15}
16	+1	+1	+1	+1	+1	y_{16}

5.2 Energy Harvesting Study

Energy harvesting is a process in which energy which would otherwise be wasted is stored and then used to power a system. The use of harvested energy could extend the operational life of devices traditionally powered by batteries. This is particularly advantageous in systems with limited accessibility such as biomedical implants and structures with embedded micro and wireless sensors. It is feasible that such devices would have the ability to generate their own power from the ambient environment. This can either prolong the life of an existing battery or eliminate the battery. Energy can be harvested using piezoelectric materials from vibrations and heat. In this study the energy harvesting system is optimized using response surface models. Based on a literature review physical and environmental parameters of

temperature (*T*), pressure (*P*), frequency (*f*) and circuitry parameters of and resistance (*R*) are used in the study. The properties of piezoelectric materials are known to change when subjected to thermal and physical strains (Mukherjee *et al.*, 2001, Sherrit *et al.*, 1996 and 1999). In a study by Mossi et al the stiffness of a piezoelectric composite was shown to be temperature dependent (Mossi *et al.*, 2005*b*). Changing composite stiffness affects the piezoelectric coefficients and in turn could affect the energy harvesting properties of the device. Also some of the possible applications where piezoelectrically harvested energy could be used operate in extreme environmental conditions making the effect of factors like temperature critical for implementation. Statistical methods are employed to explore this parameter. Using Response Surface Methodology modeling the point of inflection or the stationary point that optimizes power generation is calculated. The factor levels at the stationary point indicate the optimal parameter values.

The sensor used in this study was a piezoelectric prestressed metal composite similar to Thunder diaphragms, but circular in shape with a perforated copper layer to reduce stiffness. In a preliminary study with two other piezoelectric materials PZT and PMN-PT, the power generated by the metal composite was studied (Green *et al.*, 2005). The metal composite generated comparatively higher magnitudes of power. Thus the metal composite was selected for the vibration energy harvesting study. They were also chosen for their rugged construction and high performance when used as an actuator in synthetic jet actuators. The composition of the metal composite is described in the synthetic jet characterization chapter. It has an active PZT-5A layer sandwiched between a top and bottom layer of dissimilar metals bonded with a high temperature polyimide adhesive (*SI*).

5.2.1 Experimental Setup

The diaphragm was dynamically pressure loaded using an air compressor such that the resultant vibrations produce a voltage. The device was clamped along its edges in a circular cavity which was pressurized using air on the copper side of the device while the steel side is left open to the ambient air. Figure 5-7 a and b show a schematic of the energy harvesting cavity with connection for pressurization. A block diagram of the complete experimental setup is shown in Figure 5-8. Clean dry air (CDA) was sent to a model 42K75 regulator/filter combination manufactured by *SpeedAire* with a 0-827.4kPa (0 - 120psi) pressure gauge. The regulated pressures used during this study are 138kPa (20psi), 206.85kPa 30psi), 275.8kPa (40psi), and 344.75kPa (50psi). During initial testing it was found that the limits of the flow meter were reached at a dynamic pressure of 50psi (344.75kPa) thus this value is set as the experimental limit. The air is then sent through an *Omega FMA 1609A* flow meter which measured mass and volumetric flow rate, temperature, and absolute pressure of the air entering the pressure chamber. A three-way electric air valve routes air into the pressurized cavity. Using an adjustable timer manufactured by National Controls Corporation model *TMM-0999M-461*, the valve is switched on and off at desired frequencies. The frequencies (2.5Hz, 3.25Hz, and 5Hz) used in this study were determined by the dynamic limitations of the 3-way valve. The pressure housing was enclosed in an environmental chamber from Sun Systems Model *EC1.3W* capable of heating up to 350ºC. While in the chamber, the diaphragm can be heated to desired temperatures.

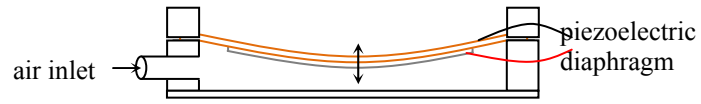

(a)

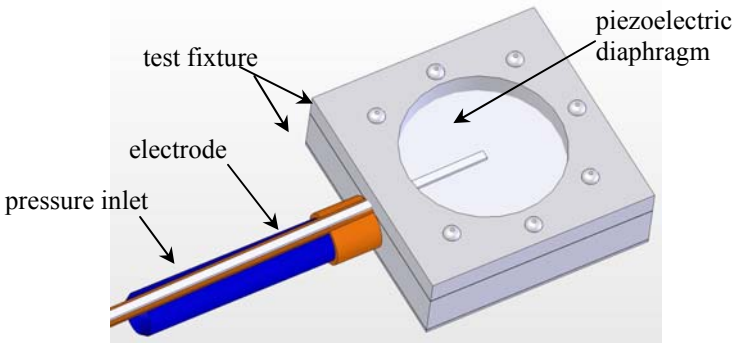

(b)

Figure 5-7 Pressurized cavity design of synthetic jet actuator
(a) cutaway schematic (b) assembly

An additional aspect of the energy harvesting process is signal conditioning, as the electrical charge generated by a piezoelectric generator is usually insufficient to power a commercial device. By using circuitry the generated signal is processed such that a usable voltage is obtained which can be applied to the device directly or used to charge a battery (Sodano *et al.*, 2005). The type of circuitry used to harvest the energy from a piezoelectric transducer is determined by the desired output to the load which most often needs to be rectified, filtered, and regulated (Ottoman, 2002 and 2003).

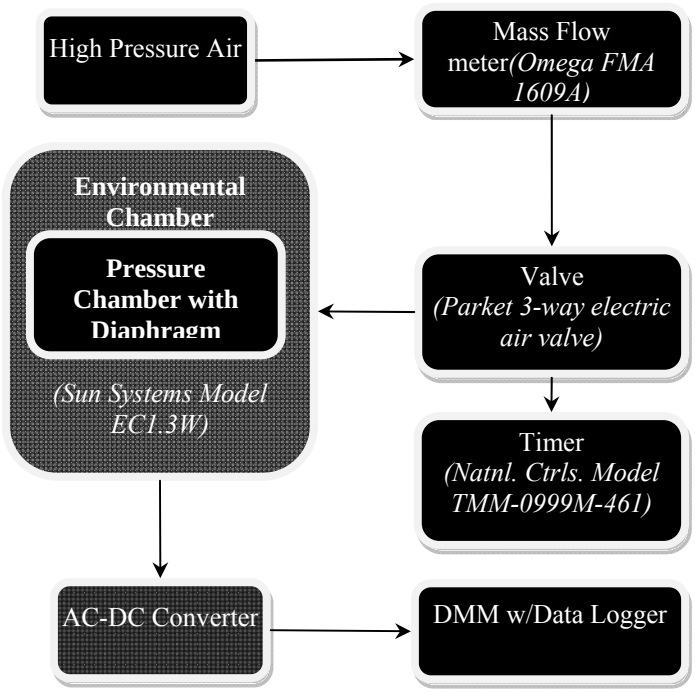

Figure 5-8 Vibration Energy Harvesting Experimental Setup

5.2.2 Energy Harvesting Circuit

The passive rectifier circuit was chosen as the energy harvesting circuit because of its simplicity and lack of active components which consume power. A schematic of the circuit is shown in Figure 5-9. The first stage of the circuit which is in parallel with the diaphragm is a *RB114* Full Wave Bridge Rectifier. A Full Wave Bridge Rectifier converts AC to DC using a system of four diodes arranged such that the polarity in is the same as the polarity out. Each time a signal travels through the diode network; there is a voltage drop that depends on the characteristics of the diode. When attached to a load, marked at R in Figure 5-9, the negative part of an input sine wave is removed and the frequency is increased by a factor of two. The output DC voltage deviates from a constant DC voltage by a parameter called a ripple voltage. When a

capacitor is added, as represented by C in Figure 5-9, ripples are smoothed and transients are filtered.

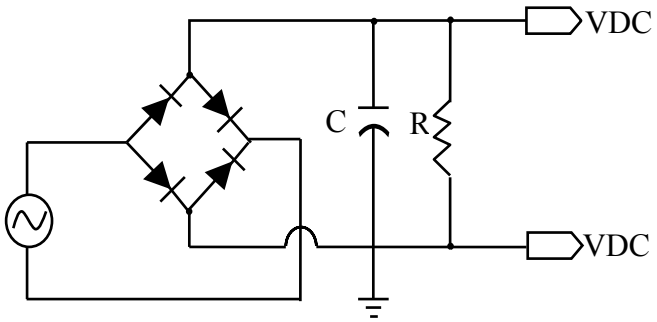

Figure 5-9 Energy Harvesting Circuit

In the first set of experiments the peak to peak AC voltages are measured without using the energy harvesting circuit. The experiments are conducted at four pressures, 138kPa, 206.85kPa, 275.80kPa, 344.75kPa; three frequencies, 2.5Hz, 3.25Hz, 5Hz; and temperatures ranging from -60^{o}C to 100^{o}C at 10^{o}C intervals. The data is acquired using Tektronix *TDS2024* oscilloscope and data acquisition software. The experimental parameters are shown in Table 5-4.

Table 5-4 Energy harvesting experimental parameters

Factor	***Parameters***
Frequency (*f*)	2.5Hz 3.25Hz 5.0Hz
Pressure (*P*)	138kPa (20.0psi) 206.85kPa (30.0psi) 275.8kPa (40.0psi) 344.75kPa (50.0psi)
Temperature (*T*)	- 60°C to 100°C
Resistance (*R*)	470kΩ 1MΩ 2MΩ

The second set of experiments was conducted using the energy harvesting AC—DC converter circuit. A standard 4.7μF capacitor is used while three loads of 470kΩ, 1MΩ and 2MΩ. The output DC voltage of the energy harvesting circuit was measured over a time interval to observe the charging and discharging behavior of the circuit. The DC measurement experiments are also conducted under the same physical conditions used in the first set of experiments using a DMM data logger device. Table 5-5 lists a table of experiments conducted during the study. Data from the experiments is used in developing response surface models.

Table 5-5 Table of experiments

	Pressure	*Frequency*	*Temperature*	*Load Resistance*	*Output*
Experiment 1	X	X	X		ACV
Experiment 2 (measured over time)	X	X	X	X	DCV

X : indicates that the factor was varied during the experiment

5.2.3 Response Surface Model

Using response surface methodology the factors selected for this study are optimized. The typical RSM procedure is described here as in many books such as Montgomery (Montgomery 2005, Box and Graper 1987). For computational convenience, the natural variables or factors are usually converted to coded or design variables, X_1, X_2, …, X_n, standardized so that the design center is at the point 0. In the current design there are three levels are designated as shown in Table 5.3, *-1*, *0*, *1*, in a confined region *R*.

The first step in RSM is to find a suitable approximation for the true functional relationship between *Y* and the set of independent variables as indicated by Equation 5-3.

$$y = F(R, P, T, f)$$

Equation 5-3

The relation will be approximated by a polynomial of first or second degree in the confined region *R* shown at Equation 5-4. The surface represented by this fit is the response surface for the experiment. The stagnation point of the surface is the optimized response and the factor levels will be the optimized system.

$$y = \beta_0 + \sum_{i=1}^{n} \beta_i x_i + \sum_{i=1}^{n} \beta_{ii} x_i^2 + \sum_{i<j} \sum \beta_{ij} x_i x_j + \varepsilon$$

Equation 5-4

$i = 1, 2, \ldots, n$ and $j = 1, 2, \ldots, n$

Here y is the response variable, $x_1, x_2, \ldots, x_n$ are the dependent factors, n is the number of factors, β_0 is the intercept term and β_i are the regression coefficients. ε is the random error which is assumed to be distributed as a normal distribution with zero mean and unknown variance.

Table 5-6 Enegy harvesting coded factor levels

Levels	***R(Ω)***	***P(kPa)***	***T(^{o}C)***	***f(Hz)***
-1	470000	138	-40	2.5
0	1000000	275	20	3.25
1	2000000	350	80	5

5.3 Integration of Energy Harvesting in Synthetic Jet Actuators Study

In this part of the dissertation sensing and actuation is integrated into the synthetic jet actuator. Integration of sensors in the synthetic jet actuator will allow the harvesting of ambient energy from vibrations generated while the jet is on. This is achieved through the integration of piezoelectric sensors in the jet design. The design has weight limitations such that the synthetic jet operation is not affected. Sensors have to be carefully selected to achieve this purpose effectively. The entire sensor selection, integration and experimental plan is described in the following sections.

5.3.1 Piezoelectric Sensors Used in Integrating Actuation and Sensing

The piezoelectric sensors selected for this study were polyvinylidene fluoride (PVDF) and a square shaped prestressed PZT metal composite sensor with an aluminum substrate layer. The sensors are required to a high piezoelectric response to efficiently harvest energy from the system. In addition they need to be lightweight, reliable and easily integrate able.

5.3.1.1 Polyvinylidene Fluoride (PVDF)

PVDF is a piezoelectric polymer with high mechanical properties and strength. Due to its chemical inertness it is capable of performing in harsh chemical environments. They have higher piezoelectric properties in comparison with other polymers. They are available in a variety of different sizes and thicknesses. A PVDF film as a transducer can be cut to very small size and are very affordable at around 50 cents per sensor.

As they are very flexible they can be easily integrated into structures. When a stress is applied they generate voltages due to the movement of electrons within the PVDF film, and

voltage can vary with different stresses. PVDF film can be bonded to a variety of substrates including itself and metals with bond strengths ranging from 50-800 psi.

In the current study PVDF films of varying thickness from 28μm to 110μm purchased from Measurement Specialties are tested. PVDF is encapsulated in lamination layers of Mylar for insulation from electrical noise. Mylar was selected for lamination as it is readily available, it has good bond strength, ease of use and it is very cheap. A picture of a laminated PVDF sample is shown in Figure 5-10. The film has layers of silver electrodes sputtered on either surface. Flat nickel wires are attached on the surfaces to measure through the thickness of the sample. The sensor integration into a synthetic jet actuator is described in the following section.

Figure 5-10 PVDF sensor incased in Mylar packaging

5.3.1.2 Prestressed PZT Metal Composite Sensor

The Prestressed PZT Metal Composite sensor is similar in construction to the prestressed metal diaphragm used in synthetic jet actuators. The sensor selected for the integration process is square shaped and has a different layering arrangement. The bottom layer is stainless steel (39 x 45 x 0.2 mm), the middle layer PZT ceramic (38 x 38 x 0.254 mm), and aluminum (37.5 x 37.5 x 0.1 mm) the top layer; LaRC™-SI adhesive is applied between the layers. The entire assembly is placed into an autoclave for processing. A mismatch in coefficients of thermal expansion cause the metal and ceramic layers to contract at different rates, and they begin to work against one another, putting the ceramic in a prestressed compression at room temperature and resulting in a

characteristic curvature of the finished product. A schematic of the end shape is shown in Figure 5-11. Due to the shape of the sensor integration in a synthetic jet actuator cavity is difficult. However this sensor was selected due to large power generation potential of prestressed composites.

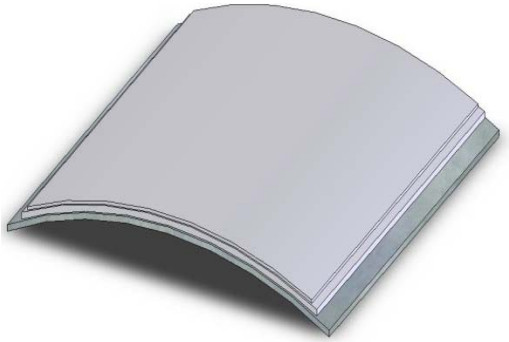

Figure 5-11 Square shaped Prestressed PZT Metal Composite Sensor

5.3.2 Sensor Integration and Experimental Setup

To integrate energy harvesting into synthetic jet actuators, piezoelectric sensors are incorporated into the design of the actuator such that vibration energy can be harvested. The synthetic jet actuator formed with a circular prestressed metal diaphragm is used in this study. The sensors are attached to the middle of the steel surface of the actuator diaphragm using a pressure sensitive FT 1122 HLP insulating adhesive as shown in Figure 5-12. As stated earlier the steel surface faces the orifice in the synthetic jet cavity. Thus sensor is exposed to the pressure changes in the cavity. As the synthetic jet diaphragm oscillates, the attached sensor also oscillates inducing vibrations. The vibrations and pressure changes in the actuator create stresses on the sensor exciting voltage generation by the sensor.

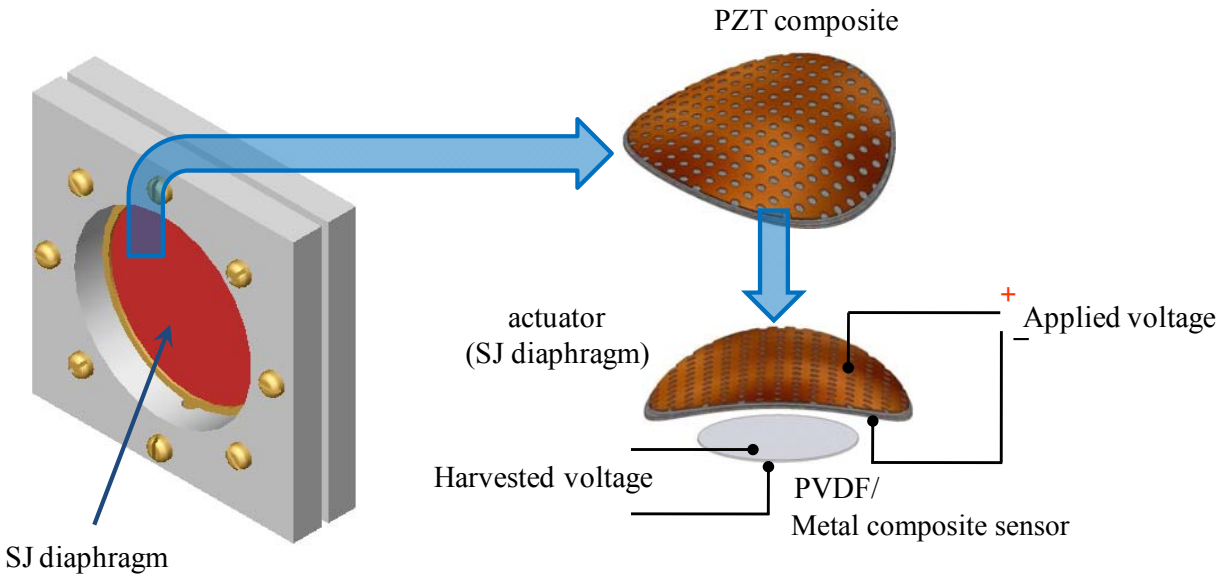

Figure 5-12 Sensor integration into a synthetic jet actuator

As the PVDF sensor is very flexible it is uniformly attached to the surface of the diaphragm. However, in case of metal composite sensor the unique shape does not allow for the complete surface area to be attached. The edges of the sensor are free and the arrangement is like a balanced seesaw with the sensor attached along a central band. As shown in Figure 5-13. This type of an arrangement is inconsistent as perfect bonding is difficult to achieve.

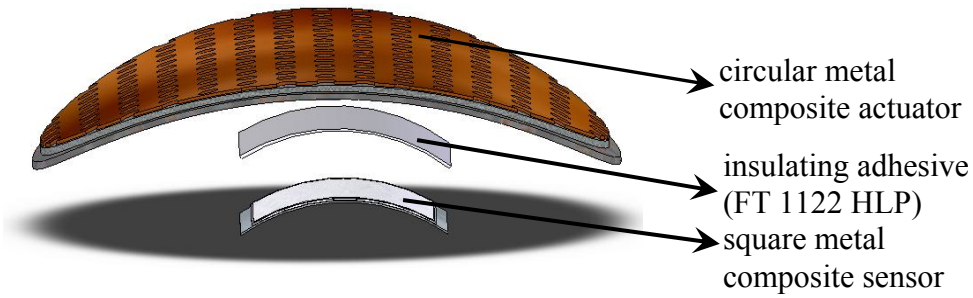

Figure 5-13 Metal composite sensor attached to synthetic jet diaphragm

For testing the integrated design the harvested sensor voltage is measured simultaneously along with the synthetic jet velocity. The experimental setup used in testing is shown in Figure 5-14. The same synthetic jet cavity design is used here as well. The jet velocity is measured using a

hotwire anemometer. The sensor voltage is monitored using a data logger which records one reading per second. The applied voltage marked in schematic is the voltage used to drive the synthetic jet diaphragm and the sensor voltage is the voltage generated by the piezoelectric velocity sensor. Tests are conducted on various diaphragm driving voltages and frequencies. AC voltages are measured for both the sensors. The energy harvesting circuit shown in Figure 5-9 is used in the AC to DC voltage conversion. The effects on sensor generated voltages can be quantified by comparing the effects on peak velocities. The experimental plan is given in the following section.

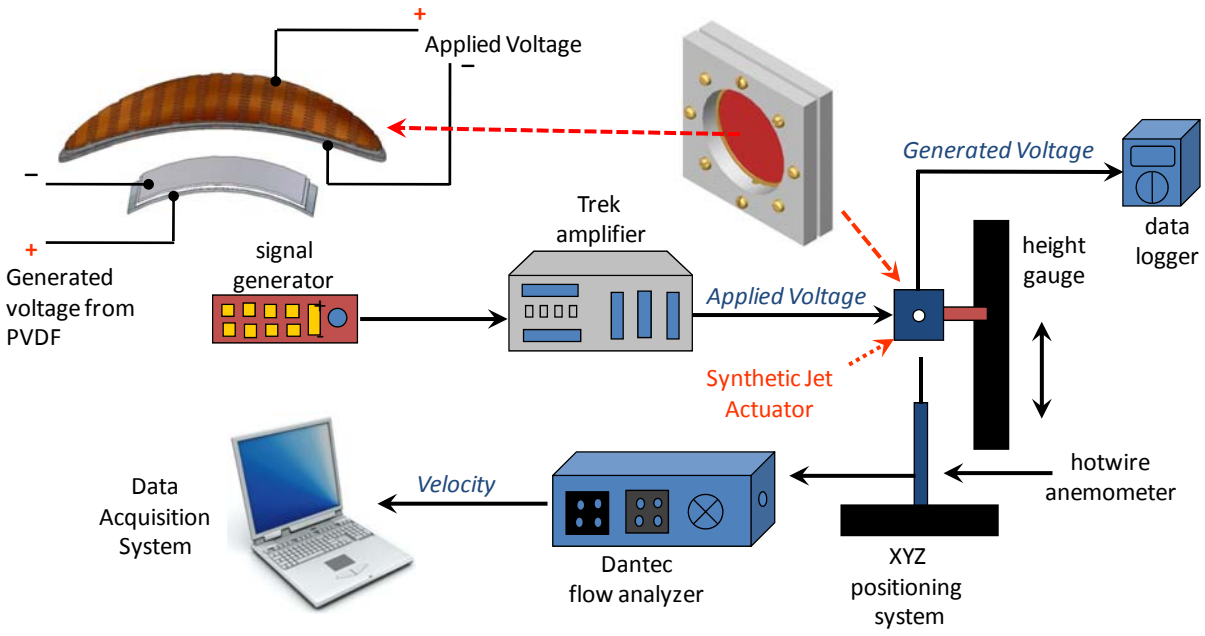

Figure 5-14 Experimental setup for testing the integration of sensing and actuation in Synthetic Jet Actuators

5.3.3 Experimental Plan

A design of experiments study is conducted using fractional factorial analysis. A two level fractional factorial analysis with one replication is conducted. The voltage generated by the sensor is related to the area and thickness of the sample these two factors are selected for the

study. Also, as energy is being harvested from vibrations the shape could have an effect on the output as each shapes has different vibration modes. Except for shape the other two factors are continuous with shape being a discrete factor. The dimensions of the shapes are selected in such a manner that the net area of the sample is constant for each shape. The DOE study is conducted only with the PVDF sensor as the composite sensor attachment mechanism is inconsistent thus affecting the results. The experimental design also includes center points to increase the accuracy of the model. Table 5-7 shows the factors and each assigned level. '-1' indicates the low level, '0' is the center point and '+1' is the high level as shown in the table. In case of the shape factor the variable is

Including center points and replications the number of runs required to conduct the analysis is 10. Table 5-8 shows the design table for the experiment. The response variable of DC power (P) is selected for the analysis. A simple linear regression fit is conducted as shown by Equation 5-5.

$$P = \mu + \beta_1 \cdot s + \beta_2 \cdot a + \beta_3 \cdot t + \varepsilon$$

Equation 5-5

Table 5-7 Factor levels

	Factor Levels		
factors	-1	0	1
shape (s)	square	rectangle	circle
areas (a)	$5cm^2$	$10cm^2$	$15cm^2$
thickness (t)	28µm	50µm	110µm

Table 5-8 2^{3-1} Fractional Factorial Design

Pattern	*s*	*a*	*t*	*P*
+−−	1	-1	-1	P_1
+−−	1	-1	-1	P_2
−+−	-1	1	-1	P_3
−+−	-1	1	-1	P_4
000	0	0	0	P_5
000	0	0	0	P_6
−−+	-1	-1	1	P_7
−−+	-1	-1	1	P_8
+++	1	1	1	P_9
+++	1	1	1	P_{10}

5.3.4 Energy Storage Mechanism

The AC harvested energy is converted to DC using a simple rectifier circuit shown in Figure 5-9. A mechanism is required to store the harvested energy into a medium. This requires efficient energy transfer to the medium. A commercially available energy harvesting module EH301 EPAD® (Figure 5-15) from Advanced Linear Devices is tested with the aim of increasing efficiency. These modules are designed to continuously and actively operate to capture, accumulate and conserve energy from an external energy source. The output from the source is directly connected to the module and it collects the energy in an inbuilt 1000 μF capacitor. As

the sensor generates voltage the energy is continuously collects in the capacitor. The operational details of the device along with the specifications are given in APPENDIX C.

Another method of storing the energy is by connecting the output of the circuit shown in Figure 5-9 to a medium such as a capacitor or a rechargeable battery. Two large capacitors of 330µF and 1000µF are tested using the rectifier circuit. Also a battery pack of rechargeable AA, NiCd batteries are charged using the same circuit.

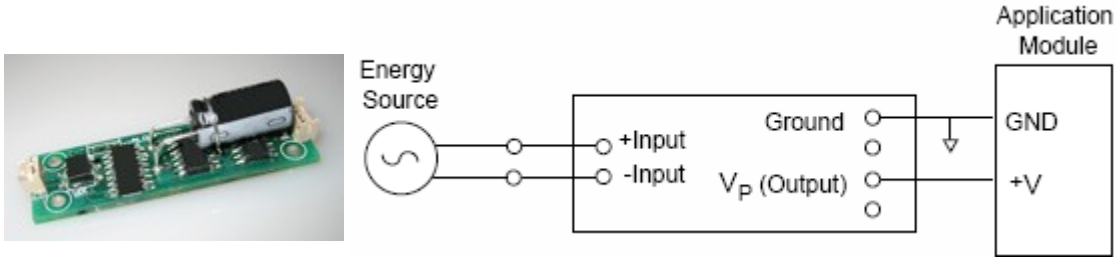

(a) (b)

Figure 5-15 ALD EH301 EPAD® Energy Harvesting Module courtesy Advanced Linear Devices (a) picture of module, (b) pin diagram

6 Results

6.1 Synthetic Jet Actuator Results

6.1.1 Driving Signal and Frequency Effects

Previous studies on synthetic jets have used the sine wave as the driving input signal. A sine wave as the driving input requires relatively high frequencies to match the actuators resonance frequency to enable a synthetic jet formation with significant velocity magnitude. High frequencies however, consume more power and also reduce the lifetime of the piezo. In this study the jets are driven using a sine and a sawtooth signal. A sawtooth signal provides the force required to produce large velocities at low frequencies thus requiring less power.

A typical velocity curve formed with a sine wave is shown in Figure 6-1. Two jets are observed with the second jet smaller in magnitude. The first jet (larger jet) follows the leading edge of the input signal and the second jet (smaller jet) follows the trailing edge. The larger jet is believed to occur during the expulsion cycle, while the smaller jet is believed to occur during the ingestion cycle. Previous studied on the synthetic jet flow fields by Smith have indicated that during the ingestion cycle the flow reenters the cavity from the sides of the orifice (Smith and Glezer, 1998, Smith, 1999).Thus the second jet may be due to the nonparallel direction of the flow, relative to the hotwire, entering the cavity. At lower frequencies, only one jet is formed

indicating that at lower frequencies the flow during ingestion cycle is nearly parallel to the hotwire anemometer and hence cannot be detected.

In the case of the sawtooth signal a single velocity jet is formed. As shown in Figure 6-2, the jet follows the leading edge of the input signal, with series of smaller jets immediately following the first jet. These jets may be caused by vibrations of the clamped actuator. The jets formed using sawtooth driving signals are larger in magnitude as compared to the ones formed with a sine wave.

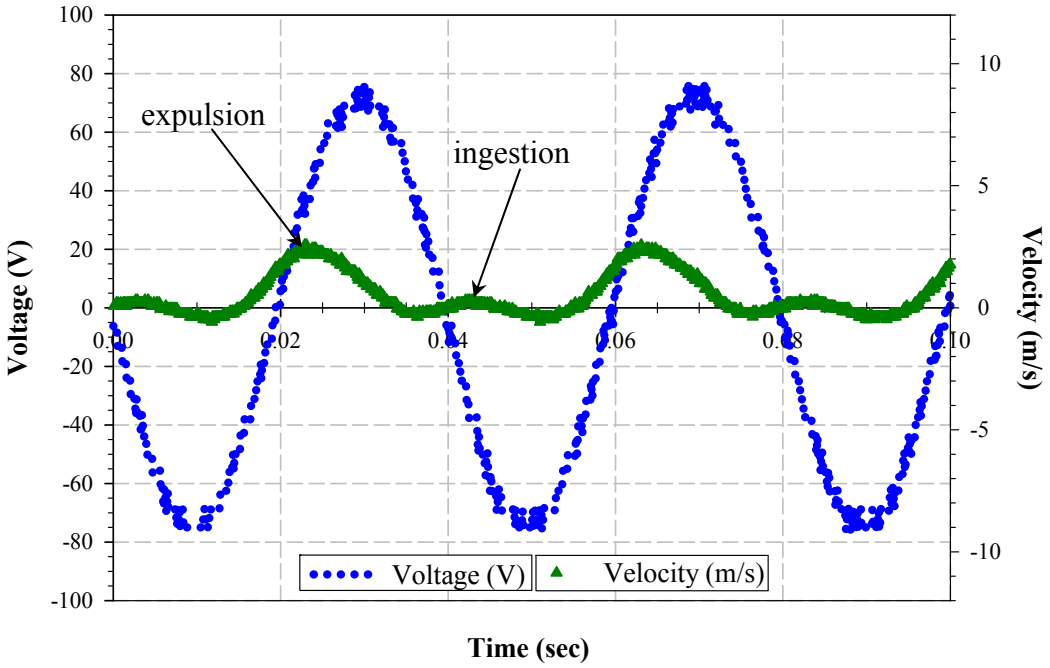

Figure 6-1 Typical Velocity Curve with Sine Driving Voltage with Cavity IV for a Bimorph Diaphragm at 100Hz and 150Vpp

The amplitude of the driving signal has an effect on the maximum jet velocity as seen in Figure 6-3 for *cavity IV*. An increase in the input voltage produces greater velocities. This effect is seen in all the cavities and frequencies for both the driving signals.

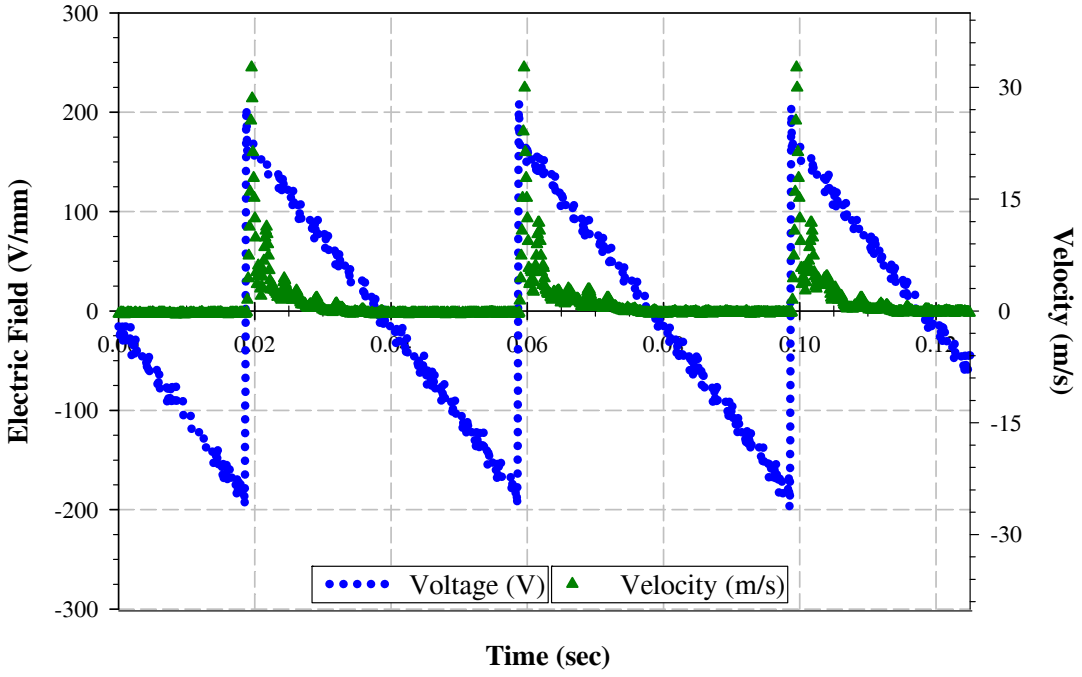

Figure 6-2 Typical Velocity Curve with Sawtooth Driving Voltage with Cavity IV for a Bimorph Diaphragm at 25Hz and 150Vpp

To test the effects of frequency on velocity, the synthetic jet actuator is operated at various frequencies up to 100Hz. As seen in Figure 6-4 with a sine wave input signal the velocity increases as frequency increases. In case of a sawtooth input, the velocity stays constant after approximately 10Hz. This behavior is observed at all voltages and for all the cavities tested. The Appendix section at the end of this document gives all the detailed results with each diaphragm.

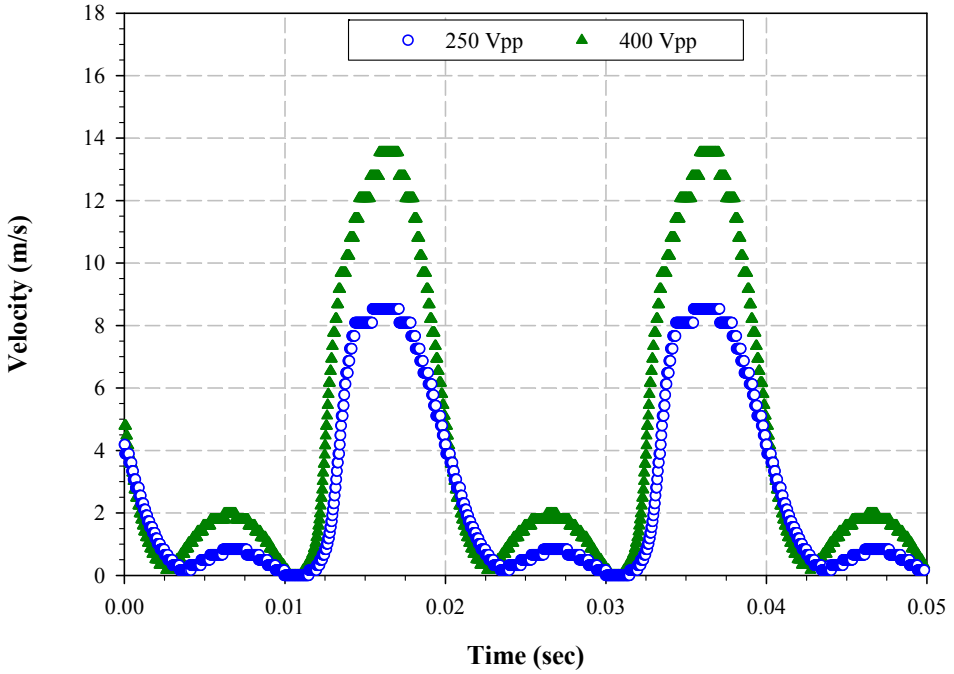

Figure 6-3 Effects of voltage on velocity magnitude with cavity IV for a prestressed metal composite diaphragm at 50Hz with a Sine Signal

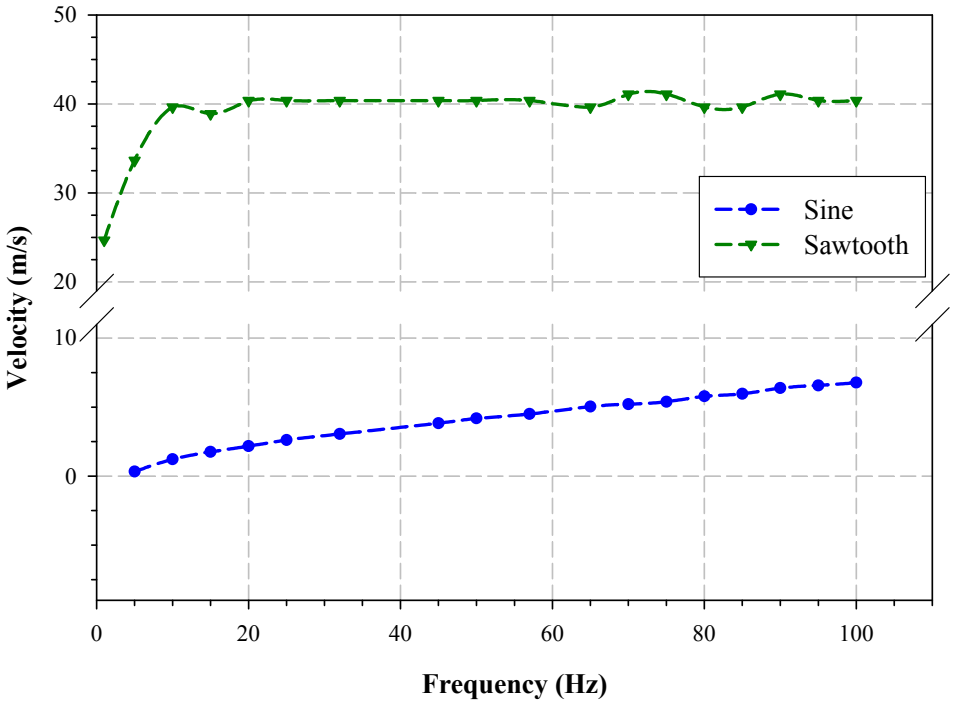

Figure 6-4 Frequency Effects on Bimorph Diaphragm Peak Velocities for Cavity IV at 150Vpp

6.1.2 Cavity Height and Orifice Size Effects

In order to test the effects of changes in cavity height, the profiles obtained from the four cavities were compared. Since *cavity III* and *cavity IV* have the same orifice diameter but different cavity heights their profile comparison will show the effects of changes in cavity height or cavity volume on the velocity magnitudes. Profiles for *cavity III* (smaller) and *cavity IV* (larger) are shown in Figure 6-5. In the case of a sine driving signal, a difference of approximately 30% is observed between the maximum velocities of the two cavities with the smaller height/volume cavity producing the higher velocity. Similarly, *cavity I* (smaller) and *cavity II* (larger) are also compared as they have the same orifice diameter, a difference of 33% is observed.

With a sawtooth driving signal the differences in velocities are smaller as shown in Figure 6-6. A comparison of *cavity I* and *II* profiles at 50Hz shows a difference of 25% and between *cavity III* and *IV* of only 13%. Similar to the sine signal, the cavity with the smaller volume produces higher velocities. The large difference between *cavities I* and *II* could be due to the relatively larger orifice of *cavities III* and *IV*.

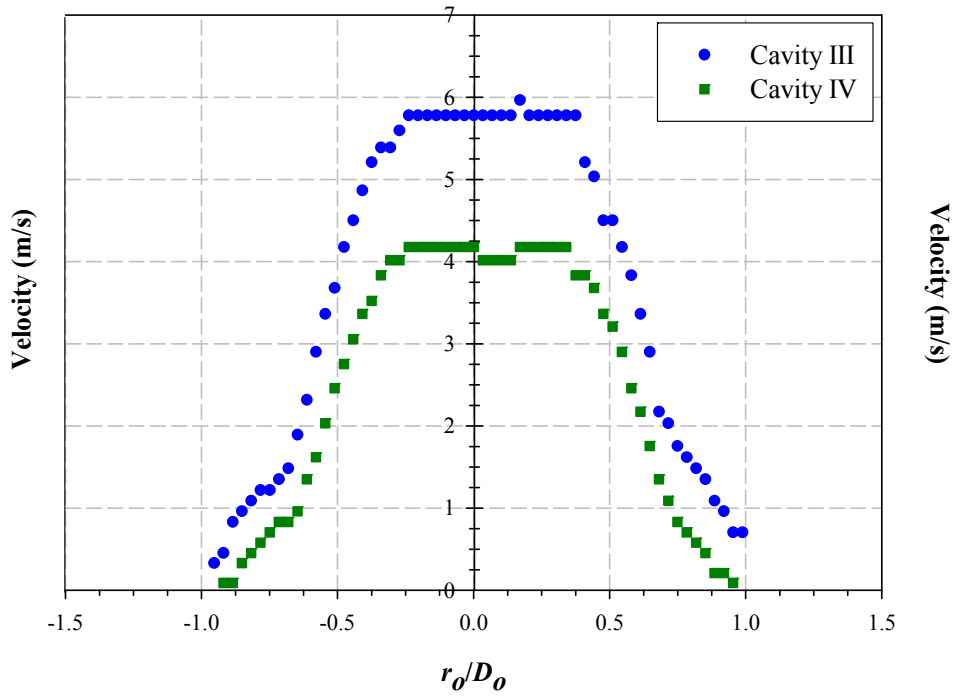

Figure 6-5 Cavity Height Effects using a Sine Driving Signal for a Bimorph Diaphragm at 50Hz and 150 Vpp

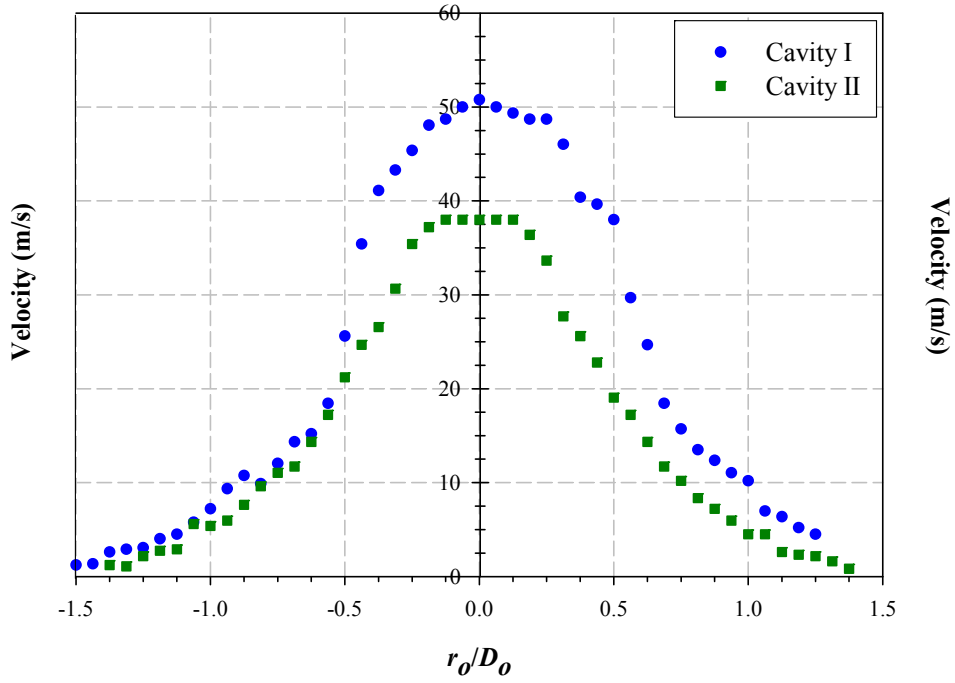

Figure 6-6 Cavity Height Effects using a Sawtooth Driving Signal for a Bimorph Diaphragm at 50Hz and 150Vpp

Next the effects of orifice size on jet velocity are studied. Figure 6-7 shows the sine wave driven profiles for *cavities I* (smaller) and *III* (larger) that have the same cavity height (smaller C_H) but different orifice diameters. It is observed that the smaller orifice diameter (smaller D_o), *cavity I*, produces 63% higher velocities than *cavity III*, larger D_o. This result is expected since to maintain a constant mass flow rate, the velocity through the smaller orifice has to be higher than the larger orifice. Similar trends are observed in the comparison between *cavities II* and *IV* with differences of 61%. In case of the sawtooth driven profiles, the differences in velocities are much smaller as shown in Figure 6-8 for *cavities I* and *III* (different C_H). Differences between *cavity I* and *III* peak velocities are 17% and between *cavity II* and *IV* are only 4%. These results indicate that the synthetic jet velocity is dependent on the type of driving signal used.

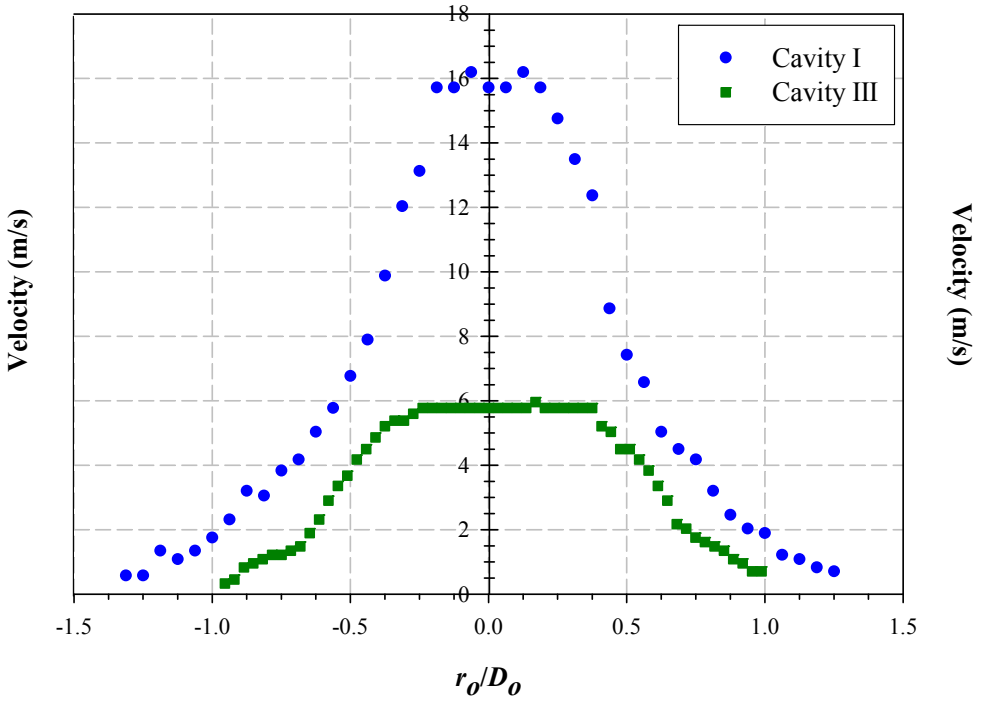

Figure 6-7 Orifice Size Effects using a Sine Driving Signal for a Bimorph Diaphragm at 50Hz and 150 Vpp

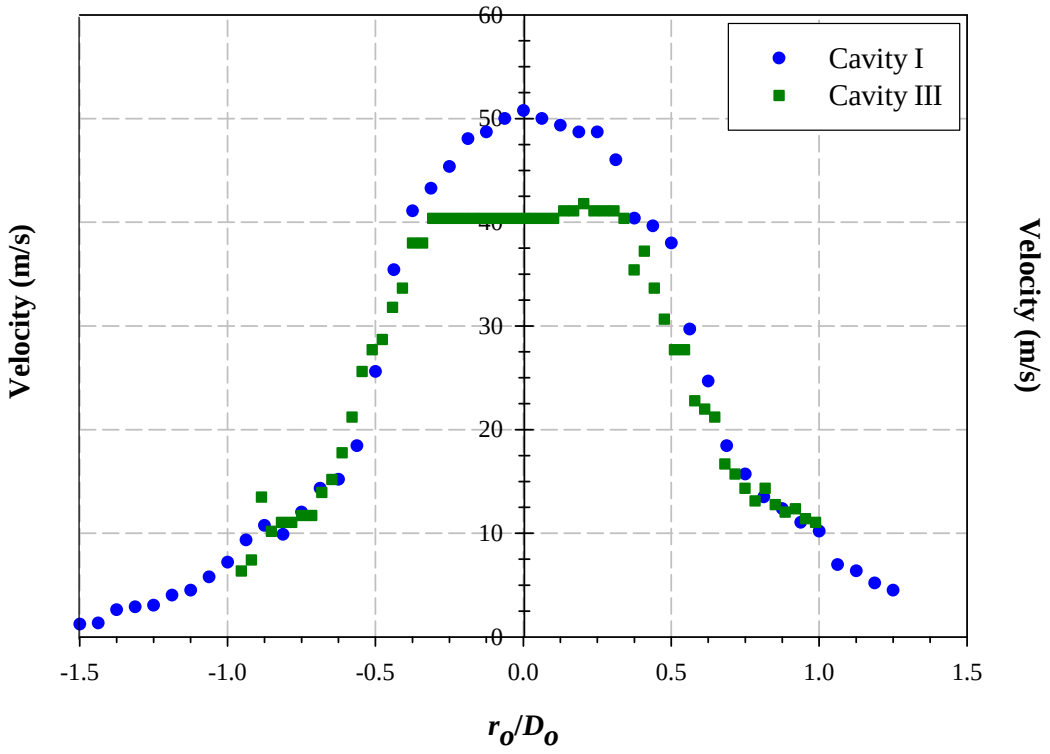

Figure 6-8 Orifice Size Effects using a Sawtooth Driving Signal for a Bimorph Diaphragm at 50 Hz and 150Vpp

6.1.3 Design of Experiments Results

The regression analysis for the 2^{5-1} fractional factorial experimental design discussed in the materials and methods chapter is shown in Table 6-1 for a Bimorph actuator. The first part of the table shows a summary output of the regression. The *R*-square value is the relative predictive power of a model. The model shown has an *R*-square value of 0.97 and an adjusted *R*-square of 0.96 indicating that 97% of the data can be predicted using the model. The adjusted *R*-square value is a better estimate of the model as it accounts for the size of the model as well. This is unlike the *R*-square value, which increases as the number of factors increase even though they might not have an effect on the experiment (Montgomery, 2005, Wheeler and Ganji, 2003).

Table 6-1 Regression Table for Bimorph diaphragm

Regression Statistics	
Multiple R	0.98
R Square	0.97
Adjusted R Square	0.96
Standard Error	3.38
Obs.	16

ANOVA

	df	*SS*	*MS*	*F*	*Sig. F*
Regression	3	4471.34	1490.45	130.19	2.03E-09
Residual	12	137.38	11.45		
Total	15	4608.72			

	Coeffs.	*Standard Error*	*t Stat*	*P-value*	*Lower 95%*	*Upper 95%*	*Lower 95.0%*	*Upper 95.0%*
Intercept	23.08	0.85	27.29	3.62E-12	21.24	24.92	21.24	24.92
F_z	-16.05	0.85	-18.97	2.58E-10	-17.89	-14.21	-17.89	-14.21
D_o	-3.47	0.85	-4.10	1.48E-03	-5.31	-1.62	-5.31	-1.62
C_H	-3.13	0.85	-3.71	3.01E-03	-4.98	-1.29	-4.98	-1.29

Following the summary is the Analysis of Variances (ANOVA). The ANOVA is sometimes called the *F*-test, and it helps determine the validity of the experimental design by testing the difference between two or more groups. When the *F*-value is larger than the *Significance F*-value, the experiment design is considered to be valid, indicating that at least one of factors have an effect on the response variable. The *F*-value shown in Table 6-1 is computed from the mean square values, and *Significance F*-value is selected from the *F*-distribution tables based on the size of the sample, the number of factors, and the significance level selected which is 95% in this case. As the *F*-value is larger than the *Significance F*-value as seen in Table 6-1, the experiment design is considered to be valid and further analysis of the design can continue.

The ANOVA only shows that the experimental design as a whole is valid but all the factors considered in the design may not be relevant. The analysis following the ANOVA helps in determining the importance of all factors. The factors are analyzed on the basis of the corresponding *p-value* generated in the table. The *p-value* or calculated probability is the estimated probability of rejecting the null hypothesis of a study question when that hypothesis is true. If the *p-value* is less than the chosen significance level then the null hypothesis is rejected. The choice of significance level at which the hypothesis is rejected is arbitrary. In the current study, the null hypothesis is that none of the factors considered in the study are significant enough such that they may affect the jet velocity. The alternate hypothesis is that one or more factors are significant and to identify these factors the corresponding *p-values* are considered. Conventionally for this analysis the 5% (less than 1 in 20 chance of being wrong) levels or the 95% confidence internal mark has be chosen such that the *p-value* has to be less than 0.05 (Montgomery, 2005).

The *p*-values for F_z, D_o and C_H are found to be below the 0.05 mark at 2.58E-10, 1.48E-03 and 3.00E-03 respectively. The remaining factors of *E* and *f*, did not appear to be significant. This does not indicate that these factors can be ignored completely. Interaction with main effects may be present but as the focus is only on linear models any additional effects are not taken into account in this study. From these results, a model is obtained as shown in Equation 6.1 such that *Y* is the velocity in m/s. This equation shows that F_z, D_o and C_H, the main effects can be linearly related to each other by Equation 6-1.

$$Y = 23.08 - 16.05 \cdot F_z - 3.47 \cdot D_0 - 3.13 \cdot C_H$$

Equation 6-1

Plots of all the effects showing the average responses are shown in Figure 6-9. The main effects, F_Z, D_o, and C_H have a large slope as seen in the plots and the remaining factors have a very small slope indicating that they do not have a significant effect on the jet velocity. The regression tables and charts for each diaphragm are shown in APPENDIX B.

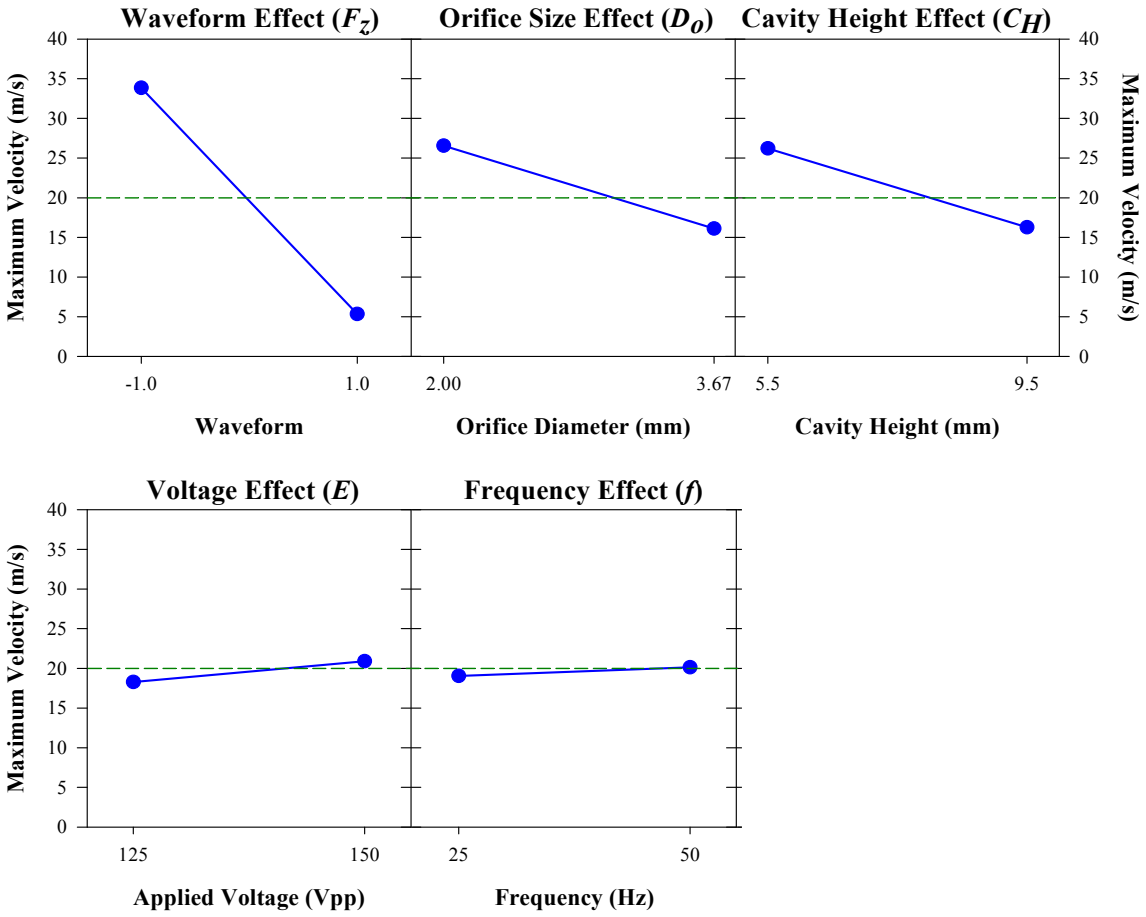

Figure 6-9 Average factor effects for a Bimorph

6.2 Energy Harvesting Results

The energy harvesting experimental parameters listed in Table 5-4 are tested using the described test setup. The ultimate goal of the experiments is optimization of harvested energy from a prestressed piezoelectric diaphragm. The diaphragm was mechanically actuated using air

in a pressurized chamber and the electrical energy converted was measured. The optimizing parameters were temperature (T), pressure (P), frequency (f) and resistant (R).

The AC voltages generated during diaphragm oscillations are measured directly without the use of a circuit. Figure 6-10 shows typical voltage curves measured with the Metal composite sensor. The figure shows curves with two temperatures and at 206.85kPa of cavity pressure. The graph clearly indicates that temperature affects the magnitude of the generated sensor voltage. For clarity the other tested temperatures have been omitted from the graph.

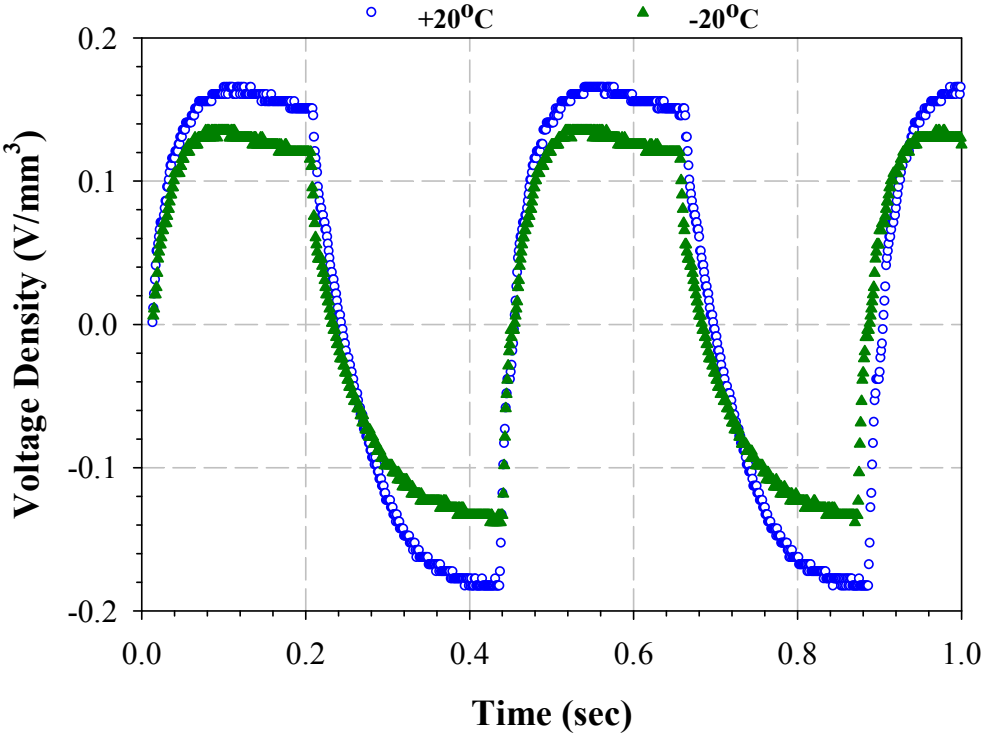

Figure 6-10 Typical vibration energy harvesting AC voltage curve

Although not shown in the figure analysis of the AC data indicates that voltages are also dependent on applied pressure. To show the dependence of temperature and pressure on AC voltage generation, a typical contour plot of the AC voltage is shown in Figure 6-11, for 5Hz frequency experiments. The high and low voltage regions are clearly visible in the figure. High

voltages were measured at pressures between 250kPa to 300kPa and at higher pressures the voltage decreases. Thus, indicating that the optimal pressure is in this range. Similar temperature ranges are difficult to identify although two regions about 20^{o}C and -30^{o}C show high voltages.

The piezoelectric diaphragm was driven at three different frequencies. Figure 6-12 shows the effect of frequency on the peak to peak AC voltage measured at 344.75kPa. As seen in Figure 6-12, the three curves are almost identical indicating that frequency does not have any effect on the generated voltage. An ANOVA of the frequency levels was also conducted and the $F < F_{critical}$ condition was in agreement with the conclusions drawn from the graphs. Also the $p-$value of 0.5 was too large to consider frequency an important factor. These results are valid only at tested frequencies. At high excitation frequencies such as in the piezo resonance region this factor could become important. For the scope of this study, frequency is ruled out as a significant factor. Another observation from Figure 6-12 is the peak in voltage seen at 20^{o}C. This is seen at all frequencies and can help in identifying the optimal energy harvesting temperature. Further analysis of this temperature and pressure dependence was conducted using DC measurements.

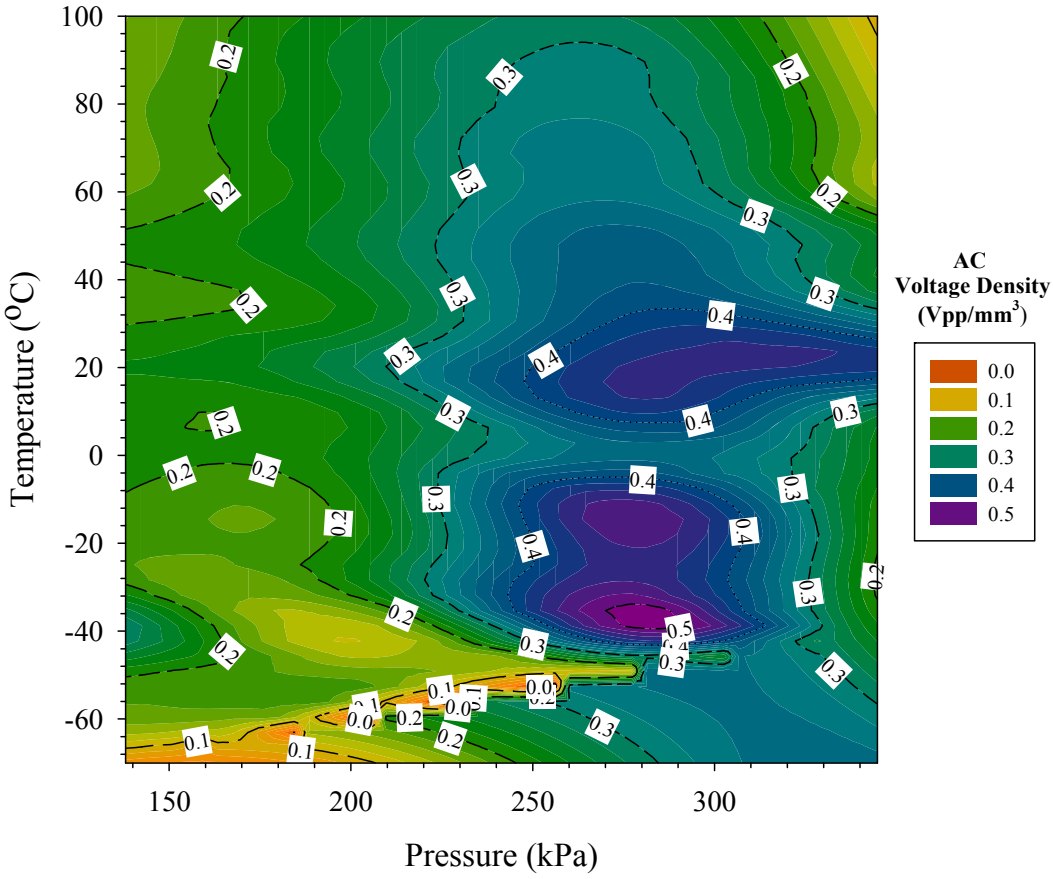

Figure 6-11 Contour plot of AC voltage region

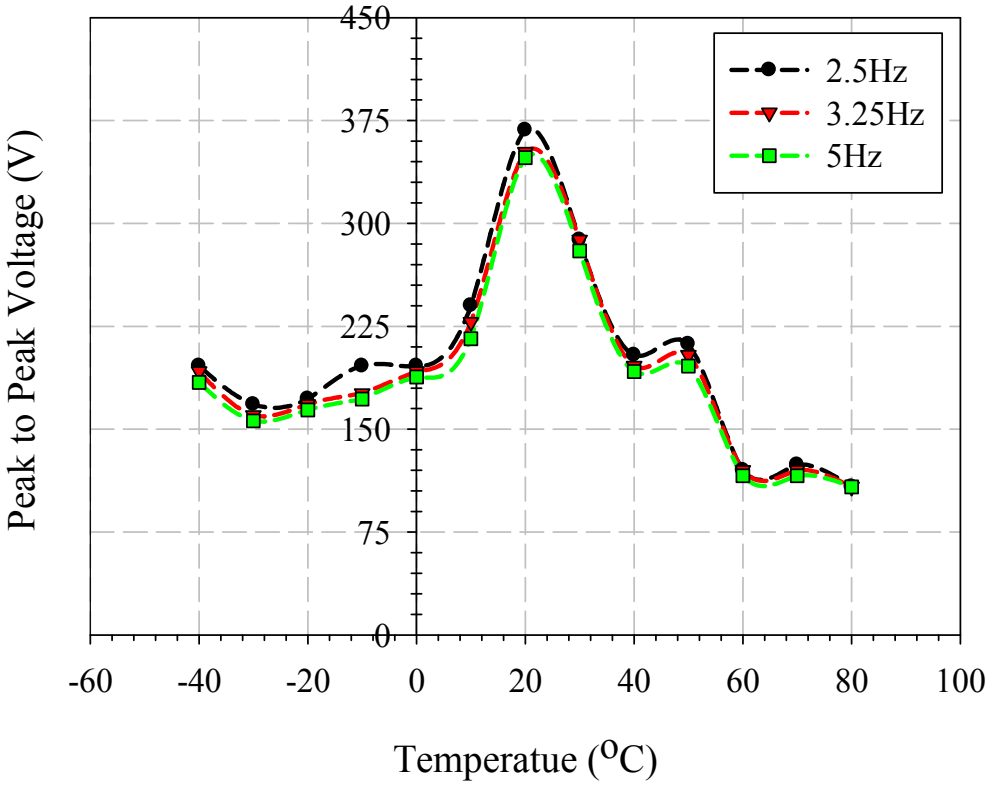

Figure 6-12 Frequency effect on vibration energy harvesting

6.2.1 DC Voltage Measurement Results

To utilize the harvested signal to power any device, the signal needs to be rectified to match the requirements of the device. Also most devices are powered with a DC voltage. To measure DC voltage an AC—DC converter circuit or energy harvesting circuit shown in Figure 5-9, is added to the setup and the DC voltage is measured across a 4.7μF capacitor. In these experiments an additional factor of *R* is included in the study simulating a load in the circuit. By varying the resistance impedance matching is achieved with different devices. Impedance matching between the source and the device maximizes power transfer to the device making the

system more efficient. Measurements are taken at different frequencies, resistances, temperatures and pressures.

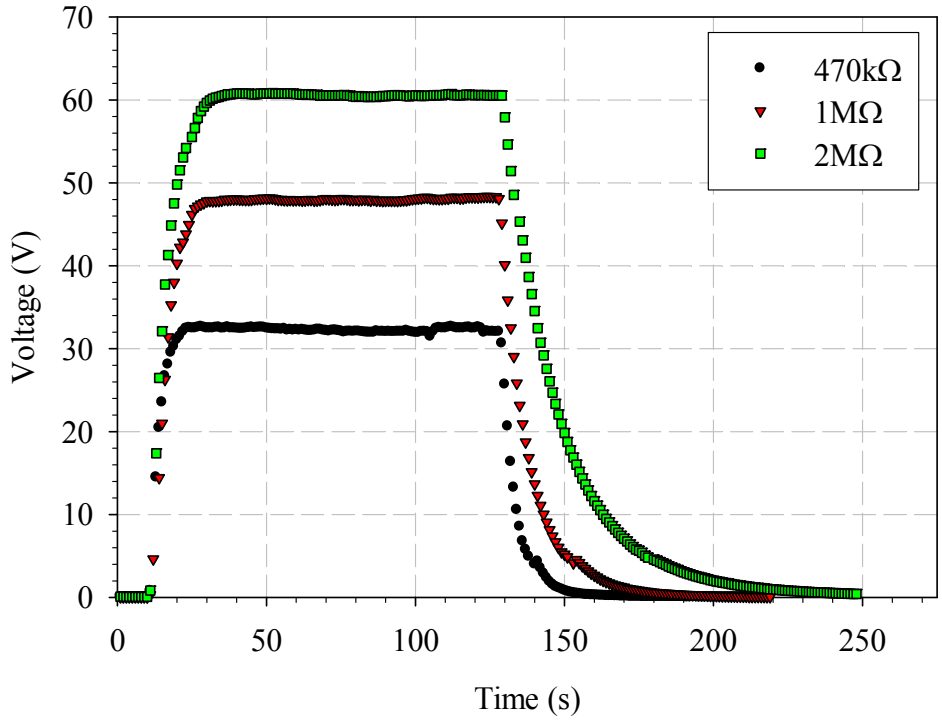

Figure 6-13 Typical DC voltage curve

Typical DC voltage curves are shown in Figure 6-13. The figure shows curves for 3.25Hz, 0^{o}C and 344.75kPa measurements. The maximum voltage is measured at 2MΩ and the lowest at 470kΩ. Similar results are seen at other temperatures and pressures. This indicates that maximum voltage is transferred to the load at 2MΩ. Thus there is greater impedance matching between the source and the load at this resistance. When the harvested voltage will be used to charge a battery or other storage devices high impedance matching will be required to ensure efficient transfer of energy. An ANOVA of the dc data also indicates that resistance is an important factor with a *p*–value of 0.00048 and the *F*–value of 89.43. It can be concluded that resistance is an important factor during energy harvesting and is dependent on the end application. However, a load of 2MΩ is not necessarily the optimal resistance for impedance

matching. The optimal value can be obtained from response surface models described in the following sections.

Using the measured voltage and the available resistance values, instantaneous power is calculated using Equation 6-2 shown below.

$$P = \frac{V^2}{R}$$

Equation 6-2

Here V is the measured voltage in volts, R is the resistance in ohms and P is the power in Watts. The maximum calculated power was 18.44mW and using ceramic volume the maximum power density was found to be 24.27μW/mm^3. These values were obtained at 20^{o}C, 344.75kPa and 5Hz. A typical power graph is shown in Figure 6-14.

Calculating area under the power curve gives the energy harvested from the system as indicated by Equation 6-3. $P(t)$ is the instantaneous power and E is the total energy harvested by the device in Joules. The maximum total energy calculated was 3.05J at -60^{o}C, 206.85kPa and 2.5Hz. The area of the shaded portion of curve gives the energy as stated in Equation 6-3.

$$E = \int_{t_i}^{t_2} P(t)dt$$

Equation 6-3

Visual analysis of the AC voltage data indicates that temperature and pressure are important factors which need to be studied in detail. Figure 6-15 shows the effect of pressure on DC voltage measurements. The graph shows the peak DC voltages measured at several positive

and negative temperatures at four increasing pressures. The temperatures follow a similar trend in which the voltage peaks at 275kPa. This pressure can be identified as the optimal pressure for this energy harvesting setup.

As discussed earlier the experimental measurements have identified trends in the energy harvesting process. In the following sections statistical methods are used to develop models which relate the variables under study. These relationships will further justify the experimental results. Furthermore such models can also be used in identifying optimal levels of the experiment indicating trends in the study.

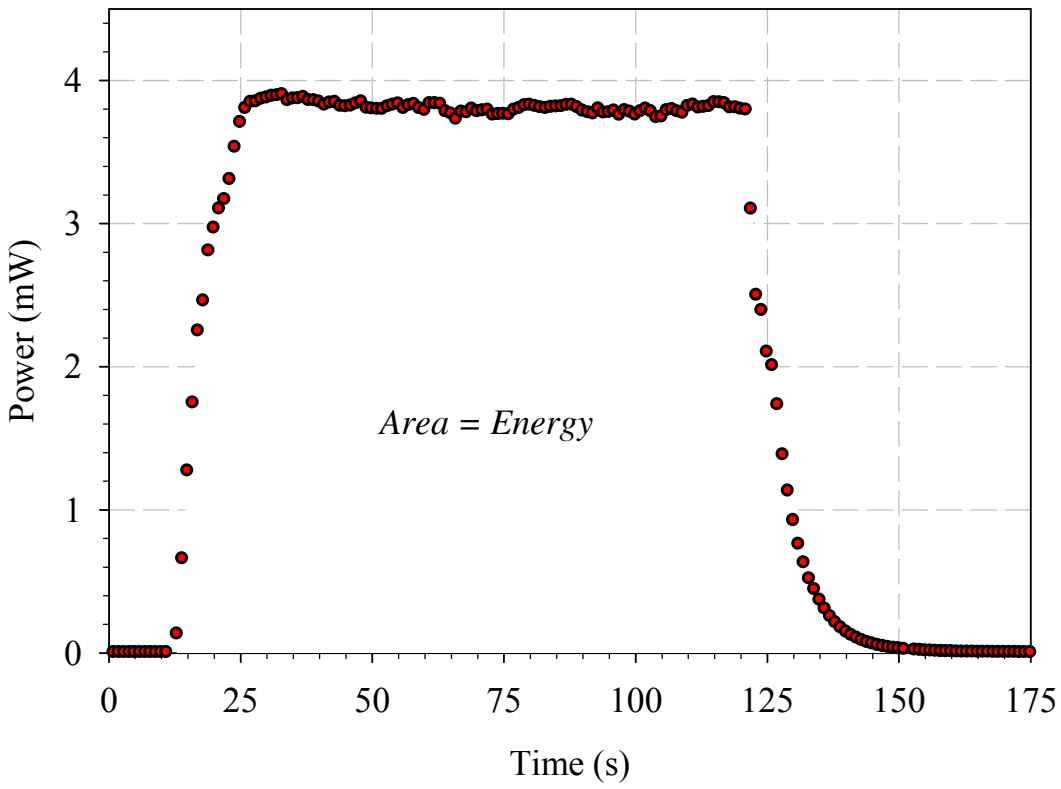

Figure 6-14 Typical Vibration Energy Harvesting Power Curve

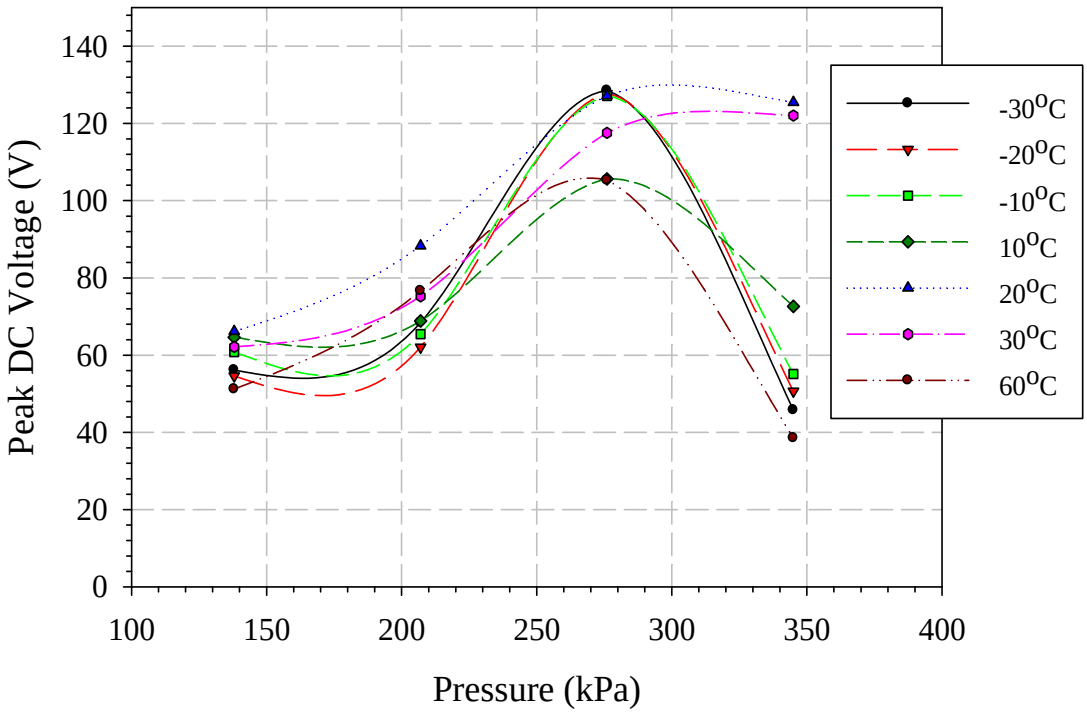

Figure 6-15 Pressure effects on DC voltage

6.2.2 Response Surface Model Results

The response surface methodology is applied to the vibration energy harvesting study. The response variable (Y) is DC voltage and the factors or dependent variables modeled are resistant (R), pressure (P), temperature (T) and frequency (f). Using this analysis approach surface maps are developed which help in optimizing the system.

A regression analysis and model fit of the DC voltage data gives a second order polynomial model given in Equation 6-4. The model fit has an R^2 value of 90%. All the first order models resulted in low R^2 values which are not acceptable. Thus a second order model was attempted.

$$VDC = 114.82 + 11.82R - 6.92P - 10.19T + 2.65f - 4.04RP - 3.51RT + 3.62PT - 1.04Rf + 2.60Pf + 0.27Tf - 9.73R^2 - 33.66P^2 - 20.84T^2 - 7.39f^2$$

Equation 6-4

As the fitted surface is an adequate approximation of the true response surface, analysis of the fitted surface is approximately equivalent to analysis of the actual system. The surface represented by the equation for VDC (response) shown in Equation 6-4 is called the response surface. Response Surface plots and contour plots play a very important role in the study of the response surface. By generating these plots using computer software for response surface analysis, the shape of the surface can be characterized. Also, location of the optimum can be determined with reasonable precision. Figure 6-16 (a) and (b) show the response surface and the contour plot of response surface. The lines of constant response are drawn in the *T*, *P* plane. The dome shape of the response surface is result of the second order model fit. The optimal point is the peak of the dome; it can also be called the stationary point, saddle point or the maximum point.

A stationary point represents the point of maximum response, to find the levels of *R*, *P*, *T*, and *f* that optimize the predicted response. The location of the stationary point can be determined using the DC measurements data. Performing the analysis discussed previously results in a x_s matrix with coded and natural factor values as shown in Table 6-2. Experimental results from previous section indicate that the optimal pressure level is approximately 250kPa which is in agreement with the predicted optimal level in the statistical analysis. Similarly 20^{o}C was

identified as the optimal temperature level in the experimental results. The model predicts the optimal temperature at approximately 12°C.

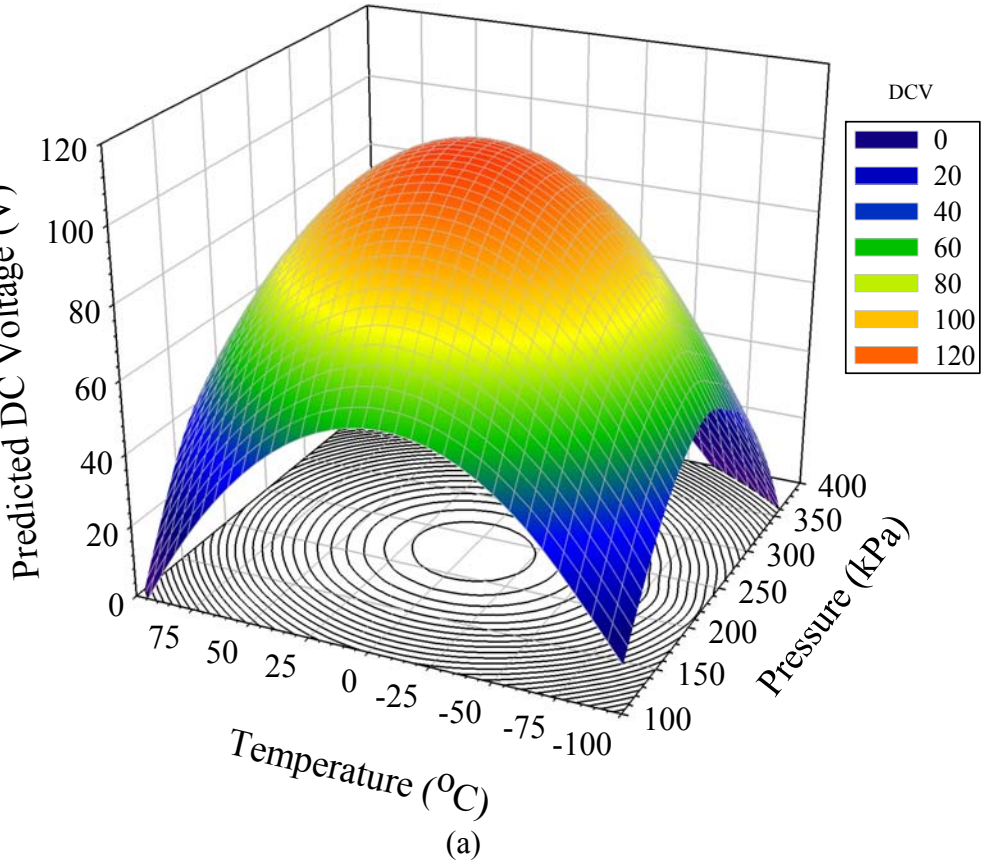

(a)

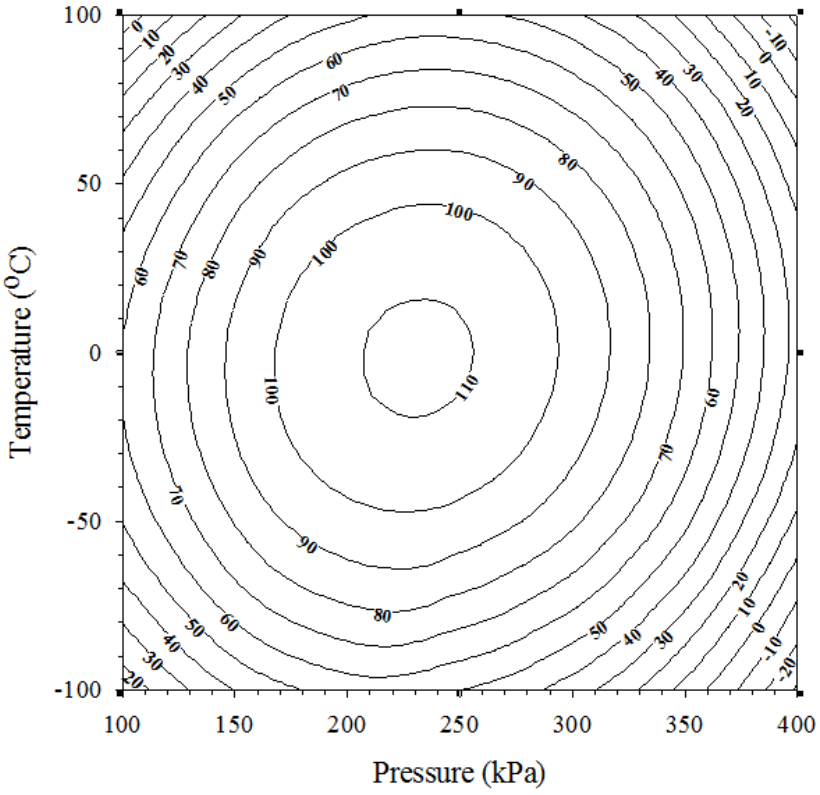

(b)

Figure 6-16 (a) 3D Response Surface showing the predicted DC voltage as a function of pressure (P) and temperature (T), (b) Contour plot of the response surface

Table 6-2 Coded factor levels

Factors	***Coded variables***	***Natural variables***
R	0.692	1MΩ
P	-0.158	237.6kPa
T	-0.132	12°C
f	0.097	3.7Hz

A surface map was plotted using optimal resistance and frequency values of 1MΩ and 3.7Hz respectively. The surface as shown in Figure 6-17 has similar results of peak voltage at 12^{o}C and 237.6kPa. Similarly voltages can be predicted for intermediate factor levels not tested in the experiments within the tested ranges.

Although PZT is a pyroelectric material, this effect is not directly involved in the study. For the pyroelectric effect to be significant the material has to be heated at a fast heating rate i.e. constant temperature should not provoke a response (Whatmore, 1986). Since the study has a very small heating and cooling rate (almost zero) the pyroelectric effect is zero and does not affect the outcome. The magnitudes of piezoelectric properties are dependent on piezoelectric coefficients of the material. The application of temperature and stress affects the coefficients and the functioning of the piezoelectric device. These stimuli are considered extrinsic contributions from the environment (Mukherjee *et al.*, 2001). Under the application of a periodic stress, a near instantaneous charge is generated due to 180^{o} domain changes and some 90^{o} domain changes thus increasing the extrinsic contribution. As studied by Mukherjee *et al.* these effects are more prominent on soft ceramics such as PZT 5A due to more domain mobility. In another study it was shown that the response of a piezoelectric material to the application of stress is a non linear function of stress, time and temperature (Sherrit *et al*., 1996). Thus there is a combined coupling effect which is also indicated in the regression model of Equation 6-4. Along with having individual effects of the outcome each factor also affects the outcome coupled with the other factors. The piezoelectric response can also be affected by multiple heating (Sherrit *et al.*, 1999).

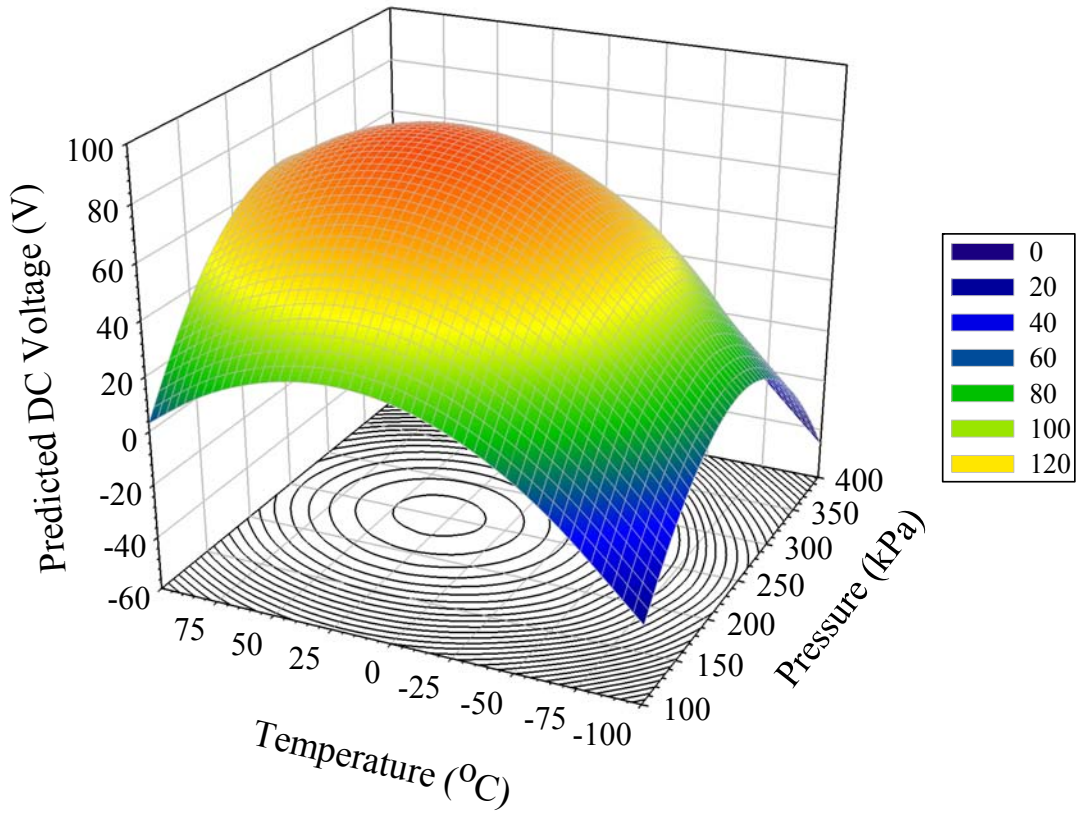

Figure 6-17 Response Surface using optimal factor level predicted in Table 5-4

In the current study the temperature is set and the device is allowed to heat until that temperature. Upon reaching a steady state condition at the temperature measurements are taken. In this manner the device is heated to various temperatures. These conditions could help in understanding the median values predicted by the regression models as the optimal conditions of the system. In a practical environment the conditions that the system will operate in will not be as varying as used in the current study. This study demonstrates that pre—stressed piezoelectric composites can be efficiently used to power devices and the efficiency is dependent on the operating conditions.

6.3 Integration of Energy Harvesting in Synthetic Jet Actuator Results

Sensing and actuation is integrated into a synthetic jet actuator using piezoelectric materials. The PVDF and Metal composite sensors are attached to the diaphragm of the actuator to harvest vibration energy from the oscillations. Only the prestressed diaphragm synthetic jet actuator is considered in this study. The diaphragm is driven using three driving signals, sine, sawtooth and square at 400Vpp and the AC voltage generated by the sensor is recorded. The AC voltage is then converted to DC using a standard rectifier circuit shown in Figure 5-9.

The voltage applied to the actuator or the oscillating diaphragm is referred to as the actuator voltage or the applied voltage and the voltage measured across the sensor is called the sensor voltage or the generated voltage. A typical graph showing the sensor voltage measured with a PVDF sensor at the diaphragm oscillating frequency of 10Hz with a square signal is shown in Figure 6-18. As expected the generated voltage follows the diaphragm applied voltage as the dynamics from the actuator are transferred to the sensor. For actuator applied voltage of 400Vpp almost 10Vpp sensor voltage is generated. Similar results are seen with the metal composite sensor but the magnitude of generated voltage is higher.

Similar tests are conducted at different frequencies in the low frequency range used in the synthetic jet actuator study of 5 - 100Hz. Figure 6-19 shows the effects of frequency and driving signal on the sensor energy generation. With the metal composite sensor the peak to peak generated sensor voltage is not affected by the frequency for the sine and square driving signals. But with the sawtooth signal the voltage increases with frequency. The prestressed metal composite attachment mechanism is unstable and thus the results are also inconsistent. Thus analysis is require to develop a more stable and consistent design.

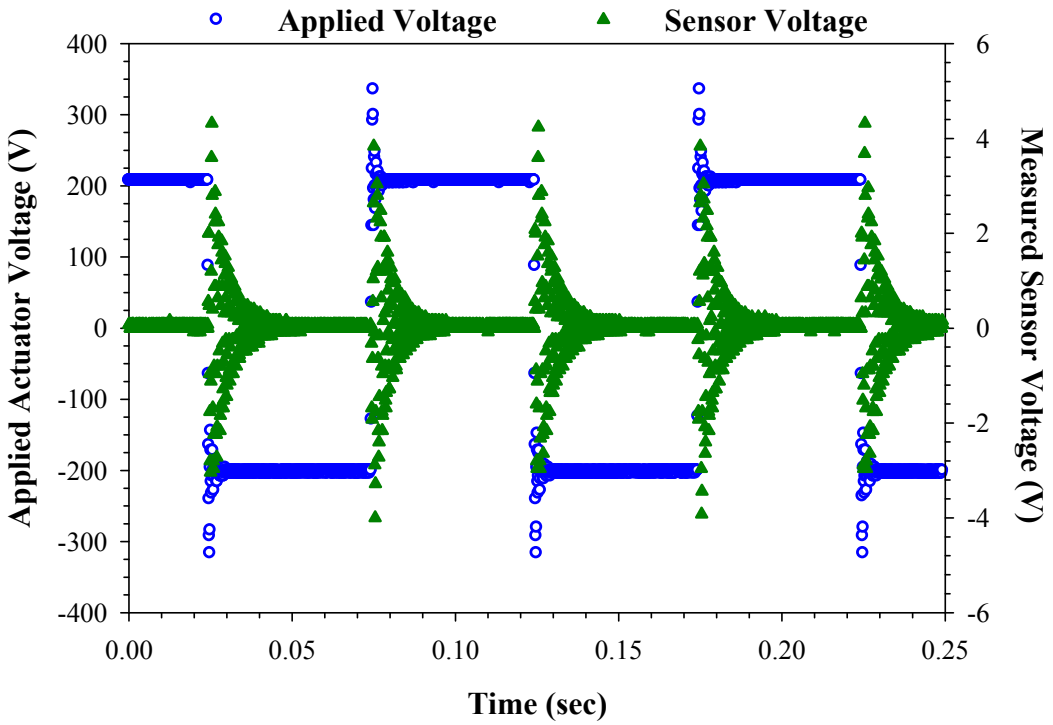

Figure 6-18 PVDF sensor voltage

With the PVDF sensor the results are different such as the voltage increases at higher frequencies with a sine signal. However the voltage decreases slightly (almost constant) with the sawtooth and square signals. Also in this case large peak voltages are generated with a sawtooth signal although the differences with square are very small (less than 5%). Results with the PVDF sensor are more consistent with the synthetic jet velocity measurements presented earlier wherein the synthetic jet velocity increases at higher frequencies with a sine signal. In general the results with the PVDF are more consistent compared to the metal composite although the magnitudes of the generated voltages are approximately 30% small while comparing the peak voltages with a square signal. Table 6-3 gives a comparison of the peak to peak voltages measured with the two sensors. The maximum voltage of 12.16 Vpp is generated by the metal composite sensor with a square driving signal.

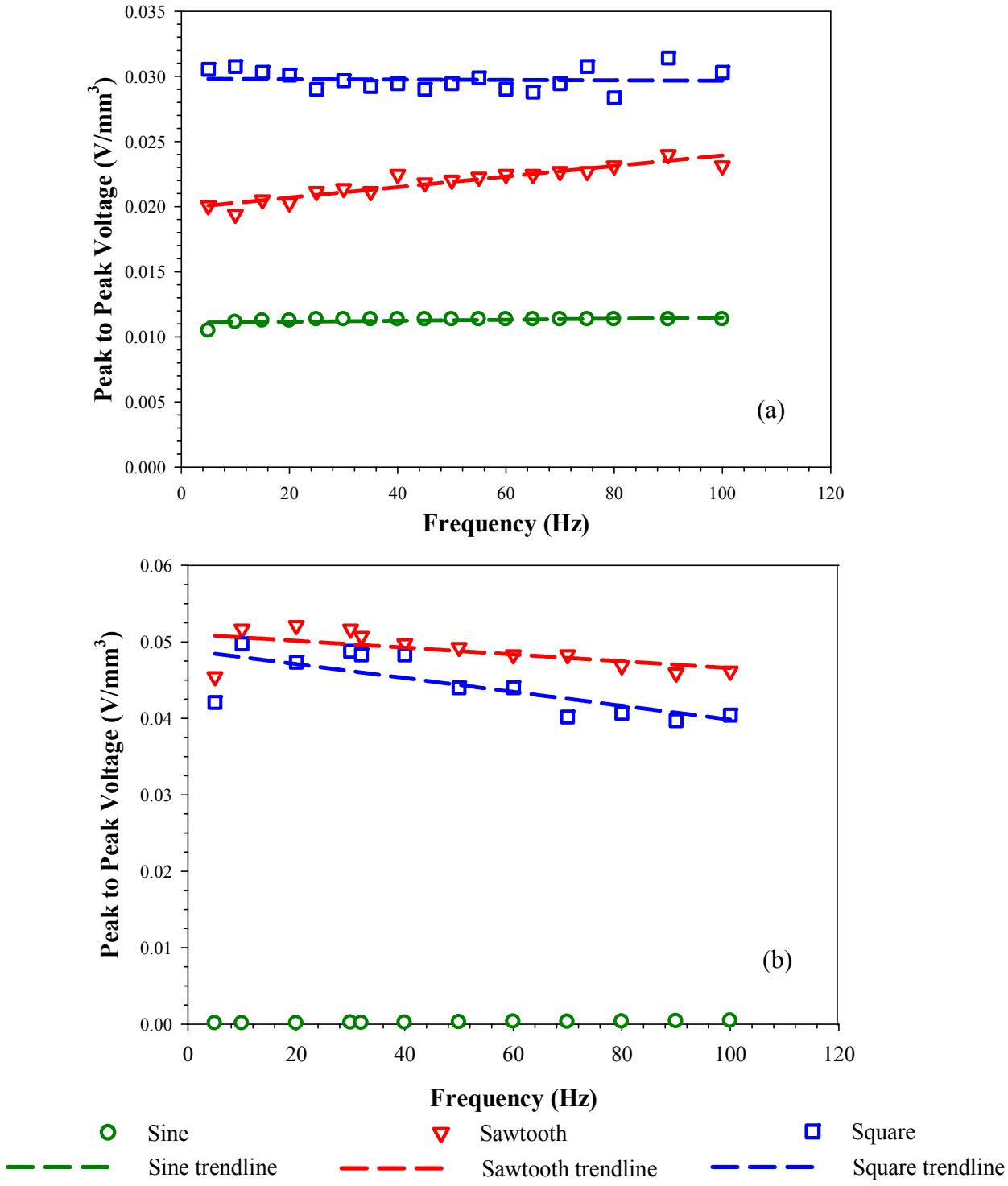

Figure 6-19 Peak to peak sensor generated voltage summary (a) Metal composite sensor (b) PVDF sensor

Table 6-3 Comparison of Sensor Voltage

	Peak to Peak Harvested Voltage (Vpp)	
	PVDF	PZT Composite
Sine	6.72	4.16
Sawtooth	6.16	8.96
Square	7.12	12.16

Due to integration of the sensor the performance of the synthetic jet actuator could be affected. The sensor adds mass to the system and more work is required which could hamper the jet output. To study the effect of sensor integration, synthetic jet velocity and sensor voltage are measured simultaneously. The peak velocities formed by the actuator are compared with results with no sensor attached. Figure 6-20 shows such a result where the jet velocity and sensor voltage are shown with the PVDF sensor and sawtooth driving signal. The peak jet velocities are in comparison with previous synthetic jet actuator results and also the characteristics of the curve are similar. Such as, the long and short velocity jets representing the expulsion and ingestion parts of the actuator cycle. The sensor voltage also follows a similar trend with unequal sized peaks following the diaphragm movement in conjunction with the jet velocity peaks.

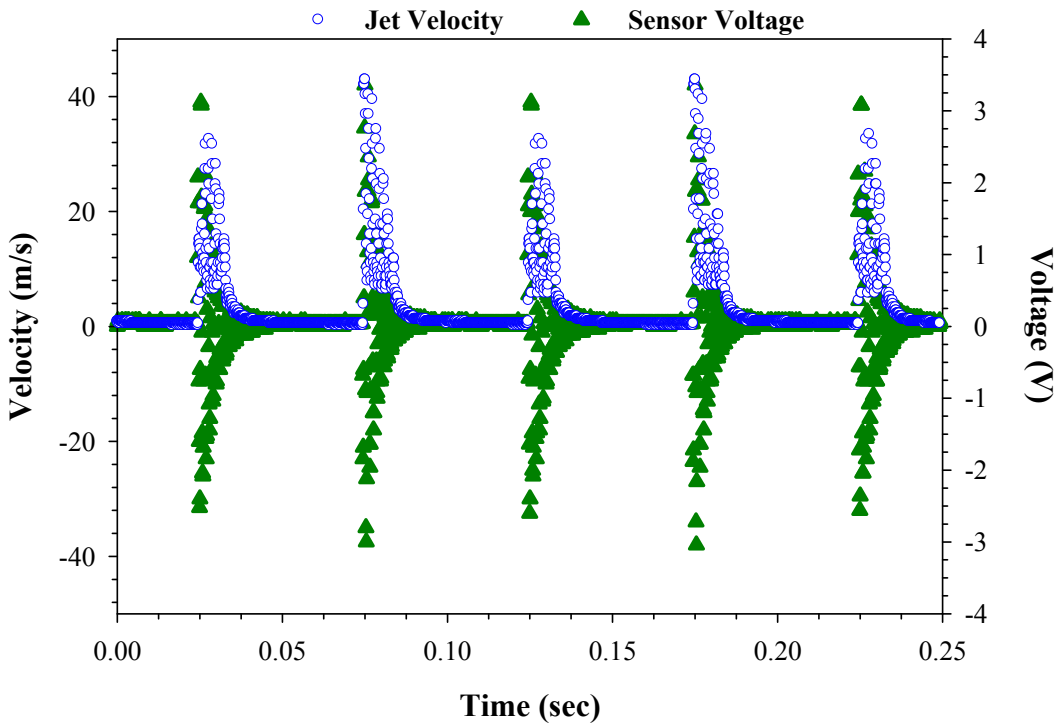

Figure 6-20 Effect of sensor integration on jet velocity with a PVDF sensor

The voltage directly measured from the sensor is converted to DC by using the full wave rectifier bridge circuit shown in Figure 5-9. Power can then be calculated using Ohm's law with the resistance in the circuit. A typical power curve is shown in Figure 6-21. Energy is the area under the power curve as indicated by the shaded part of the graph. Maximum power density of $0.167\mu W/m^3$ was measured with the PVDF sensor and peak energy of 0.407mJ was harvested.

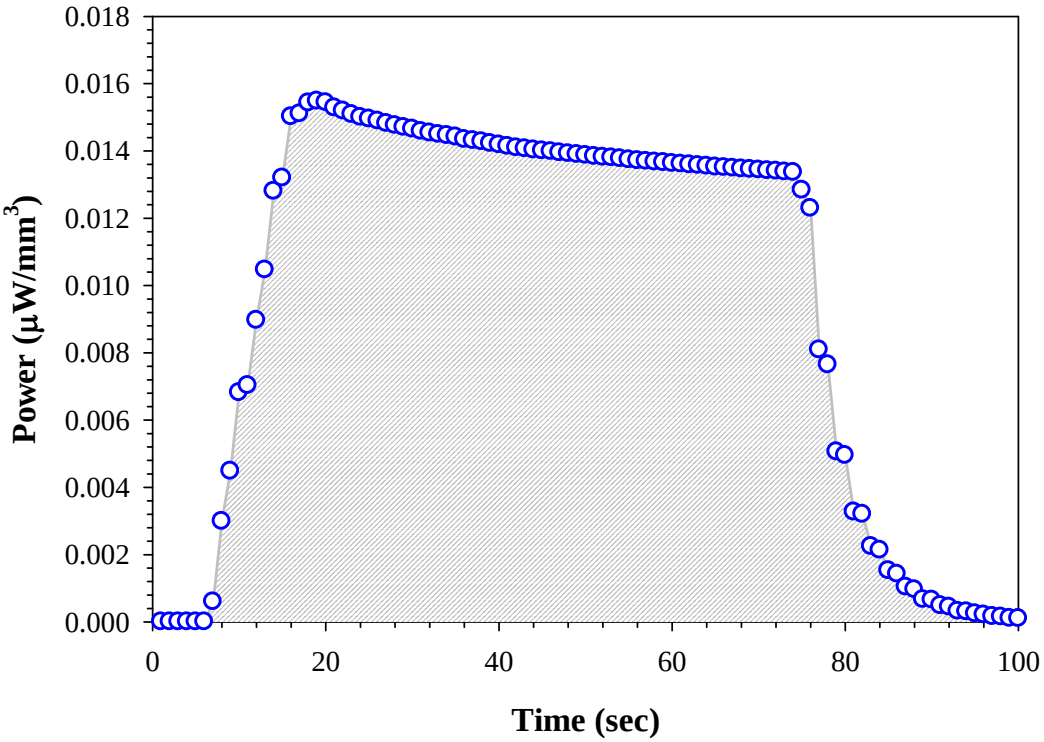

Figure 6-21 Typical power graph showing energy generation with a PVDF sensor

6.3.1 Screening Design Results

For the screening design of experiments power (*P*) is selected as the response variable. A two level fractional factorial experimental design is conducted with one replication and one center point as represented by Table 5-8. Three factors and their levels are identified as indicated in Table 5-7. The results of a linear regression analysis are shown in Table 6-4.

The R-square value of the regression is 0.919. Only main factor effects are considered ignoring interaction effects. Since this analysis was conducted with a 95% confidence interval, factors with *p*-values under 0.05 are considered significant. Thus area and thickness are clearly important factors which have a direct effect on the power generation. Since shape is a discrete variable each level of the factor is considered separately. The *p*-value for '-1' level is significant

which is the square shaped sample. Since one of the levels is significant the entire factor is considered important and included in the linear model. The prediction expression is shown below in Equation 6-5. Depending on the driving signal being used the coefficient will be different as indicated in the equation.

Table 6-4 Regression analysis results with a PVDF sensor integrated into a SJA

Term	***Scaled Estimate***	***p—value***
Intercept	2.054	0.0010*
s[0]	0.363	0.4735
s[1]	0.973	0.0558
s[-1]	-1.336	***0.0191****
a	1.433	***0.0061****
t	1.472	***0.0054****

$$P = 2.054 + Match(s)\begin{Bmatrix} "0" & \Rightarrow 0.363 \\ "1" & \Rightarrow 0.973 \\ "-1" & \Rightarrow -1.336 \end{Bmatrix} + 1.433a + 1.472t$$

Equation 6-5

In the regression analysis it is also seen that the regression coefficients or scales estimates for the two important factors of area and thickness have a positive value. This indicates that the response increases as the factor levels increase. Thus with a sensor of larger area and thickness the energy harvested will be larger. Similar conclusions are difficult to draw when the variables are not continuous. Contour plots of the prediction expression are shown in Figure 6-22. As expected the contour lines have a negative slope with area and thickness as the X and Y variables.

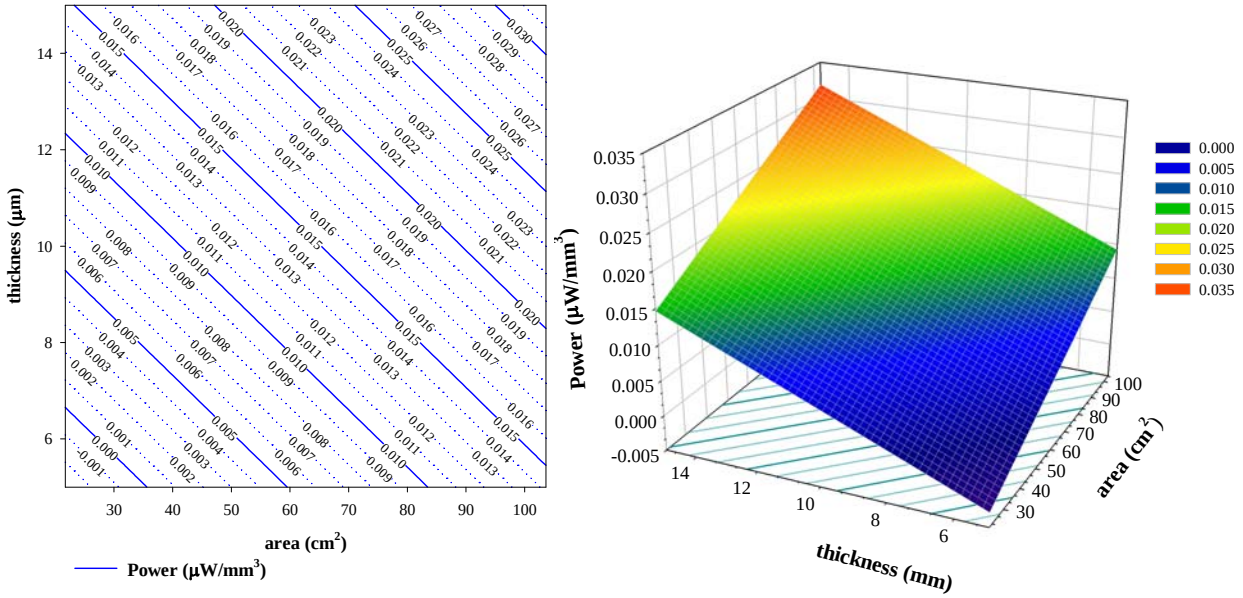

Figure 6-22 Contours of the response variable Power (*P*) with the significant factors of area (*a*) and thickness (*t*)

6.3.2 Energy Collection in a Storage Medium

As the power harvested by the piezoelectric sensors is very small (µW) it not possible to directly charge an application. However, if the energy is stored in a medium it can be eventually used to power a device such as a wireless sensor. With the PVDF and metal composite sensors the energy generated while the synthetic jet actuator is operational is accumulated in the EH301 energy harvesting module shown in Figure 5-15. Figure 6-23 shows the charging of the capacitor integrated in the module over time. The capacitor was charged while the synthetic jet actuator was operated using a square signal at 50Hz. Peak voltage of almost 5V was observed with the metal composite sensor.

In another set of tests the rectifier circuit shown in Figure 5-9 was used to charge two large capacitors of 300µF and 1000µF. Figure 6-24 shows the charging of the capacitors using a

PVDF sensor. In this case as well a 50Hz square driving signal was used. Using the circuit the voltage collected was very small for the same duration as tested with the module. Thus indicating that the module is more efficient compared to the circuit.

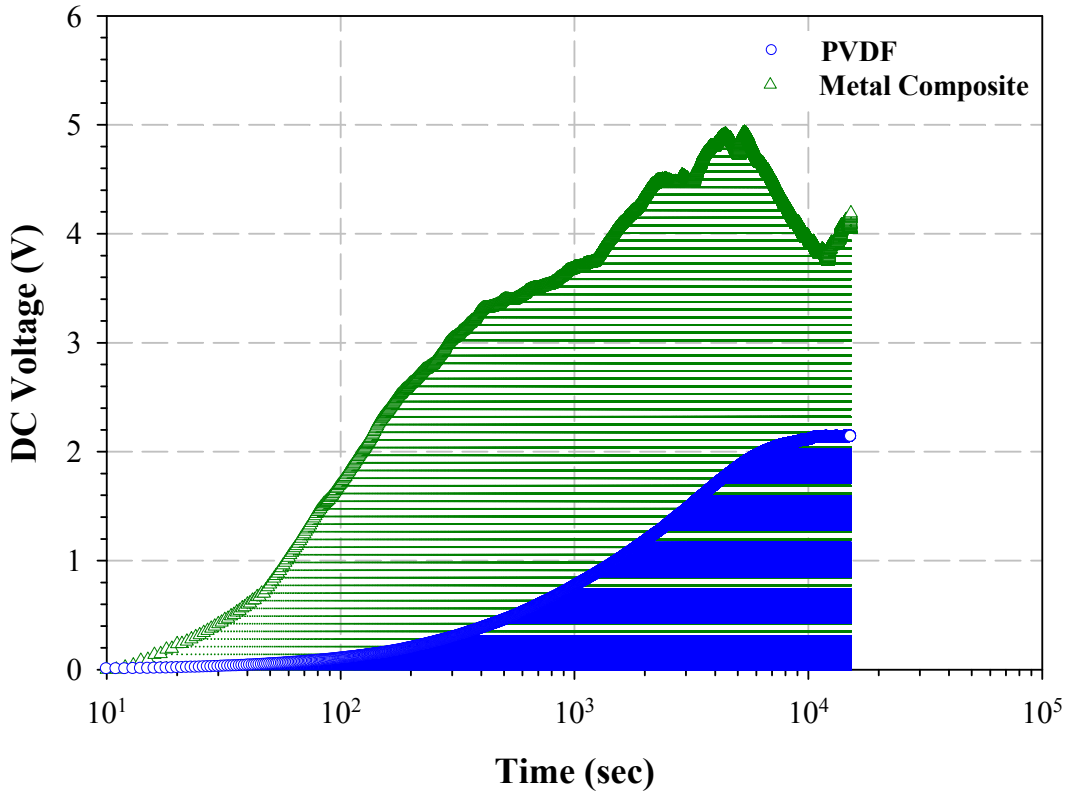

Figure 6-23 Charging of the EH301 energy harvesting module

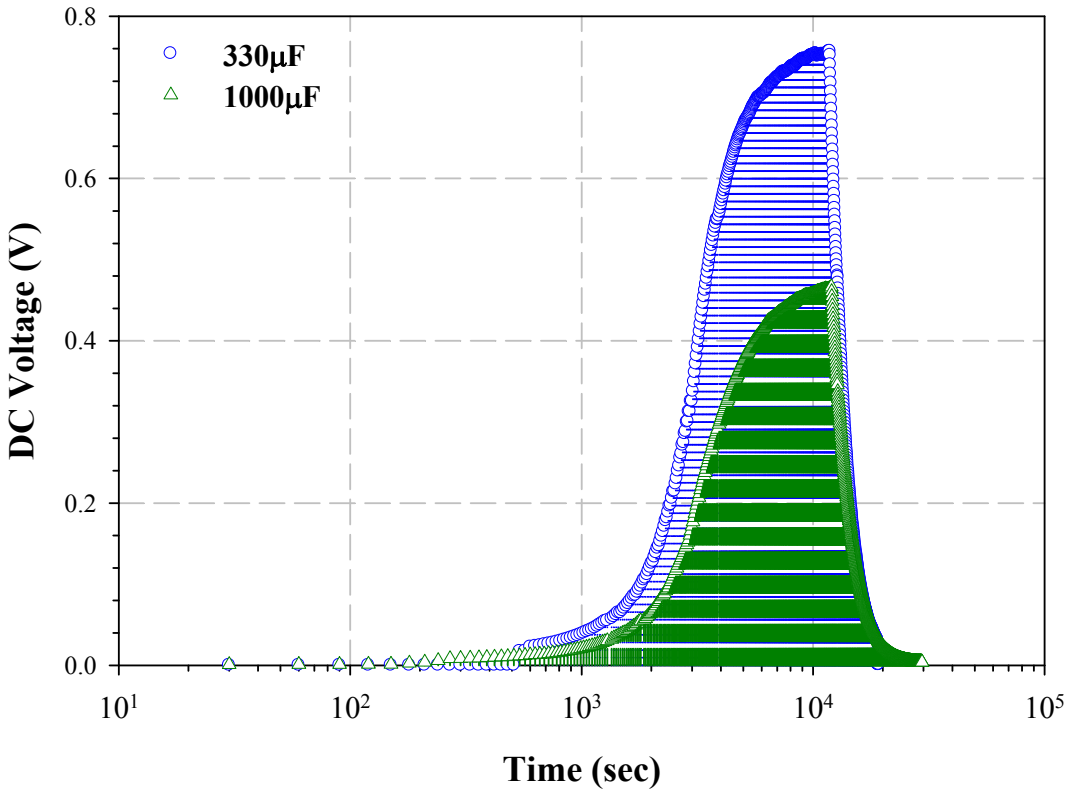

Figure 6-24 Charging of capacitors using PVDF sensor

Experiments were conducted to recharge a NiCd, AA battery pack. The source was connected to the rectifier circuit used in previous testing and the DC output was directly fed into the battery pack. The battery charging is shown in Figure 6-25 using a metal composite sensor. Thus it was successfully demonstrated that energy harvesting can be integrated into synthetic jet actuators and generated power can be collected in a storage device.

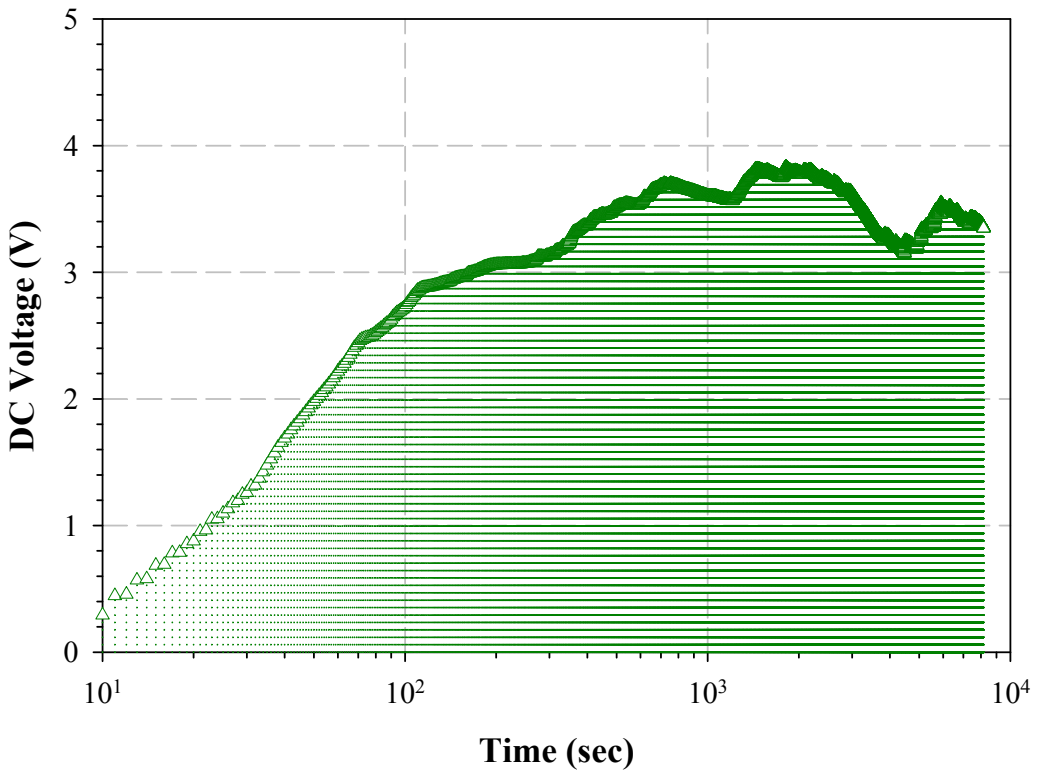

Figure 6-25 Charging of an Energizer AA NiCd battery pack using a prestressed metal composite sensor

7 Conclusions

Four diaphragms, Bimorph, Prestressed PZT Metal Composite, Lipca and RFD are studied as synthetic jet diaphragms. Using statistical analysis tools such as screening designs and fractional factorial models, an analysis of significance is performed on several variables with peak jet velocity as the objective function. The factors studied were the driving signal used to excite the diaphragms, the magnitude and frequency of the signal, the volume of the cavity described by the cavity height, and the size of the exit or orifice. A 2^{5-1} fractional factorial design with regression analysis showed that three factors were statistically significant in all piezoelectric diaphragms; driving signal, orifice diameter, and cavity height. In contrast, frequency was found a non-significant factor in all. A comparison of the regression coefficient sizes for each actuator suggests the possibility of a larger model that could include the diaphragm as a factor. This study indicates that to optimize performance of a synthetic jet, diaphragm and driving signal should be included in any design of a piezoelectric synthetic jet actuator.

Comparing the peak jet velocity magnitudes the Bimorph diaphragm generated the largest velocities followed by the metal composite diaphragm. Due to the uniform drum like deflection of the Bimorph diaphragm the effective volumetric displacement inside the cavity is higher thus leading to larger peak velocities. On the other hand with its uneven prestressed shape the metal composite displays lower volumetric displacement. Although Bimorphs generate large velocities they are very brittle and also have very small force capabilities. In comparison the metal composite is very robust and can operate in harsh environments.

A prestressed piezoelectric diaphragm was dynamically pressure loaded to harvest energy and to assess the devices performance under harsh environments. Parameters involved in the energy harvesting process such as temperature, pressure, resistance and frequency are optimized using statistical techniques. Response surface methodology is used to develop models to identify optimal parameter ranges and also to predict power generation for specific parameter levels. The model predicted optimal levels of $12^{o}C$, 237kPa, 1MΩ and 3.7Hz. These levels were in agreement with the experimental results. Maximum power densities of approximately $24.27\mu W/mm^3$ are measured at optimal conditions. The results can be explained by studying the combined effect the factors have on the piezoelectric response of the material. Piezoelectric coefficients are affected by stress and temperature and repeated heating and cooling cycles further introduce thermal hysteresis effects into the system.

The study demonstrates that prestressed piezoelectric composites can be used to power devices and response surface methodology can be utilized to optimize a system efficiently. In future studies the harvested energy can be collected in storage mediums to power small devices such as wireless sensors which are getting miniaturized with advances in technology. As piezoelectric energy harvesting is operating conditions dependent using a storage medium could act as an interface between different applications.

PVDF and metal prestressed piezoelectric devices are integrated into the synthetic jet actuator for energy harvesting. These devices are attached to the oscillating diaphragm of the synthetic jet actuator. As the diaphragm oscillates, the devices generate energy which is then measured. Effects of oscillation frequency and driving signal on the device voltage are studied. The metal prestressed piezoelectric devices generate larger peak to peak voltages with a square driving signal than a sinusoidal waveform. However, its high stiffness and due to its unique

shape, this device is difficult to incorporate into the synthetic jet design. PVDF on the other hand is very flexible and conforms to surfaces fairly easily. Peak power density of $0.167\mu W/m^3$ was harvested with a PVDF sensor.

A fractional factorial analysis is conducted on three variables; sensor shape, area and thickness; with power as the response variable using the PVDF experimental data. A linear regression analysis indicated that area and thickness are important factors that significantly affect the power generated by the sensor. Such that as the area and thickness increases the power increases. As shape is not a continuous factor each level is considered separately. For the tested shapes, square was identified as important although the other shapes cannot be ignored.

The energy harvested by the two sensors; Metal composite and PVDF can be stored in mediums such as large capacitors and batteries. The charging of both these mediums is demonstrated in this study. A commercially available energy harvesting module is also used which has embedded circuitry to accumulate and store the energy in a capacitor included in the package. With the PVDF sensor maximum voltage of approximately 0.8V could be accumulated in a 330μF capacitor using the rectifying circuit. However, with the metal composite sensor almost 5V could be stored in a similar rating capacitor by using the energy harvesting module, indicating that the module has much higher efficiency. Within four hours the Energizer AA NiCd battery pack was recharged as demonstrated with a Thunder sensor. Thus in this dissertation the synthetic jet actuator efficiency was increased using a prestressed metal composite and energy harvesting was incorporated into the design of the actuator to successfully generate enough power to recharge a battery and to store in a large capacitor. This energy can then be used to power small devices such as wireless sensors.

8 Dissertation Contributions

This dissertation makes significant contributions to active flow control and energy harvesting hence addressing the global need for energy. An active flow control tool called synthetic jet actuator is designed and tested using an interdisciplinary approach combining experiments and statistics.

The synthetic jet actuator is formed using prestressed piezoelectric composites which have never been used for this application. This is a very significant contribution to active flow control as using these composites increases the efficiency of the actuator as demonstrated in this dissertation. This dissertation also suggests the possibility of using alternate driving signals other than sine; such that the actuator can be operate at low off resonance frequencies in turn increases the life time of the actuator. Also, the complexity of the electronics for designing piezoelectric power supplies is diminished making its implementation easier.

Another aspect of this dissertation is the harvesting of energy from ambient vibrations. Prestressed composites are used to harvest energy from vibrations induced using pulsating pressures. The power densities generated by the composite are larger than previously published literature. Response surface methodology is used to model the energy harvesting system and optimal conditions are identified for power generation. Such an approach is unique to this dissertation and is effective in developing an understanding of the system.

The most important contribution of this dissertation is the integration of energy harvesting into synthetic jet actuators. In other words sensing and actuation is integrated such that a piezoelectric sensor harvests energy while the actuator is operational. It is also demonstrated that the energy harvested from the sensor can be stored in a medium such as a large capacitor and a rechargeable battery.

A summary of the dissertation contributions are as follows:

1. Prestressed piezoelectric composites are used as diaphragms in a synthetic jet actuator as they provide robustness, and enhanced durability.
2. Nontraditional waveforms are investigated to provide an insight onto the issue of powering piezoelectric diaphragms.
3. Prestressed composites are used as energy conversion devices and produce higher power densities as compared to previously published literature.
4. In the current project actuation and sensing is integrated into the same application by harvesting energy from synthetic jet actuators.
5. Energy harvested from synthetic jet actuators is used in charging a large storage capacitor.

9 Future Work

This dissertation demonstrated the use of prestressed composites in synthetic jet actuators using an interdisciplinary experimental and statistical approach. Current CFD tools are insufficient in modeling synthetic jet actuators thus a coupled approach combining experiments, statistics and numerical techniques could be more successful. Also further research is required into incorporating synthetic jet actuators in automotive and aerospace applications.

Although extensive research has gone into harvesting energy with piezoelectrics, still many issues remain such as energy efficiency. Further work needs to look in to means of increasing the efficiency of piezoelectric energy harvesting systems. Also, not much work has gone into the energy management issues which deal with energy conversion and transfer to devices requiring power.

Integration of sensing and actuation into one device could lead to self powered systems. Very little research has been done on this topic and the scope is tremendous. Further research is required into integration without the loss of efficiency. This concept can be used in structural and biological health monitoring. For use in biological systems an insulating mechanism needs to be developed for piezoelectric as they are non bio degradable.

10 References

Aimmanee, S. (2004) "*Deformation and Force Characteristics of Laminated Piezoelectric Actuators*," *Engineering Mechanics*, Virginia Tech, Blacksburg, Virginia, p. 280.

Aimmanee, S. and Hyer, M.W. (2004) "*Analysis of the manufactured shape of rectangular THUNDER-type actuators*," Smart Materials and Structures, **13**(6), pp. 1389–1406.

Amitay, M., Honohan, A., Trautman, M., and Glezer, A. (1997) "*Modification of the aerodynamic characteristics of bluff bodies using fluidic actuators*," 4th AIAA Shear Flow Control Conference, AIAA Paper 97–2004.

Amitay, M., Smith, B., and Glezer, A. (1998) "*Aerodynamic flow control using synthetic jet technology*," 36th AIAA Aerospace Sciences Meeting and Exihibit, AIAA Paper 98–0208.

Anderson, E., Hagood, N., Goodlife, J. (1992) "*Self-sensing Piezoelectric Actuation: Analysis and Application to Controlled Structures*," 33rd AIAA/ASME/ASCE/AHS/ASC Structures, Structural Dynamics, and Materials Conference, AIAA Paper 92–2465, pp. 2141–2155.

Anderson, J.D. (1995) "Computational Fluid Dynamics The Basics With Applications," McGraw-Hill, Edition1.

APC International, Ltd. www.americanpiezo.com

August, J.A., and Joshi, S.P. (1996) "*Preliminary Design of Smart Structure Fins for High Speed Missiles*," SPIE Smart Structures and Materials 1996: Industrial and Commercial Applications of Smart Structures Technologies, **2721**, pp. 58–65.

Balakrishnan, S. and Nierecki, C. (2002) "*Investigation of Thunder Actuators as Underwater Propulsors,"* Journal of Intelligent Material Systems and Structures, 2002. **13**(4), pp. 193–207.

Ballato, A. (1996) "*Piezoelectricity: History and New Thrusts,"* IEEE Ultrasonics Symposium, pp. 575–583.

Barron, B.W., Li,G., and Haertling, G.H. (1996) "*Temperature Dependent Characteristics of Cerambow Actuators*," IEEE International Symposium on Applications of Ferroelectrics, Part 1, IEEE, **96CH35948**, IEEE, Piscataway, New Jersey, pp. 305–308.

Bent, A.A. (1999) "*Active Fiber Composite Material Systems for Structural Control Applications*," *Proceedings of the SPIE Conference on Industrial and Commercial Applications of Smart Structures*, Vol. 3674, Newport Beach, California, March, pp. 166–175.

Bent, A.A., and Hagood, N.W. (1993) "*Development of Piezoelectric Fiber Composites for Structural Actuation*," *Proceedings of the 34th AIAA/ASME/ASCE/AHS Structures, Structural Dynamics, and Materials Conference*, AIAA Paper 93-1717, La Jolla, California, April.

Bent, A.A., and Hagood, N.W. (1997) "*Piezoelectric Fiber Composites with Interdigitated Electrodes*," Journal of Intelligent Material Systems and Structures, **8**, pp. 903–919.

Bernhard, A.P.F., and Chopra, I. (1996) "*Development and Hover Testing of a Smart Trailing Edge Flap with a Piezo-Induced Bending-Torsion Coupled Actuator*," Annual Forum Proceedings—American Helicopter Society, **3**, pp. 107–137.

Bindal, V., and Chandra, M. (1977) "*A Piezoelectric Displacement Transducer for Fine Movement and Its Performance*," Indian Journal of Pure and Applied Physics, **15**, pp. 109–114.

Boucher, D. (1987) "*Trends and Problems in Low Frequency Sonar Projectors and Design*," Power Sonic and Ultrasonic Transducers Design, B. Hamonic and J.N. Decarpigny, eds., Springer-Verlag, Heidelberg, pp. 100–120.

Box, G.E., and Draper, N.R. (1987) "*Empirical Model Building and Response Surfaces*," New York: John Wiley & Sons, Inc.

Boyd, J.G. (1993) "*Thermomechanical response of shape memory composites*," Intelligent Materials and Structures, **5**, pp. 333–346.

Bruneau, H., Le Letty, R., Claeyssen, F., Barillot, F., Lhermet, N., and Bouchilloux, P. (1999) "*Semi-Passive and Semi-Active Vibration Control Using New Amplified Piezoelectric Actuators*," Proceedings of the SPIE—The International Society for Optical Engineering, **3668**, pp. 814–822.

Bryant, R.G. (1996) ''*LaRC-SI: A Soluble Aromatic Polyimide*," High Performance Polymers, **8(**4), pp. 607–615.

Bryant, R.G., Effinger, R.T., Aranda, I.Jr., Copeland, B.M., Jr., Covington, E.W., III, and Hogge, J.M. (2004) "*Radial Field Piezoelectric Diaphragms*," Journal of Intelligent Material Systems and Structures, **15**.

Capozzoli, M., Gopalakrishnan, J., Hogan, K., Massad, J., Tokarchik, T., Wilmarth, S., Banks, H.T., Mossi, K.M., and Smith, R.C. (1999) "*Modeling Aspects Concerning THUNDER Actuators*," Proceedings of the SPIE—The International Society of Optical Engineering, **3667**, pp. 719–727.

Chandra, R., and Chopra, I. (1999) "*Actuation of Trailing Edge Flap in a Wing Model Using a Piezostack Device*," Journal of Intelligent Material Systems and Structures, **9**, pp. 847–853.

Chandrakasan, A., Goodman, R.J. and Rabiner, W. (1998) "*Trends in low power digital signal processing*," IEEE International Symposium on Circuits and Systems.

Chandran, S., Kugel, V.D., and Cross, L.E. (1996) "*Characterization of the Linear and Non-Linear Dynamic Performance of Rainbow Actuator*," Proceedings of the Tenth IEEE International Symposium on Applications of Ferroelectrics, **2**, East Brunswick, New Jersey, pp. 743–756.

Chandran, S., Kugel, V.D., and Cross, L.E. (1997) "*Crescent: A Novel Piezoelectric Bending Actuator*," Proceedings of the SPIE—The International Society for Optical Engineering, **3041**, pp. 461–469.

Chen, Q.X., and Payne, P.A. (1995) "*Industrial Applications of Piezoelectric Polymer Transducers*," Measurement Sciences and Technology, **6**, pp. 249–267.

Chonan, S., Jiang, Z.W., and Koseki, M. (1996) "*Soft-Handling Gripper Driven by Piezoceramic Bimorph Strips*," Smart Materials and Structures, **5**, pp. 407–414.

Cole, D.J., Allen, M.G., Trautman, A.G., and Glezer, A. (1994) "*Micromachined jets for manipulation of macto flows*," Soild-State Sensors and Actuators Workshop, Hilton Head, SC, pp. 243–247.

Collis, S., Joslin, R., Seifert, A., Theofilis, V., 2004, *Issues in Active Flow Control: Theory, Control, Simulation, and Experiment*, Progress in Aerospace Science, **40**, p. 237–289.

Crook, A., Sadri, A.M., and Wood, N.J. (1999) "*The Development and Implementation of Synthetic Jets for the Control of Separated Flow*," AIAA, 99–3176.

Cudney, H.H., Inman, D.J., and Oshman, Y. (1990) "Distributed Structural Control Using Multilayered Piezoelectric Actuators," 31st AIAA/ASME/ASCE/AHS/ASC Structures, Structural Dynamics and Materials Conference, New Orleans, LA, pp. 2257–2266.

Curie, P. and Curie, J. (1880) "*Development by pressure of polar electricity in hemihedral crystals with inclined faces,"* Bulletin de la Société Chimique de France, **3**: pp. 90–93.

Dausch, D.E., and Wise, S.A. (1998) "*Composition Effects on Electromechanical Degradation of RAINBOW Actuators*," NASA TM–1998–206282, pp. 2–3.

Davis, W.R., Zhang, N., Camera, K., Markovic, D., Smilkstein, T., Ammer, M.J., Yeo, E., Augsburger, S., Nikolic, B., and Brodersen, R.W. (2002) "*A design environment for high-throughput low-power dedicated signal processing systems*," IEEE Journal of Solid-State Circuits, **37**, pp. 420–431.

De Boer, E. (1961) "*Theory of Motional Feedback*," IRE Transactions on Audio, **AU-9**, pp. 15–21.

Dogan, A., Xu, Q., Onitsuka, K., Yoshikawa, S., Uchino, K., and Newnham, R.E. (1994) "*High Displacement Ceramic Metal Composite Actuators (Moonies)*," Ferroelectrics, **156**, pp. 1–6.

Dogan, A., Fernandez, J.F., Uchino, K., and Newnham, R.E. (1996) "*The Cymbal Electromechanical Actuator*," IEEE International Symposium on Applications of Ferroelectrics, **1**, pp. 213–216.

Dogan, A., Uchino, K., and Newnham, R.E. (1997) "*Composite Piezoelectric Transducer with Truncated Conical Endcaps 'Cymbal*," IEEE Transactions on Ultrasonics, Ferroelectrics, and Frequency Control, **44**, pp. 597–605.

Dogan, A., Tressler, J., Newnham, R.E. (2001) "*Solid-State Ceramic Actuator Designs*," AIAA, **39**(7).

Dongi, F., Dinkler, D., and Kroplin, B. (1995) "Active Panel Flutter Suppression using Self-Sensing Piezoactuators," 36th AIAA/ASME/ASCE/AHS/ASC Structures, Structural Dynamics and Materials Conference, New Orleans, LA, **95-1078**, pp. 2264–2272.

Donovan, J.F., Kral, L.D., and Cary, A.W., "*Active Flow Control Applied to an Airfoil*," AIAA, 98–0210.

Dosch, J.J., Inman, D.J. (1992) "*A self-sensing piezoelectric actuator for collocated control*," Journal of Intelligent Material Systems and Structures, **3**, pp. 166–185.

Elissalde, C., and Cross, L.E. (1995) "*Dynamic Characteristics of Rainbow Ceramics*," Journal of the American Ceramic Society, **78**, pp. 2233–2236.

Elvin, N., Elvin, A., Choi, D. H., 2003, *A Self Powered Damage Detection System*, Journal of Strain Analysis for Engineering Design, **38**, 2, p. 115–124.

Ericka, M., Vasic, D., Costa, F., Poulin, G., Tliba, S., 2005, *Energy Harvesting From Vibration Using a Piezoelectric Membrane*, Journal de Physique IV (Proceedings), **128**, pp. 187–93.

"*Flexural-Extensional Electromechanical Transducer*," 1967, Journal of the Acoustical Society of America, **41**, pp. 764.

Fanson, J.L., and Caughey, T.K. (1987) "Positive Position Feedback Control for Large Space Structures," 28th AIAA/ASME/ASCE/AHS/ASC Structures, Structural Dynamics and Materials Conference, Monterey, CA, **87-0902**, pp. 588–598.

Fox, R., Hellbaum, R., Bryant, R., and Copeland, B.(1997) "*Advanced Layered composite polylaminate electroactive actuator and sensor*,". US patent.

Fukada, E., Yasuda, J. (1964) "Piezoelectric Effects in Collagen," Japanese Journal of Applied Physics, 3, pp. 117.

Fukami, A., Yano, M., Tokuda, H., Ohki, M., and Kizu, R. (1994) "*Development of Piezo-Electric Actuators and Sensors for Electronically Controlled Suspension*," International Journal of Vehicle Design, **15**, pp. 348–357.

Fulton, M., and Ormiston, R.A. (1998) "*Use of Piezoelectric Actuators as Elements of Intelligent Structures*," Proceedings of the 54th American Helicopter Society Forum, Washington, D.C.

Frampton, K.D., Clark, R.L., and Dowell, E.H. (1995) "Active Control of Panel Flutter with Linearized Potential Flow Aerodynamics," 36th AIAA/ASME/ASCE/AHS/ASC Structures, Structural Dynamics and Materials Conference, New Orleans, LA, **95-1079.**

Jaffe, B., Cook, W., and Jaffe, H. (1971) "*Piezoelectric Ceramics*," R. A. N. Publishers, Marietta, OH, pp. 317.

Gad-el-Hak, M. (1998) "*Flow Control: Fundamentals and Practices*," Springer–Verlag, New York, pp. 527.

Gad-el-Hak, M. (2000) "*Flow Control: Passive, Active, and Reactive Flow Management*," Cambridge University Press, Cambridge United Kingdom.

Gogola, M., and Goldfarb, M. (1999) "*Design of a PZT-Actuated Proportional Drum Brake*," IEEE/ASME Transactions on Mechatronics, **4**, pp. 409–416.

Green, C., Mossi, K., Bryant, R. (2005) "*Scavenging energy from piezoelectric materials for wireless sensor applications*," ASME Proceedings of IMECE05, *ASME International Mechanical Engineering Congress and Exposition,* Orlando - Florida, USA, **IMECE2005-80426**.

Haertling, G.H., (1994a) "*Rainbow Ceramics—A New Type of Ultra High Displacement Actuator*," American Ceramic Society Bulletin, **73**(1), pp. 93–96.

Haertling, G.H. (1994b) "*Chemically Reduced PLZT Ceramics for Ultra High Displacement Actuators*," Ferroelectrics, **154**, pp. 101–106.

Haertling, G.H., and Robinson, G.C. (1997) "*Rainbow Actuators and Sensors: A New Smart Technology*," Proceedings of the SPIE—The International Society for Optical Engineering, **3040**, pp. 81–92.

Hall, S.R., and Prechtl, E.F. (1996) "*Development of a Piezoelectric Servoflap for Helicopter Rotor Control*," Smart Materials and Structures, **5**(1), pp. 26–34.

Hassan, A.A. (1998) "*Numerical Simulations and Potential Applications of Zero-Mass Jets for Enhanced Rotorcraft Aerodynamic Performance*", AIAA, 98–0211.

Hellbaum, F.R., Bryant, R.G., and Fox, R.L. (1997) "*Thin Layer Composite Unimorph Ferroelectric Driver and Sensor*," U.S. Patent No. **5,632,841**.

Herakovic, N. (1996) "*Die Untersuchung der Nutzung des Piezoeffektor zur Ansteurung Fluide Ventille,"* Ph. D. Dissertation, University of Aachen, Germany.

Ho, C.H., Tai, Y.C. (1996) "*Review: MEMS and Its Applications for Flow Control*," Journal of Fluids Engineering, **118**, pp. 437–447.

Hooker, M.W. (1997) "*Properties and Performance of Rainbow Piezoelectric Actuator Stacks*," Proceedings of the SPIE—The International Society for Optical Engineering, **3044**, pp. 413–420.

Hopkins, M., Henderson, D., Moses, R., Ryall, T., Zimcik, D., and Spangler, R. (1998) "*Active Vibration Suppression Systems Applied to Twin Tail Buffeting*," Proceedings of the SPIE—The International Society for Optical Engineering, **3326**, pp. 27–33.

Hyer, M.W. and Jilani, A.B. (2002) "*Deformation characteristics of circular RAINBOW actuators.* Smart Materials and Structures, **11**: pp. 175–195.

Janocha, H. (2004) "*Actuators: Basics and Applications*," 1st Edition, Saarbrucken: Springer, 336.

Jiles, D. (1995) "*Theory of the Magnetomechanical Effect*," Journal of Physics D: Applied Physics, **28**, pp. 1537–1546.

Jones, L., Garcia, E., and Waites, H. (1994) "*Self-sensing Control as applied to a Stacked PZT actuator used as a micropositioner*," Smart Materials and Structures, **3**, pp. 147–156.

Kaneko, T., Ohmi, T., Ohya, N., and Kawahara, N. (1998) "*A Compact and Quick-Response Dynamic Focusing Lens*," *Sensors and Actuators A*, **70**, pp. 92–97.

Katzir, S. (2003) "*The Discovery of the Piezoelectric Effect*," Archive of the History of Exact Sciences, **57**(1), pp. 61–91.

Kawai, H. (1969) "*The Piezoelectricity of Poly(vinylidene Fluoride)*," Japanese Journal of Applied Physics, 8, pp. 975–976.

Kim, S., Clark, W.W., Qing-Ming, W., 2005, *Piezoelectric energy harvesting with a clamped circular plate: experimental study*, *Journal of Intelligent Material Systems and Structures*, **16**, pp. 855–863.

Koratkar, N.A., and Chopra, I. (1999) "*Design, Fabrication and Testing of a Mach Scaled Rotor Model with Trailing-Edge Flaps*," Annual Forum Proceedings—American Helicopter Society, **1**, pp. 558–578.

Kral, L.D., Donovan, J.F., Cain, A.B., and Cary, A.W. (1997) "*Numerical simulation of synthetic set actuators*," 28th AIAA Fluid Dynamics Conference, 97–1824.

Kugel, V.D., Chandran, S., and Cross, L.E. (1997) "*A Comparative Analysis of Piezoelectric Bending-Mode Actuators*," Proceedings of the SPIE—The International Society of Optical Engineering, **3040**, pp. 70–80.

Lachman, G.V. (1961) "Boundary Layer Flow Control," Pergamon Press, **1**(2).

Le Letty, R., Claeyssen, F., Lhermet, N., and Bouchilloux, P. (1997) "*A New Amplified Piezoelectric Actuator for Precise Positioning and Active Damping*," Proceedings of the SPIE—The International Society for Optical Engineering, **3041**, pp. 496–504.

Lee, C.K. (1990) "*Theory of Laminated Piezoelectric Paltes for the Design of Distributed Sensors/Actuators, Part I and II*," Journal of Acoustic Society of America, **89**, pp. 1141–1158.

Lee, C.K., and Moon, F.C. (1990) "*Modal Sensors/Actuators*," Journal of Applied Mechanics, 57, pp. 434–441.

Lee, T., and Chopra, I. (1999) "*Development and Validation of a Refined Piezostack-Actuated Trailing Edge Flap Actuator for a Helicopter Rotor*," Proceedings of the SPIE—The International Society for Optical Engineering, **3668**, pp. 22–36.

Lorenz, R. (2001) "*Self-sensing motion control for electrical and hybrid electrical vehicles*," IEE Power Conversions and Applications Lecture, midlands Engineering Center, Birmingham, UK.

Mallinson, S.G., Reizes, J.A., Hong, G., and Buttini, M. (1999) "Synthetic Jet Actuators for Flow Control," SPIE Conference, **3891**, pp. 146–156.

Mane, P., Mossi, K., Rostami, A., Bryant, R., and Castro, N. (2007) "*Piezoelectric actuators as synthetic jets: Cavity dimension effects*," Journal of Intelligent Materials Systems and Structures, **18 (11),** 221–232.

Mane, P., Mossi, K., Bryant, R. (2008) "*Piezoelectric Synthetic Jets in Quiescent Air: Experimental Design and Analysis*," Smart Materials and Structures, **17**(1), 015013, 12pp.

Martinez, D.R., Hinnerichs, T.D., and Redmond, J.R. (1996) "*Vibration Control for Precision Manufacturing Using Piezoelectric Actuators*," Journal of Intelligent Material Systems and Structures, **7**, pp. 182–191.

McGowan, A.R., Wilkie, W.K., Moses, R.W., Lake, R.C., Florance, J.P., Wieseman, C.D., Reaves, M.C., Taleghani, B.K., Mirick, P.H., and Wilbur, M.L., (1998) "*Aeroservoelastic and Structural Dynamics Research on Smart Structures Conducted at NASA Langley Research Center*," Proceedings of the SPIE—The International Society for Optical Engineering, **3326**, pp. 188–201.

McLean, J.D., Crouch, J.D., Stoner, R.C., Sakurai, S., Seidel, G.E., Feifel, W.M., and Rush, H.M. (1999) "*Study of the application of separation control by unsteady excitation to civil transport aircraft*," Technical Report CR–1999–209338, NASA.

Montgomery, D.C. (2005) "*Design and Analysis of Experiments*," John Wiley & Sons Inc., New Jersey.

Moses, R.W. (1997) "*Vertical Tail Buffeting Alleviation Using Piezoelectric Actuators—Some Results of the Actively Controlled Response of Buffet-Affected Tails (ACROBAT) Program*," SPIE's 4th Annual Symposium on Smart Structures and Materials, Industrial and Commercial Applications of Smart Structures Technologies, **3044**, San Diego, California, pp. 87–98.

Moses, R. (1999) "*Contributions to Active Buffeting Alleviation Programs by the NASA Langley Research Center*," 40th AIAA/ASME/ASCE/ AHS/ASC Structures, Structural Dynamics, and Materials Conference, AIAA 99-1318, St. Louis, Missouri.

Mossi, K., Selby, G., Bryant, R. (1998) "*Thin-Layer Composite Unimorph Ferroelectric Driver and Sensor Properties*," Materials Letters, **35**, pp. 39–49.

Mossi, K.M., Bishop, R.P., Smith, R.C., and Banks, H.T. (1999) "*Evaluation Criteria for Thunder TM Actuators*," Proceedings of the SPIE—The International Society of Optical Engineering, **3667**, pp. 738–743.

Mossi, K., and Bryant, R.G. (2003) "*Piezoelectric Actuators for Synthetic Jet Applications*," Materials Research Society*, Material Research Society Fall Meeting,* **D11.8.**

Mossi, K., and Bryant, R.G. (2004) "*Pre-stressed Circular Actuators*," American Ceramic Society, pp. 445–454.

Mossi, K., Mane, P., and Bryant, R. (2005*a*) "*Velocity Profiles for Synthetic Jets Using Piezoelectric Circular Actuators*," AIAA, 2005-2341.

Mossi, K., Bryant, R., and Mane, P. (2005*b*) "*Piezoelectric composites as bender actuators,*" *Integrated Ferroelectrics*, **71**, pp. 221–232.

Mossi, K., Green, C., Ounaies, Z., Hughes, E. (2005*c*) "*Harvesting Energy Using a Thin Unimorph Prestressed Bender: Geometrical Effects*," *Journal of Intelligent Material Systems and Structures*, **16**, pp. 249–261.

Mukherjee, B.K., Ren, W., Liu, S-F, Masys, A.J., and Yang, G. (2001) "*Non-Linear Properties of Piezoelectric Ceramics*," SPIE Smart Structures and Materials, San Diego, CA.

Murphy, T.P. (2004) "*Comparing the SMART Stent with the Wallstent Iliac Endoprosthesis: Reading Between the Line,"* Journal of Vascular and Interventional Radiology, **15,** pp. 907–909.

Niezrecki, C., Brei, D., Balakrishnan, S., and Moskalik, A. (2001) "*Piezoelectric Actuation: State of the Art*." The Shock and Vibration Digest, **33**(4), pp. 269–280.

Onitsuka, K., Dogan, A., Tressler, J.F., Xu, Q., Yoshikawa, S., and Newnham, R. (1995) "*Metal-Ceramic Composite Transducer, the Moonie*," Journal of Intelligent Material Systems and Structures, **6**, pp. 447–455.

Ottoman, G.K., Hofmann, H.F., Bhatt, A.C., Leisieutre (2002) "*Adaptive Piezoelectric Energy Harvesting Circuit for Wireless Remote Power Supply*," IEEE Transactions on Power Electronics, **17**(5).

Ottoman, G.K., Hofmann, H.F., Leisieutre (2003) "*Optimized Piezoelectric Energy Harvesting CircuitUsing Step-Down Converter in Discontinuous Conduction Mode*," IEEE Transactions on Power Electronics, **18**(2).

Ounaies, Z., Mossi, K, Smith, R., and Bernd, J. (2001). "*Low-field and high-field characterization of THUNDER actuators*," SPIE Smart Structures and Materials, San Diego, CA.

Park, C.H. (2001) "*On the circuit model of piezo-ceramics*," Journal of Intelligent Material Systems and Structures, **12(**7), pp. 515–522.

Park, K.H., Kim, Y.B., Kim, Y.S., Park, H.C., and Yoon, K.J. (2001) "*Experimental Performance Evaluation of Lightweight Piezo-Composite Curved Actuators*," SPIE Conference, 4699–41.

Pokines, B.J., and Garcia, E. (1998) "*A Smart Material Microamplification Mechanism Fabricated Using LIGA*," Smart Materials and Structures, **7**, pp. 105–112.

Pratt, J. (1993) "*Design and analysis of a self-sensing Terfenol-D magnetostrictive actuator*," M.S. Thesis, Iowa State University.

Prechtl, E.F., and Hall, S.R. (1997) "*Design of a High Efficiency Discrete Servo Flap Actuator for Helicopter Rotor Control*," Proceedings of the SPIE—The International Society for Optical Engineering, **3041**, pp. 158–182.

Prechtl, E.F., and Hall, S.R. (1998) "*An X-Frame Actuator Servo-Flap Actuation Systme for Rotor Control*," Proceedings of the SPIE—The International Society for Optical Engineering, **3329**, pp. 309–319.

Ramsay, J.V., and Mugridge, E.G.V. (1962) "*Barium Titanate Ceramics for Fine-Movement Control*," Journal of Scientific Instruments, **39**, pp. 636–637.

Rathnasingham, R., Breuer, K., S. (1997*a*) "*Coupled fluid-structural characteristics of actuators for flow control*," AIAA, **J 35**, pp. 832–837.

Rathnasingham, R., Breuer, K., S. (1997*b*) "*System Identification and Active Control of a Turbulent Boundary Layer*," PhD Dissertation, MIT.

Redmond, J., and Barney, P. (1997) "*Vibration Control of Stiff Beams and Plates Using Structurally Integrated PZT Stack Actuators*," Journal of Intelligent Material Systems and Structures, **8**, pp. 525–535.

Rizetta, D.P., Visbal, M.R., and Stanek, M.J. (1999) "Numerical Investigation of Synthetic Jet Flow Fields, AIAA Jounal, **9**, pp. 919–927.

Roundy, S. (2003) "*Energy Scavenging for Wireless Sensor Nodes with a Focus on Vibration to Electricity Conversion*," Mechanical Engineering. Berkley: University of California Berkley.

Roundy, S., Wright, P.K., and Rabaey, J. (2003) "*A Study Of Low Level Vibrations as a Power Source for Wireless Sensor Nodes,"* Computer Communications, **26**(11), pp.1131–1144.

Roundy, S., Wright, P. K., and Rabaey, J. (2004) "*Energy Scavenging For Wireless Sensor Networks*," Kluwer Academic Publishers, Boston.

Royster, L.H. (1970) "*The Flextensional Concept: A New Approach to the Design of Underwater Acoustic Transducers*," Applied Acoustics, **3**, pp. 117–126.

Rumsey, C.L., Gatski, B., Sellers, W.L., Vatsa, V., and Viken A. (2004) "*Summary of the 2004 CFD Validation Workshop on Synthetic Jets and Turbulent Separation Control*," AIAA, 2004-2217

Samak, D.K., and Chopra, I. (1996) "*Design of High Force High Displacement Actuators for Helicopter Rotors*," Smart Materials and Structures, **5**, pp. 58–67.

Sawyer, C.B. (1931) "*The Use of Rochelle Salt Crystals for Electrical Reproducers and Microphones*," Proceedings of the Institute of Radio Engineers, **19**, pp. 2020–2029.

Schaeffler, N., and Jenkins, L. (2004) "*The Isolated Synthetic Jet in Crossflow: A Benchmark for Flow Control Simulation*," AIAA, 2004–2219.

Schwartz, R.W., Laoratanakul, P., Nothwang, W.D., Ballato, J.M., Moon, Y., and Jackson, A. (2000) "*Understanding Mechanics and Stress Effects in Rainbow and Thunder Stress-biased Actuators*," Proceedings of the SPIE—The International Society for Optical Engineering.

Schwartz, R.W., and Moon, Y.W. (2001) "*Domain Configuration and Switching Contributions to the Enhanced Performance of Rainbow Actuators*," Proceedings of the SPIE—The International Society for Optical Engineering, **4333** (408).

Schwartz, R.W. and Narayanan, M. (2002) "*Development of High performance stress-biased actuators through the incorporation of mechanical pre-load*," Sensors and Actuators A, **101**: pp. 322–331.

Schubauer G.B. and Skramstad H.K. (1947) "Laminar Boundary Layer Oscillations and Stability of Laminar Flow." Journal of the Aeronautical Sciences, 14(2), pp. 69–78.

Seifert, A., Bachar, T., Koss, D., Shepshelovich, M., Wygnanski, I. (1993) "*Oscillatory Blowing: A Tool to delay Boundary-Layer Separation*," AIAA Journal, **31(**11).

Seifert, A., Darabi, A., Wygnanski, I. (1996) "*Delay of Airfoil Stall by Periodic Excitation*," Journal of Aircraft, **33(**4).

Seifert, A., and Pack, L.G. (1999) "*Oscillatory Control of Separation at High Reynolds Numbers*", AIAA Journal, **37**, pp. 1062–1071.

Shakeri, C., Bordonaro, C.M., Noori, M.N., and Champagne, R. (1999) "*Experimental Study of THUNDER: A New Generation of Piezoelectric Actuators*," Proceedings of the SPIE—The International Society for Optical Engineering, **3675**, pp. 63–71.

Sherrit, S., Stimpson, R.B., Weiderick, H.D., Mukherjee, B.K. (1996) "*Stress and temperature dependence of the direct piezoelectric charge coefficient in lead zirconate titanate ceramics*," SPIE Smart Structures and Materials Conference, San Diego, CA.

Sherrit, S., Yang, G., Wiederick, H.D., Mukherjee, B.K. (1999) "*Temperature Dependence of the Dielectric, Elastic and Piezoelectric Material Constants of Lead Zirconate Titanate Ceramics*," Smart Material, Structures and Systems, Bangalore, India.

Shu, S.G., Lagoudas, D.C., Hughes, D., and Wen, J.T. (1997) "*Modeling of a flexible beam actuated by shape memory alloy wires*," Smart Materials and Structures, 6, pp. 265–277.

Simmers Jr., G.E., Hodgkins, J.R., Mascarenas, D.D., Gyuhae, P., and Sohn, H. (2004) "*Improved Piezoelectric Self-sensing Actuation*," Journal of Intelligent Material Systems and Structures, 15(12), pp. 941–953.

Smith, B.L.,and Glezer, A. (1998) "*The formation and evolution of synthetic jets*," Physics of Fluids, **10**, pp. 2281–2297.

Smith, B.L. (1999) "*Synthetic Jets and their Interaction with Adjacent Jets*," PhD Thesis, Georgia Institute of Engineering, pp. 143.

Sodano, H.A., Park, G., and Inman, D.J. (2004) "*An investigation into the performance of macro-fiber composites for sensing and structural vibration applications*," Mechanical Systems and Signal Processing, **18**, pp. 683–697.

Sodano, H.A., Leo, D., Inman, D.J. and Park, G. (2005) "*Comparison Of Piezoelectric Energy Harvesting Devices For Recharging Batteries*," Journal of Intelligent Material Systems and Structures, **16**(10), pp. 799–807.-

Sodano, H. A., Lloyd, J., and Inman, D.J. (2006) "*An experimental comparison between several active composite actuators for power generation*," Smart Materials and Structures, **15**, pp. 1211–1216.

Spangler, R.L., and Hall, S.R. (1989) "*Piezoelectric Actuators for Helicopter Rotor Control*," Report No. SSL I-89, SERC 14-90, MIT Space Engineering Research Center, Massachusetts Institute of Technology.

Steel, M.R., Harrison, F., and Harper, P.G. (1978) "*The Piezoelectric Bimorph: An Experimental and Theoretical Study of Its Quasistatic Response*," Journal of Physics D: Applied Physics, **11**, pp. 979–989.

Stiffler, R. and Henneke II, E.G. (1983) "*The Application of Polyvinylidene Fluoride as an Acoustic Emission Transducer for Fibrous Composite Materials*," Materials Evaluation, 44(8), pp. 956–960.

Straub, F.K. (1993) "*A Feasibility Study of Using Smart Materials for Rotor Control*," 49th Annual Forum of the American Helicopter Society, St. Louis, Missouri.

Straub, F.K. (1999) "*Development of a Full Scale Smart Rotor System*," *8th ARO Workshop on Aeroelasticity of Rotorcraft Systems*, State College, Pennsylvania.

Straub, F.K., Ngo, H.T., Anand, V., and Domzalski, D.B. (1999) "*Development of a Piezoelectric Actuator for Trailing Edge Flap Control of Rotor Blades*," SPIE Symposium on Smart Structures and Materials, **3688**, Newport Beach, California, pp. 2–13.

Sugawara, Y., Onitsuka, K., Yoshikawa, S., Xu, Q.C., Newnham, R.E., and Uchino, K. (1992) "*Metal-Ceramic Composite Actuators*," Journal of the American Ceramic Society, **75**, pp. 996–998.

Suplee, C. (1997) "*Is the Sky the Limit in the Future?*," Virginia Post, pp. D4.

Tamura, M., Yamguchi, T., Oyaba, T., and Yoshimi, T. (1975) "*Electroacoustic Transducers with Piezoelectric High Polymer Films*," Journal of Audio Engineering Society, 23(1), pp. 21–26.

Tang, H., Zhong, S., Jabbal, M., Garcillan, L., Guo, F., Wood, N., and Warsop, C. (2007) "*Towards the Design of Synthetic-jet Actuators for Full-scale Flight Conditions Part 2: Low-dimensional Performance Prediction Models and Actuator Design Method*," Flow Turbulence Combust, **78**, pp. 309–329.

Tasaka, S., and Miyata, S. (1985) "*Effect of Crystal-Structure on Piezoelectric and Ferroelectric Properties of CoPoly-(Vinylidenefluoride-Tetrafluoroethylene)*," Journal of Applied Physics, **57**(3), pp. 906–910.

Tzou, H.S., and Hollkman, J.J. (1994) "*Collocated Independent Modal Control with Self-Sensing Orthogonal Piezoelectric Actuators (Theory and Experiment)*," Smart Materials and Structures, 3, pp. 147–156.

Timoshenko, S., 1959, *Theory of Plates and Shells*, New York: McGraw-Hill, Second Edition.

Tzou, H.S. (1989) "*Development of a Light-Weight Robot End-Effector Using Polymeric Piezoelectric Bimorph*," Proceedings of the 1989 International Conference on Robotics and Automation, **3**, IEEE, **89CH2750**, IEEE Computer Society, Washington, DC, pp. 1704–1709.

U.S.F.D.A, *New Device Approval*, in *CDRH Consumer Information*. 2003.

Usher, T. and Sim, A. (2005) "*Nonlinear dynamics of piezoelectric high displacement actuators in cantilever mode,"* Journal of Applied Physics, **98**.

Vallone, P. (1995) "*High-performance Piezo-based Self-sensing for structural Vibration Control*," Proceedings of 2nd SPIE Smart Structures and Materials Conference, Newport Beach, CA, 2443, pp. 643–655.

Vinogradov, A. M., Schumacher, S. C., Rassi, E. M., 2005, Dynamic response of the piezoelectric polymer PVDF, Jounral of Applied Electromagnetics and Mechanics, 22(1-2), pp. 39–51.

Walz, C., and Chopra, I. (1994) "*Design, Fabrication, and Testing of a Helicopter Rotor Model with Smart Trailing Edge Flaps*,"Proceedings of the AIAA/ASME/ASCE/AHS/ASC 35th Structures, Structural Dynamics, and Materials Conference—Adaptive Structures Forum, Hilton Head, South Carolina, pp. 298–319.

Wang, T.T., Herbert, J.M., and Glass, A.M. (1988) "*The Applications of Ferroelectric Polymers*," Chapman and Hill, New York.

Webber, K.G., Hopkinson, D.P., and Lynch, C.S. (2006) "*Application of a Classical Lamination Theory Model to the Design of Piezoelectric Composite Unimorph Actuators*," Journal of Intelligent Material Systems and Structures, 2006. **17**(1), pp. 29–34.

Whatmore, R.W. (1986) "*Pyroelectric devices and materials*," Reports on Progress in Physics, **49**, pp. 1335–1386.

Wheeler, A.J., and Ganji, A.R. (2003) "*Introduction to Engineering Experimentation*," Prentice Hall, Second Edition.

Winslow, W. (1947) "Method and means for translating electrical impulses into mechanical force," Patent No. **2,417,850**, USA.

Winslow, W. (1949) "*Induced fibration of suspensions*," Applied Physics, **20,** pp. 1137–1140.

Wise, S.A. (1998) "*Displacement Properties of Rainbow and Thunder Piezoelectric Actuators*," Sensors and Actuators A, **69**, pp. 33–38.

Wood, N.J., Sadri, A.M., and Crook, A. (2000) "Control of Turbulent Separation by Synthetic Jets," AIAA, 2000–4331.

Yang, R., Jouaneh, M., and Schweizer, R. (1996) "*Design and Characterization of a Low-Profile Micropositioning Stage*," Precision Engineering, **18**, pp. 20–29.

Yang, G., Liu, S.-F., Ren, W., and Mukherjee, B.K. (2000) "*Uniaxial Stress Dependence of the Piezoelectric Properties of Lead Zirconate Titanate*," Proceedings of SPIE Smart Structures and Materials Conference, Newport Beach, CA, 3992, pp. 103–106.

Yao, C., Chen, F., Neuhart, D., and Harris, J (2004) "*Synthetic Jet Flow Field Database for CFD Validation*," AIAA, 2004-2218.

Yoon, K.J., Shin, S., Park, H.C., and Goo, N.S. (2002) "*Design and Manufacture of Lightweight Piezoceramic Curved Actuator,*" Smart Materials and Structures, **11**, pp. 163–168.

Yoon, K.J., Park, K.H., Park, H.C., Lee, S.K., and Goo, N.S. (2003*a*) "*Analytical Design Model for a Piezo-Composite Unimorph Actuator and its verification using Lightweight Piezo-Composite Curved Actuators*", Smart Materials and Structures, **13**, pp. 459–467, 2003*a*.

Yoon, K.J., Park, K.H., Park, H.C. and Perraux, D. (2003*b)* "*Thermal Deformation Analysis of Curved Actuator LIPCA with Piezoceramic Layer and Fiber Composite Layers*," Composites Science and Technology, **63**, pp. 501–506, 2003*b*.

Yoon, H.S., Washington, G., and Danak, A. (2005) "*Modeling, Optimization, and Design of Efficient Initially Curved Piezoceramic Unimorphs for Energy Harvesting Applications*," Journal of Intelligent Material Systems and Structures, **16**, pp. 877–888.

Zhong, S., Garcillan, L., Pokusevski, Z., Wood, N. (2004) "*A PIV study of synthetic jets with different orifice shape and orientation*," AIAA, 2004–2213.

Zhong, S., Jabbal, M., Tang, H., Garcillan, L., Guo, F., Wood, N., and Warsop, C. (2007) "*Towards the Design of Synthetic-jet Actuators for Full-scale Flight Conditions Part 1: The Fluid Mechanics of Synthetic-jet Actuators*," Flow Turbulence Combust, **78**, pp. 283–307.

Appendix A

Hotwire Calibration

Mathcad Program for Converting Hotwire Voltages to Velocities

i:=0..2501

Bridge=

	0
0	0.969
1	0.975
2	0.969
3	0.963
4	0.963
5	0.956
6	0.956
7	0.95

Enter Bridge Voltage Displayed:

Data Collected

10.22698071	1.1972
11.390362	1.2147
12.56376891	1.2342
14.06382435	1.253
15.02994005	1.266
16.79627886	1.2842
18.19159262	1.2971
19.25816471	1.3103
19.90040502	1.3214
21.78147118	1.3384
23.88705169	1.3583

Velocity Voltage

$x := fit^{\langle 0 \rangle}$ $y := fit^{\langle 1 \rangle}$

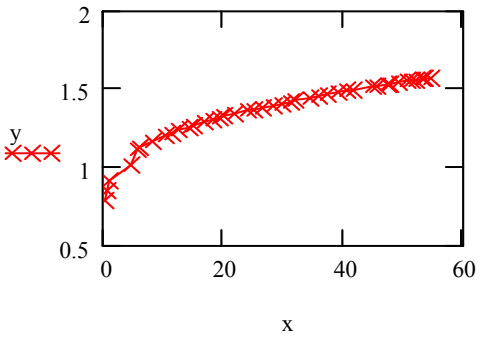

Plot of x and y

$X := fit^{\langle 0 \rangle}$ $Y := fit^{\langle 1 \rangle}$ $n := rows(fit)$

Enter degree of polynomial to fit:

$k := 4$

Number of data points:

$n = 41$

$z := regress(X, Y, k)$

Polynomial fitting function:

$fit(x) := interp(z, X, Y, x)$

$coeffs := submatrix(z, 3, length(z) - 1, 0, 0)$

Coefficients:

$$coeffs^T = \begin{pmatrix} 0.827 & 0.056 & -2.409 \times 10^{-3} & 5.076 \times 10^{-5} & -3.842 \times 10^{-7} \end{pmatrix}$$

R^2:
$$\frac{\overrightarrow{\sum (fit(X) - mean(Y))^2}}{\overrightarrow{\sum (Y - mean(Y))^2}} = 0.994$$

Degrees of freedom: $n - k - 1 = 36$

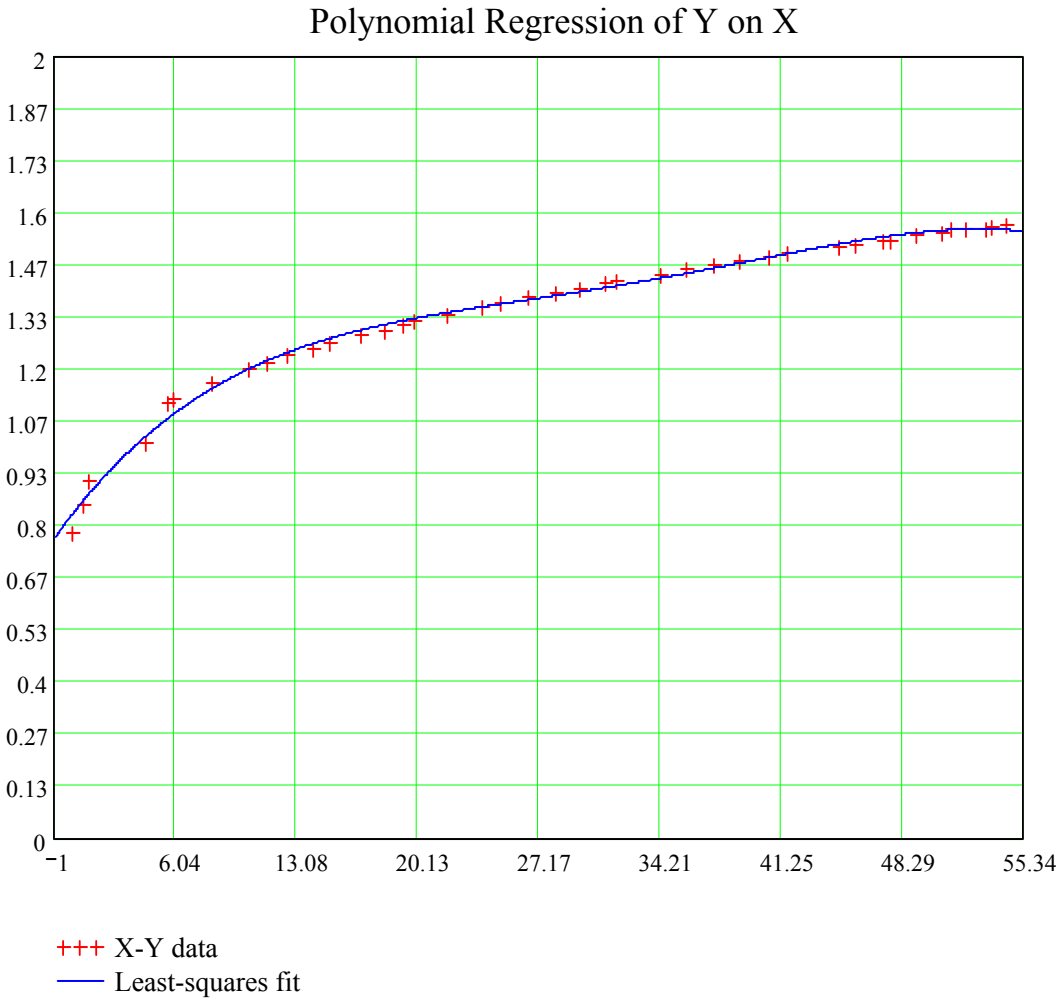

$$\text{scale} := \max\left(\left|\overrightarrow{\text{fit}(X) - Y}\right|\right) \cdot 1.1$$

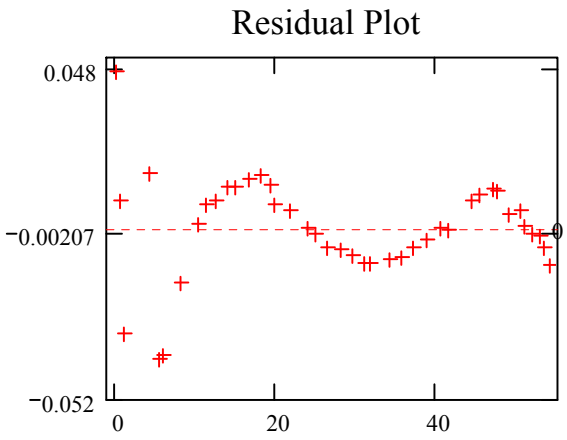

$$\text{coeffs} = \begin{pmatrix} 0.827 \\ 0.056 \\ -2.409\times 10^{-3} \\ 5.076\times 10^{-5} \\ -3.842\times 10^{-7} \end{pmatrix}$$

$$\text{velocity}_i := \text{root}\left(\text{coeffs}_{0,0} + \text{coeffs}_{1,0}\cdot g + \text{coeffs}_{2,0}\cdot g^2 + \text{coeffs}_{3,0}\cdot g^3 + \text{coeffs}_{4,0}\cdot g^4 - \text{Bridge}_i, g, -1, 54.4\right)$$

Velocity determined from the bridge voltage is:

velocity =

	0
0	2.862
1	3.001
2	2.862
3	2.725
4	2.725
5	2.567
6	2.567
7	2.433
8	2.301
9	2.301
10	2.301
11	2.021
12	2.171
13	2.021
14	2.021
15	2.021

Calibration Setup

The calibration setup consisted of a standard pipe flow, with a pitot tube and an electronic pressure transducer as the calibration standard. As fully developed flow is required for calibration, the pipe had to be sufficiently long. In order to reduce turbulence, flow straightening devices were distributed along the length of the pipe that consisted of honeycombed PVC pipe distributed in several sections was used. Various experiments were conducted with different combinations of length and number of the honeycombs until fully developed flow was achieved. Different types of nozzles and diffusers were considered in finding the desired flow condition, fully-developed flow. The nozzle used at the mouth of the wind tunnel was a 9.53 mm male quick release fitting, mounted onto an aluminum bracket that is fixed into a 187.33 mm diameter coupler. The coupler was reduced to an 88.9 mm outside diameter pipe that was 2.52 m in length. The nozzle was situated in the wind tunnel pipe, which was fitted into the 88.9 mm diameter *PVC* pipe. Foam was used around the pipe to dampen the oscillations that the tunnel would produce during operation as they could have a significant effect on the pressure. The actual wind tunnel pipe that would become the calibration diameter was 19.05 mm diameter. This section of pipe was cut to a length of 2.65 m and measurements were taken at 2.48 m from the nozzle at the tunnel inlet. The hotwire was calibrated for use in airflows having velocities ranging from 0 to 60 m/sec. A picture of the nozzle flow coupler is shown in Figure A-1 (a) and (b). The calibration facility along with the air supply assembly is shown in Figure A-1 (b).

(a)

(b)

Figure A–1 Hotwire Calibration Facility, (a) nozzle flow coupler, (b) calibration pipe and air supply assembly

Appendix B

Additional Results from Synthetic Jet Actuator Study

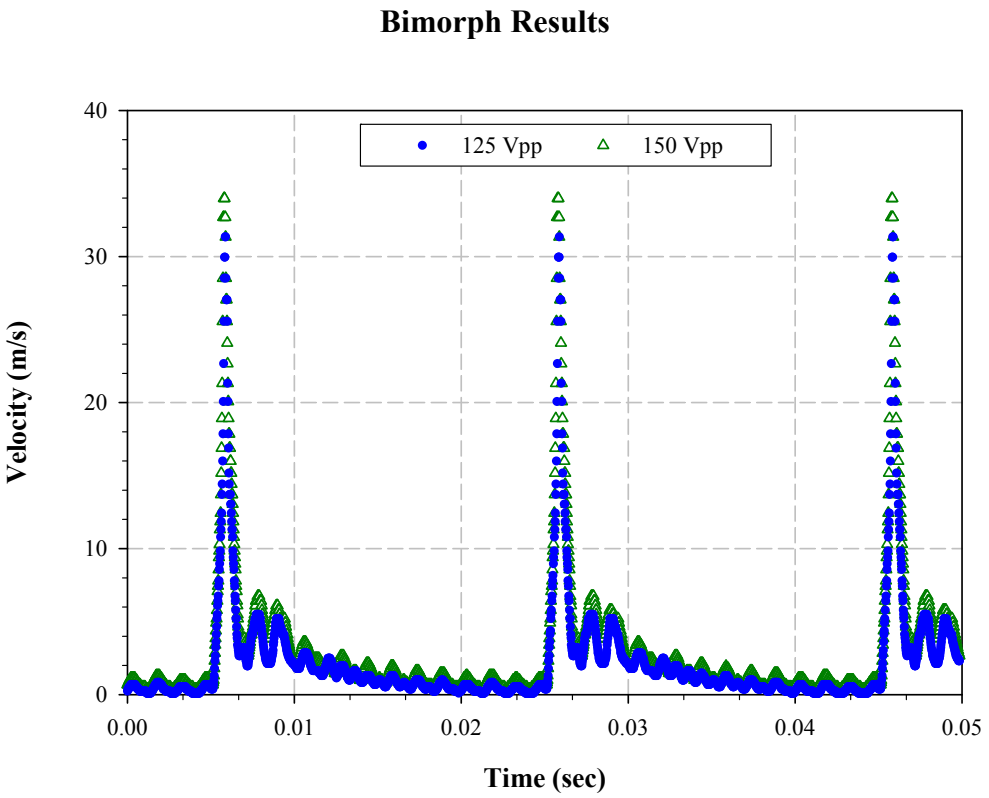

Figure B-1 Effect of Voltage on Velocity Magnitude with Cavity IV for a Bimorph Diaphragm at 50 Hz using a Sawtooth Signal

Metal Composite Results

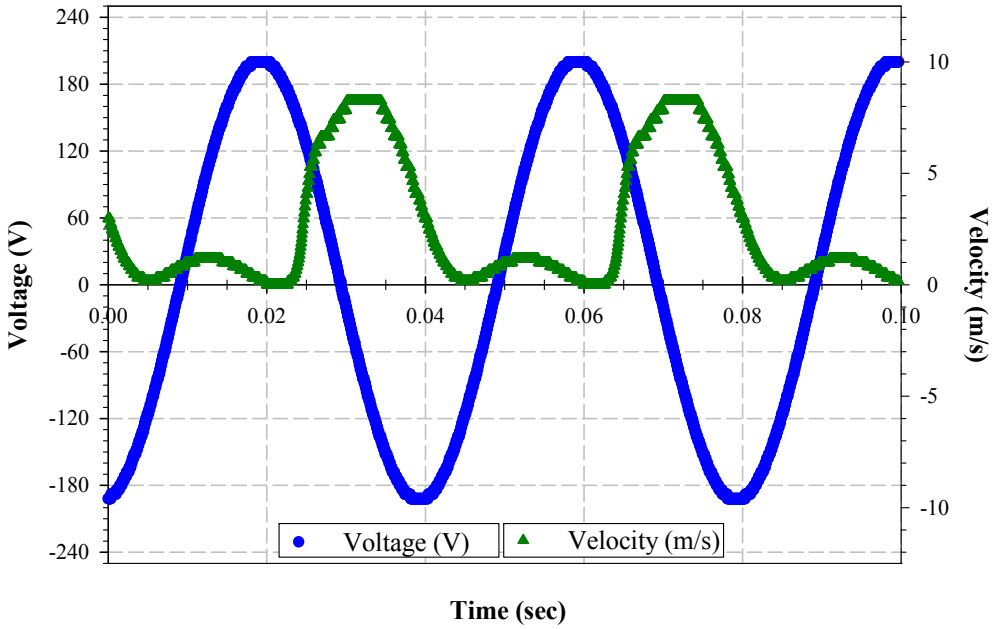

Figure B-2 Typical Velocity Curve with Sine Driving Voltage with Cavity IV for a Prestressed Metal composite Diaphragm at 25 Hz and 400 Vpp

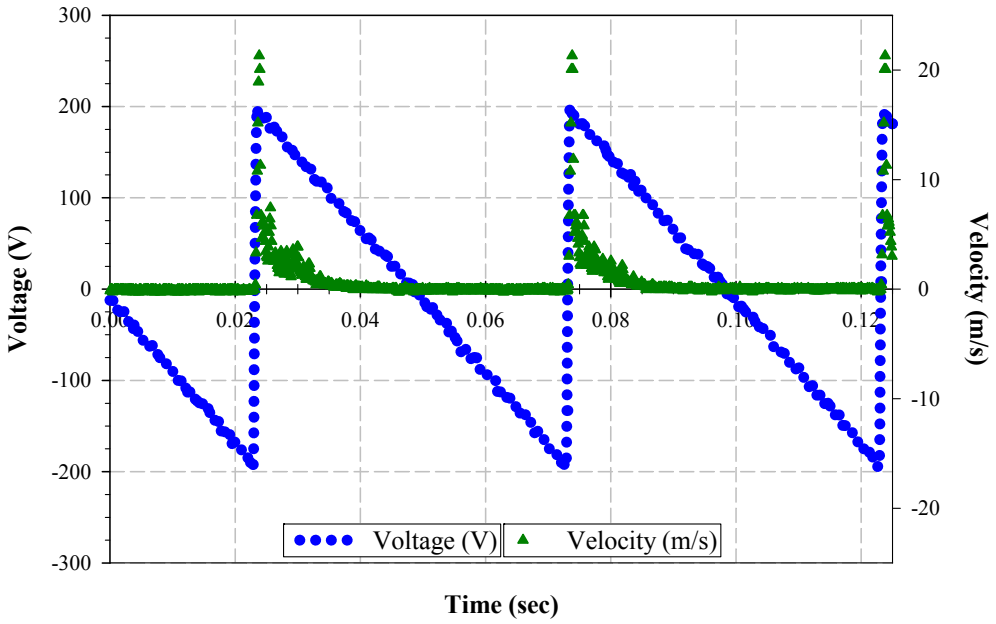

Figure B-3 Typical Velocity Curve with Sawtooth Driving Voltage with Cavity IV for a Prestressed Metal composite Diaphragm at 25 Hz and 400 Vpp

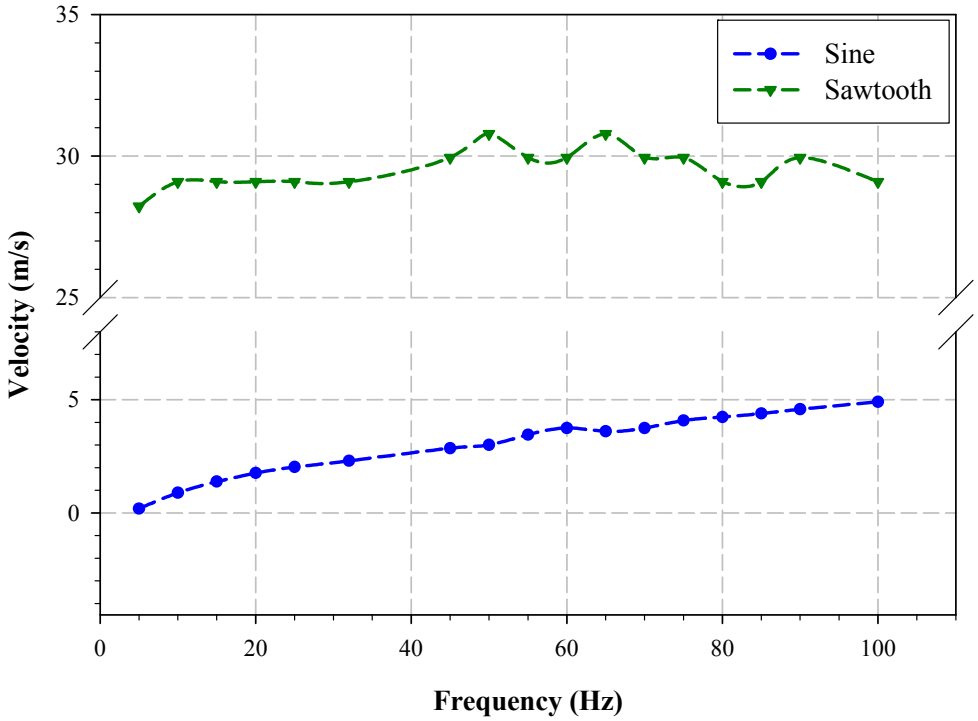

Figure B-4 Frequency Effects on Prestressed Metal composite Diaphragm Peak Velocities for Cavity IV at 400 Vpp

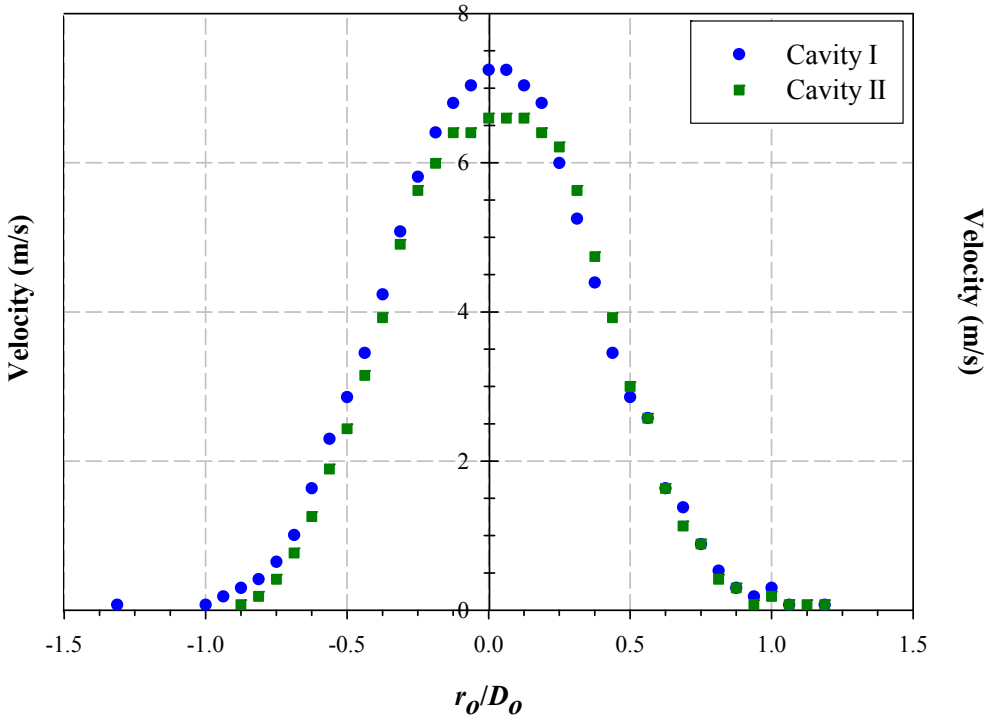

Figure B-5 Cavity Height Effects shown using Cavities I and II for a Prestressed Metal composite Diaphragm at 32 Hz and 400 Vpp with a Sine Driving Signal

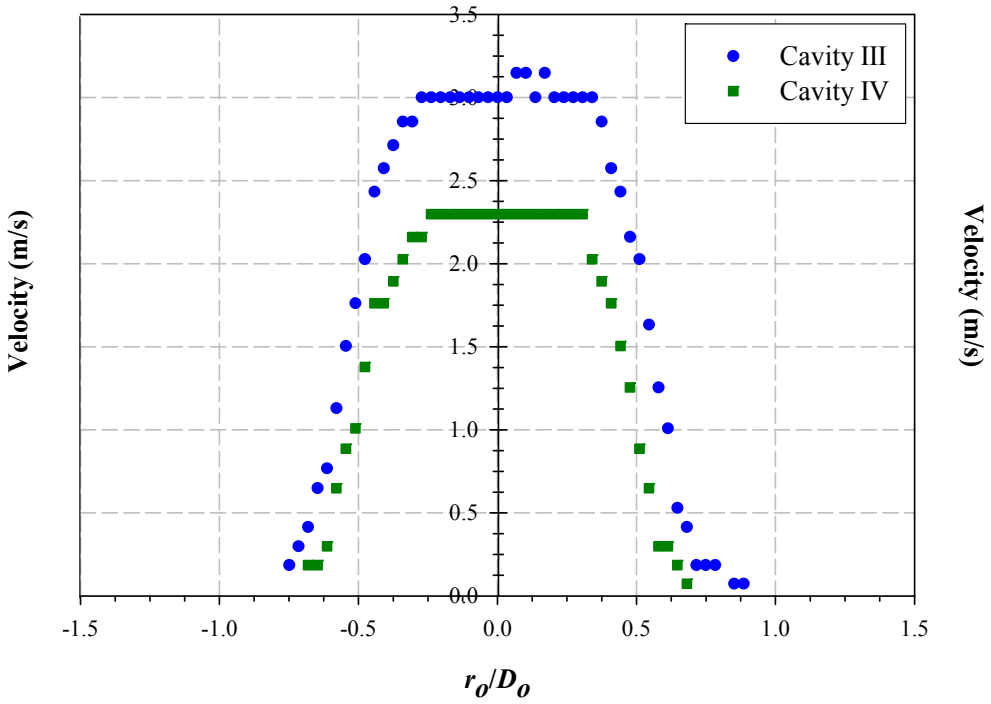

Figure B-6 Cavity Height Effects shown using Cavities III and IV for a Prestressed Metal composite Diaphragm at 32 Hz and 400 Vpp with a Sine Driving Signal

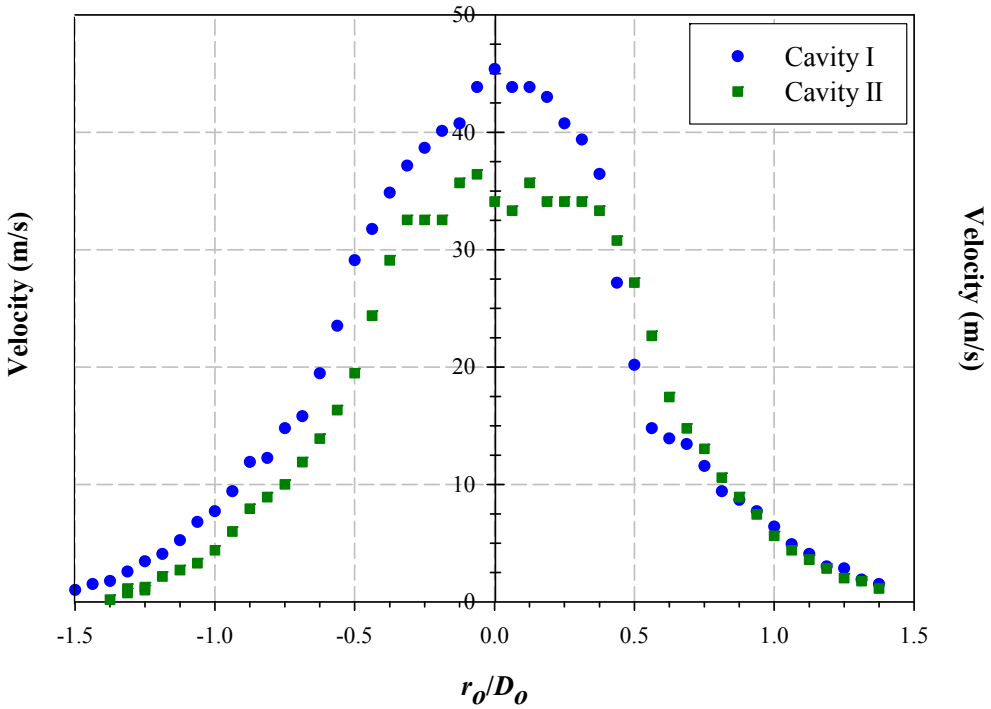

Figure B-7 Cavity Height Effects using a Sawtooth Driving Signal for a Prestressed Metal composite Diaphragm at 32 Hz and 400 Vpp

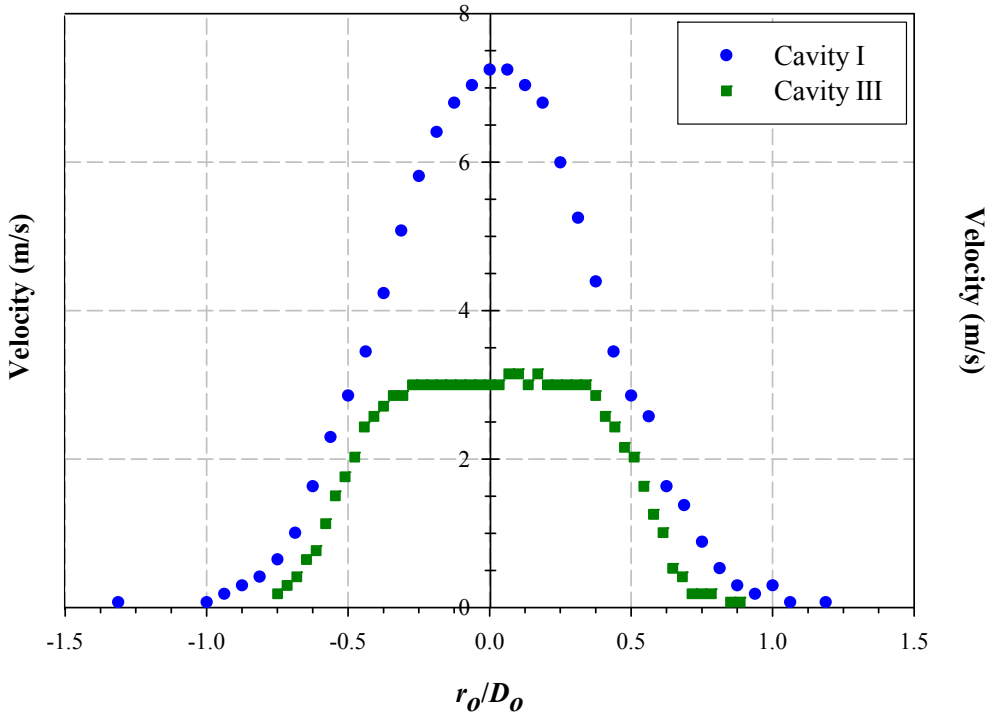

Figure B-8 Orifice Size Effects using a Sine Driving Signal for a Prestressed Metal composite Diaphragm at 32 Hz and 400 Vpp

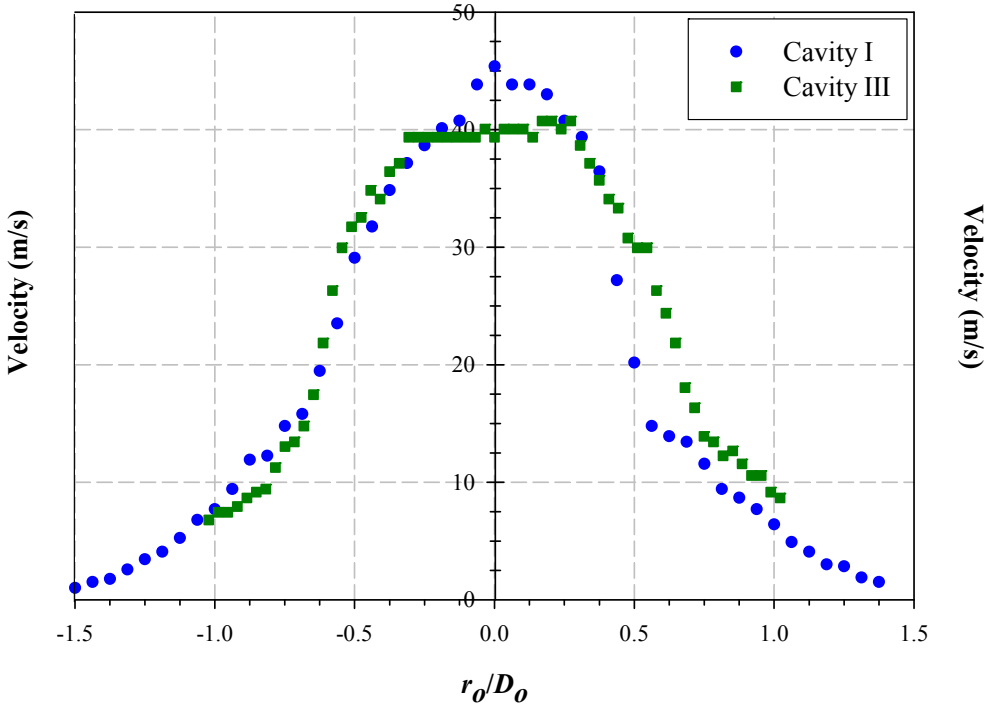

Figure B-9 Orifice Size Effects using a Sawtooth Driving Signal for a Prestressed Metal composite Diaphragm at 32 Hz and 400 Vpp

Table B-1 Regression Analysis for a Prestressed Metal composite Device

SUMMARY

Regression Statistics	
Multiple R	0.96921
R Square	0.93936
Adjusted R Square	0.91732
Standard Error	4.54818
Obs.	16

ANOVA

	df	*SS*	*MS*	*F*	*Sig. F*
Regression	4	3525.13489	881.28372	42.60305	1.245E-06
Residual	11	227.54521	20.68593		
Total	15	3752.68010			

	Coeffs.	*Standard Error*	*t Stat*	*P-value*	*Lower 95%*	*Upper 95%*	*Lower 95.0%*	*Upper 95.0%*
Intercept	18.28700	1.13704	16.08292	5.460E-09	15.78438	20.78962	15.78438	20.78962
F_z	-13.91638	1.13704	-12.23908	9.495E-08	-16.41899	-11.41376	-16.41899	-11.41376
E	2.69675	1.13704	2.37172	0.03704	0.19413	5.19937	0.19413	5.19937
D_o	-3.15625	1.13704	-2.77584	0.01804	-5.65887	-0.65363	-5.65887	-0.65363
C_H	-3.06938	1.13704	-2.69943	0.02068	-5.57199	-0.56676	-5.57199	-0.56676

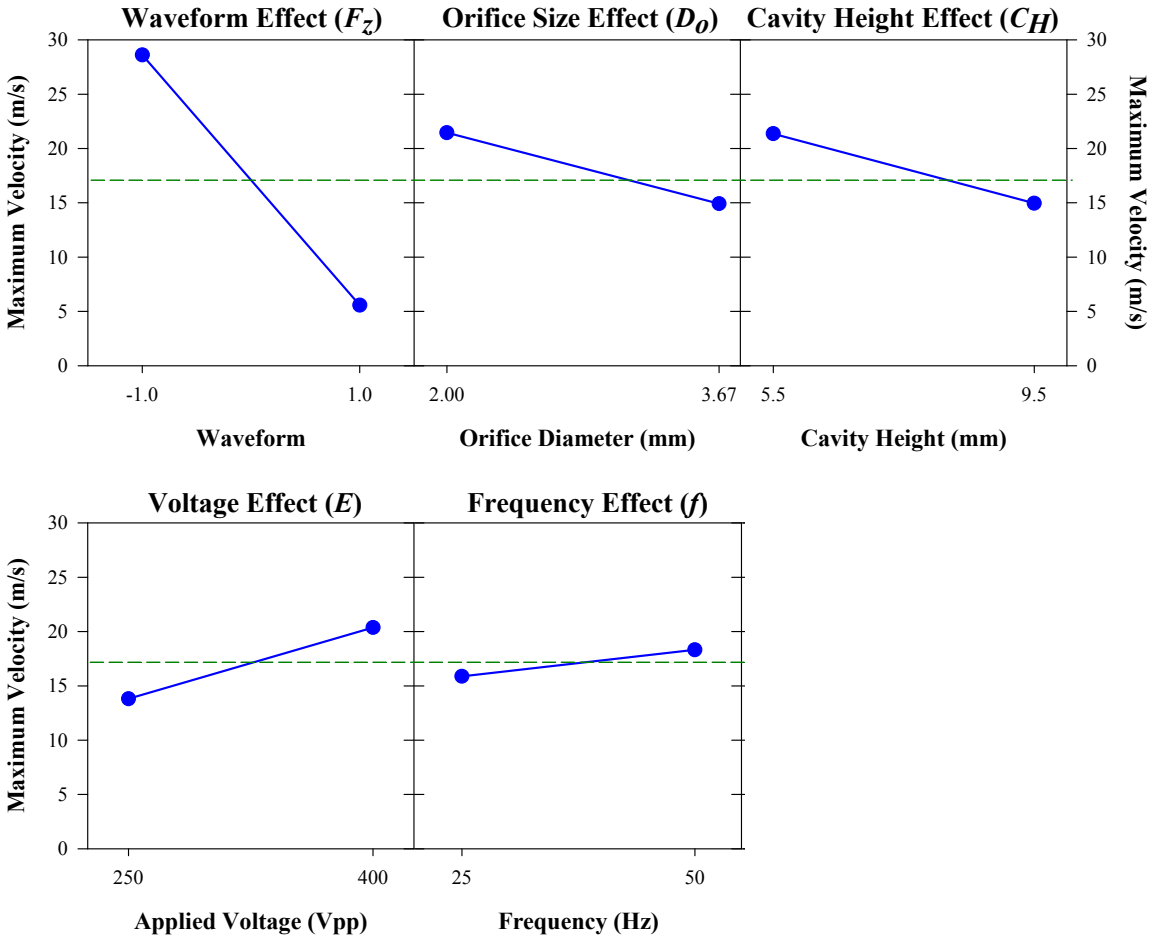

Figure B-10 Average factor effect size

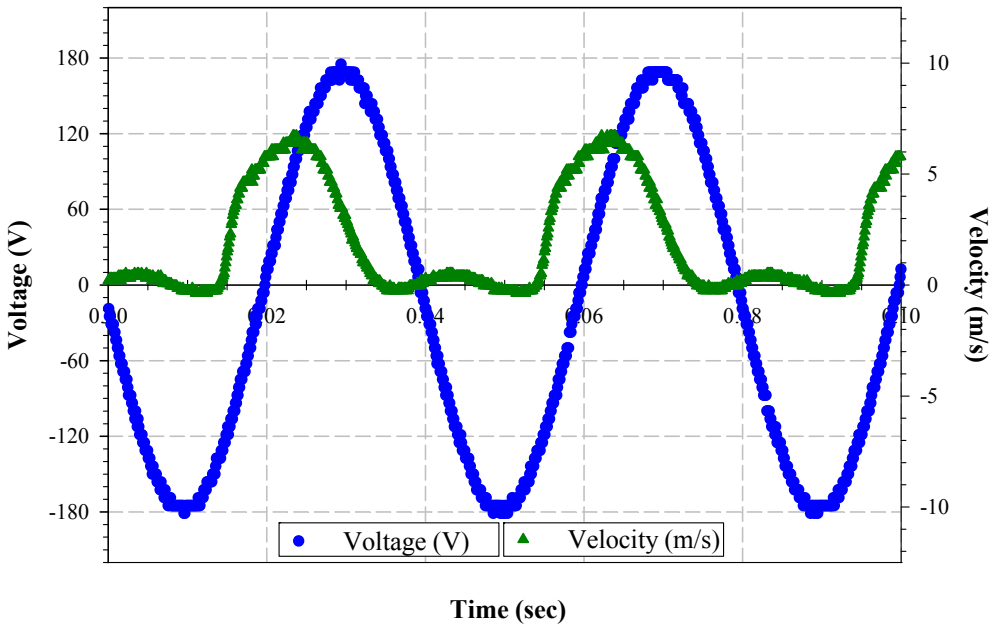

Figure B-11 Typical Velocity Curve with Sine Driving Voltage with Cavity I for a Lipca Diaphragm at 25 Hz and 350 Vpp

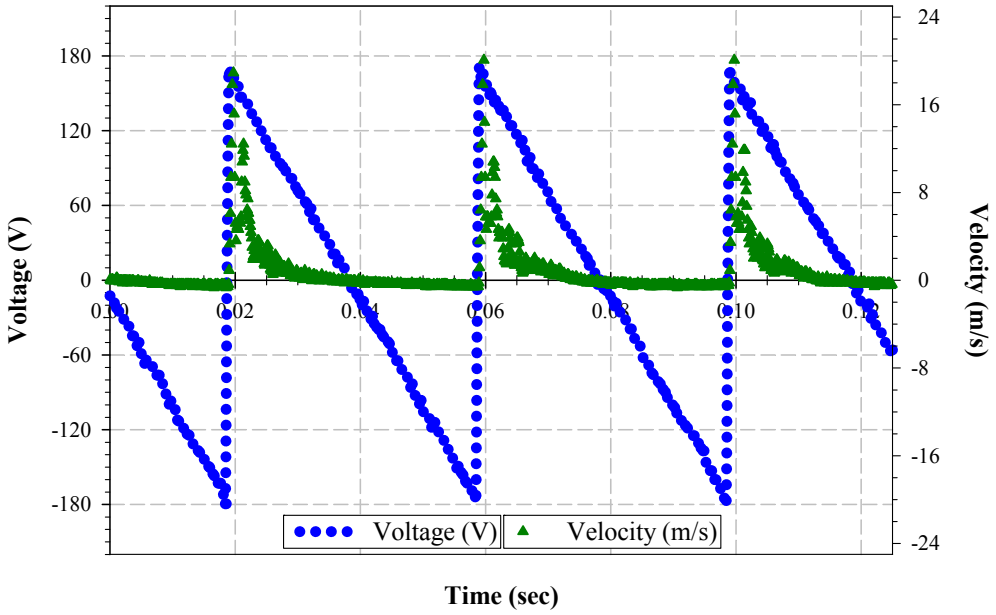

Figure B-12 Typical Velocity Curve with Sawtooth Driving Voltage with Cavity IV for a Lipca Diaphragm at 25 Hz and 350 Vpp

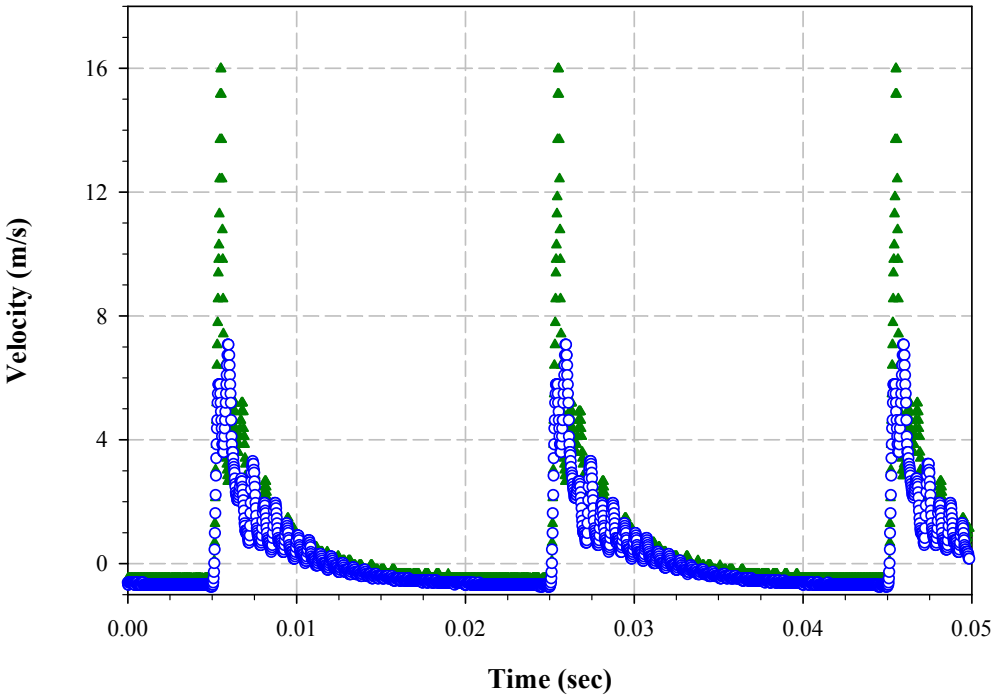

Figure B-13 Effect of Voltage on Velocity Magnitude with Cavity IV for a Lipca Diaphragm at 25 Hz with a Sawtooth Signal

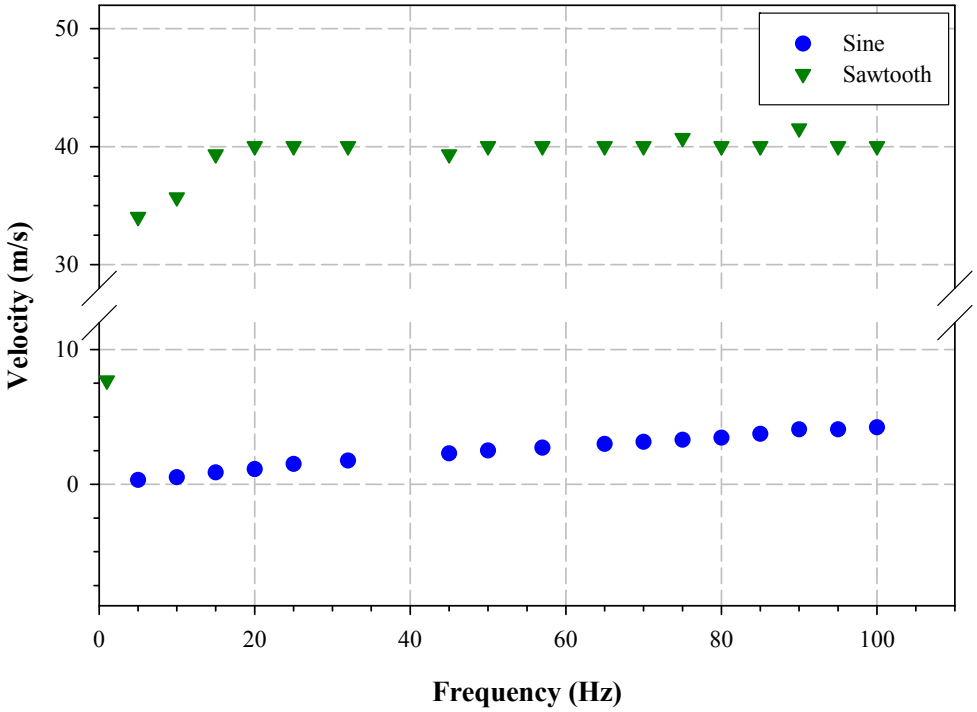

Figure B-14 Frequency Effects on Lipca Diaphragm Peak Velocities for Cavity IV at 350 Vpp

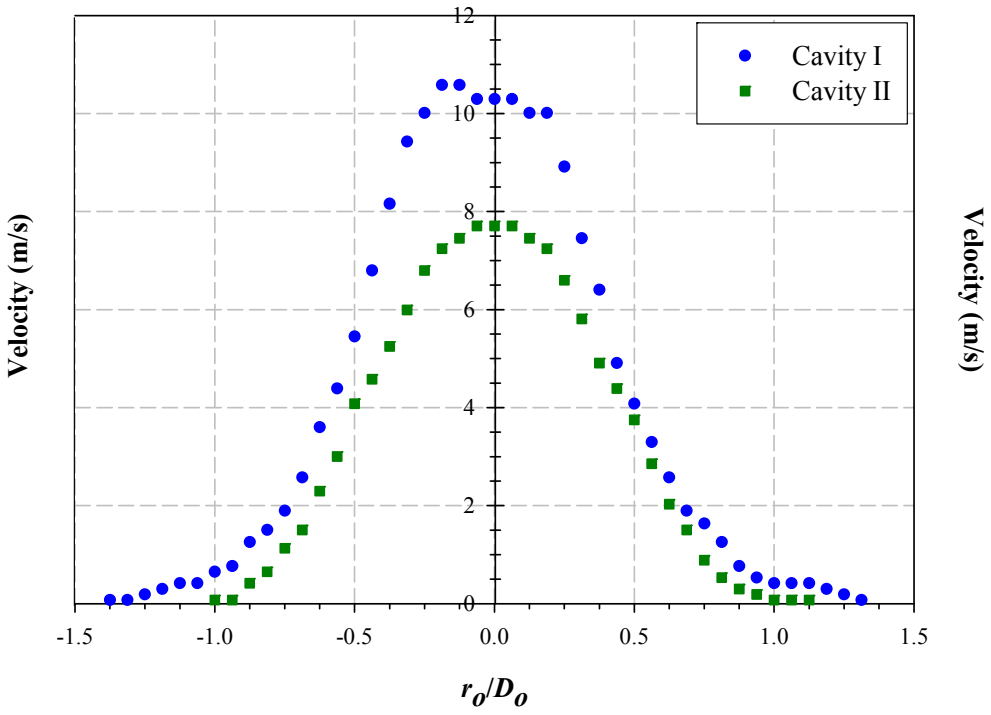

Figure B-15 Cavity Height Effects using a Sine Driving Signal for a Lipca Diaphragm at 50 Hz and 350 Vpp

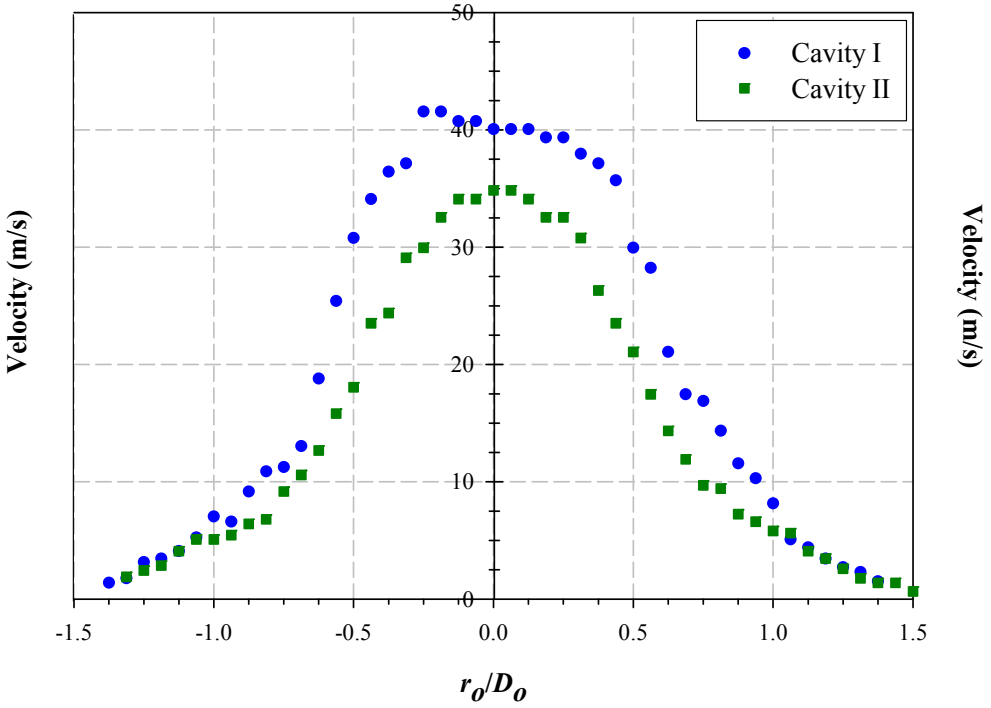

Figure B-16 Cavity Height Effects using a Sawtooth Driving Signal for a Lipca Diaphragm at 50 Hz and 350 Vpp

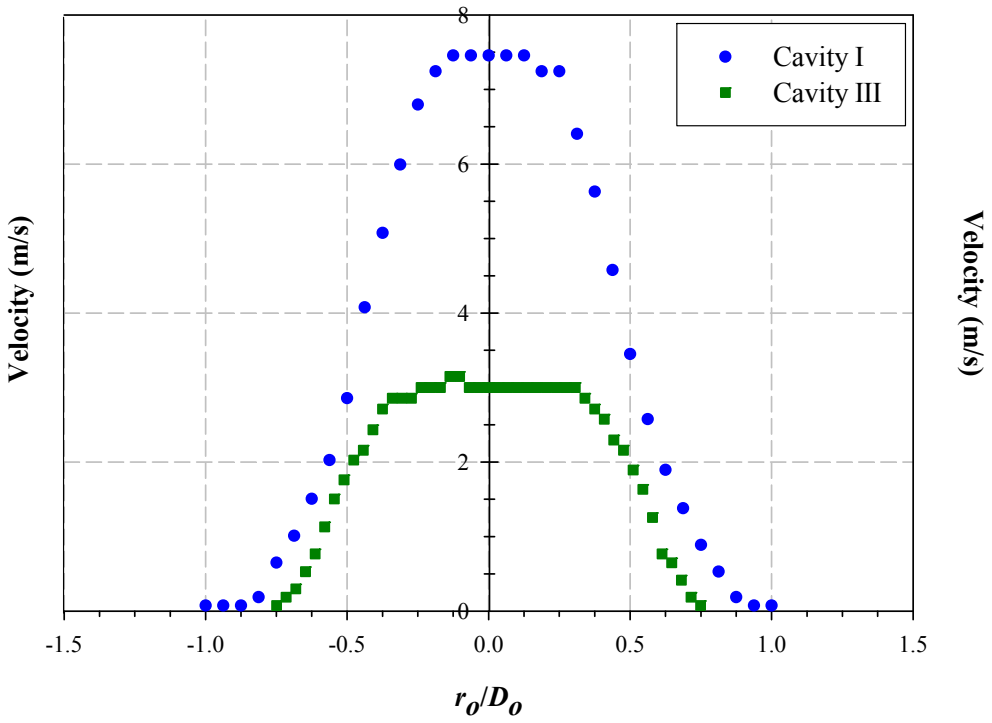

Figure B-17 Orifice Size Effects using a Sine Driving Signal for a Lipca Diaphragm at 32 Hz and 350 Vpp

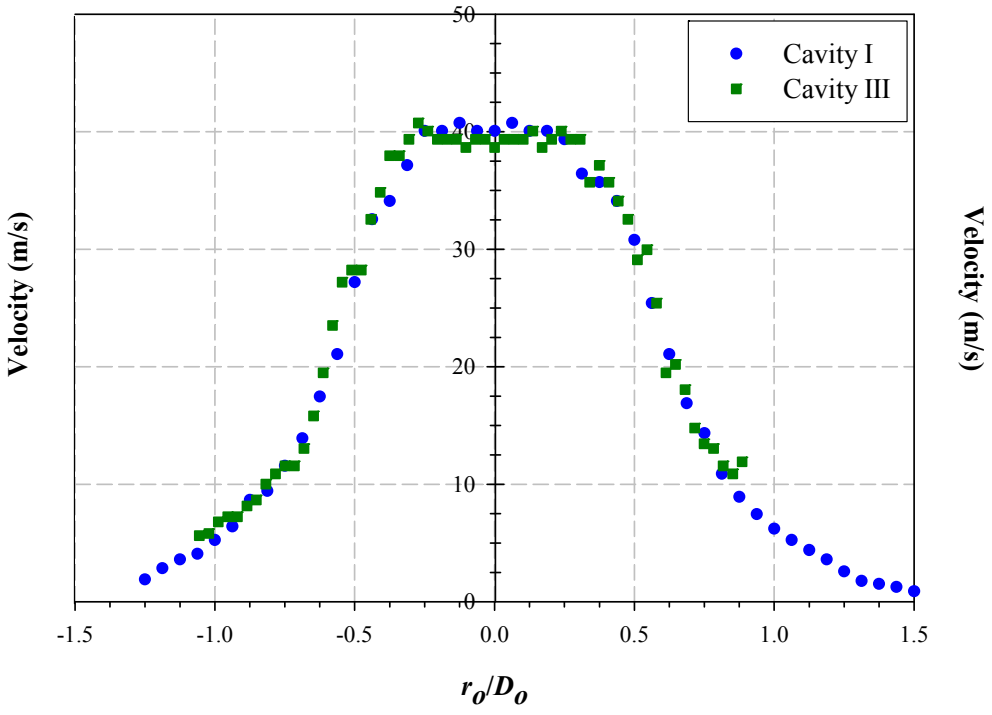

Figure B-18 Orifice Size Effects using a Sawtooth Driving Signal for a Lipca Diaphragm at 32Hz and 350 Vpp

Table B-2 Regression Analysis for a Lipca Device

SUMMARY

Regression Statistics	
Multiple R	0.97008
R Square	0.94106
Adjusted R Square	0.91963
Standard Error	4.32153
Obs.	16

ANOVA

	df	*SS*	*MS*	*F*	*Sig. F*
Regression	4	3279.90553	819.97638	43.90633	1.067E-06
Residual	11	205.43142	18.67558		
Total	15	3485.33694			

	Coeffs.	*Standard Error*	*t Stat*	*P-value*	*Lower 95%*	*Upper 95%*	*Lower 95.0%*	*Upper 95.0%*
Intercept	17.61694	1.08038	16.30622	4.718E-09	15.23903	19.99484	15.23903	19.99484
F_z	-13.40644	1.08038	-12.40899	8.237E-08	-15.78434	-11.02853	-15.78434	-11.02853
E	2.79056	1.08038	2.58294	0.02546	0.41266	5.16847	0.41266	5.16847
D_o	-2.78031	1.08038	-2.57345	0.02589	-5.15822	-0.40241	-5.15822	-0.40241
C_H	-3.12156	1.08038	-2.88932	0.01472	-5.49947	-0.74366	-5.49947	-0.74366

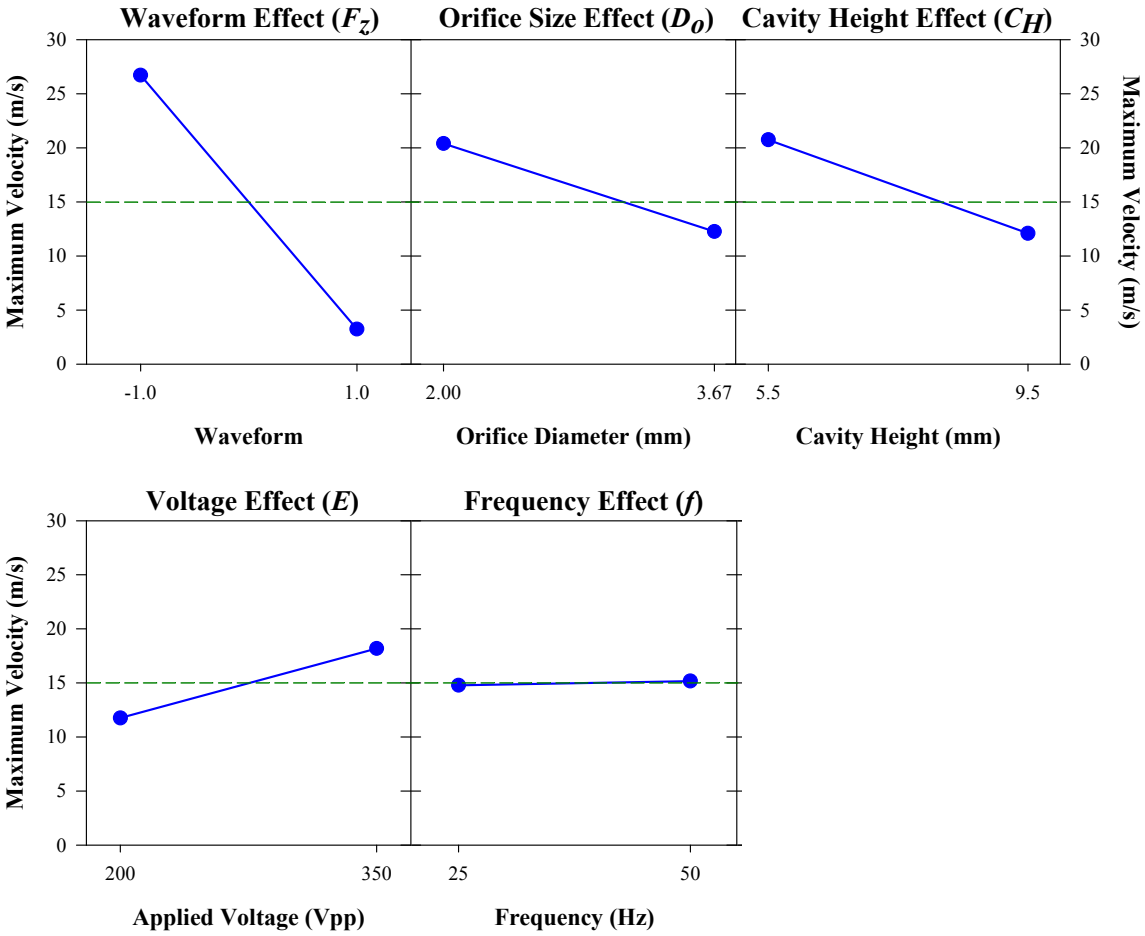

Figure B-19 Average factor effects for a Lipca device

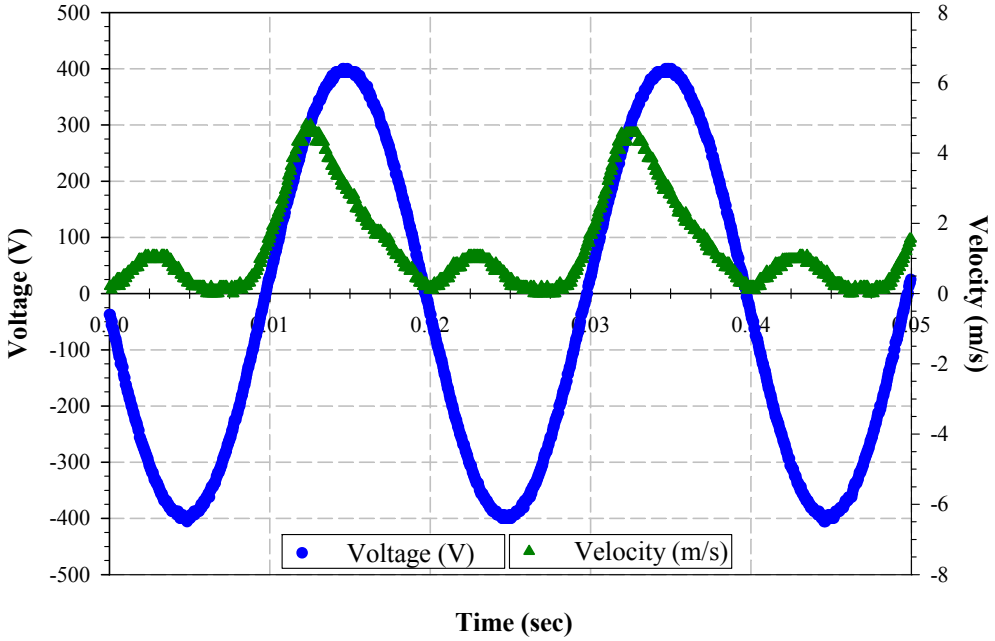

Figure B-20 Typical Velocity Curve with a Sine Driving Signal with Cavity IV for a RFD Diaphragm at 50 Hz and 800 Vpp

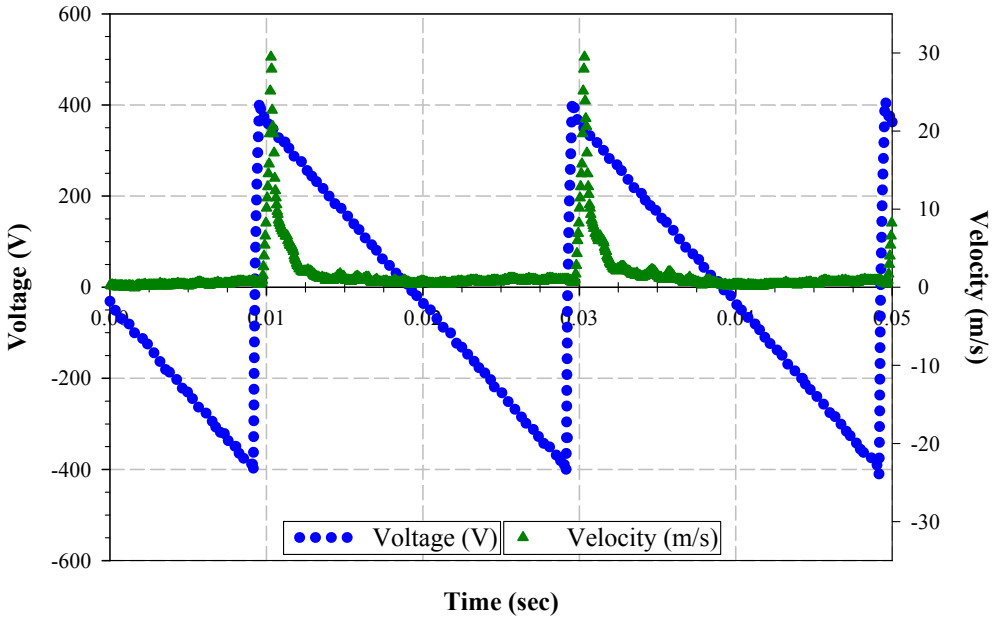

Figure B-21 Typical Velocity Curve with a Sawtooth Driving Signal with Cavity IV for a RFD Diaphragm at 50 Hz and 800 Vpp

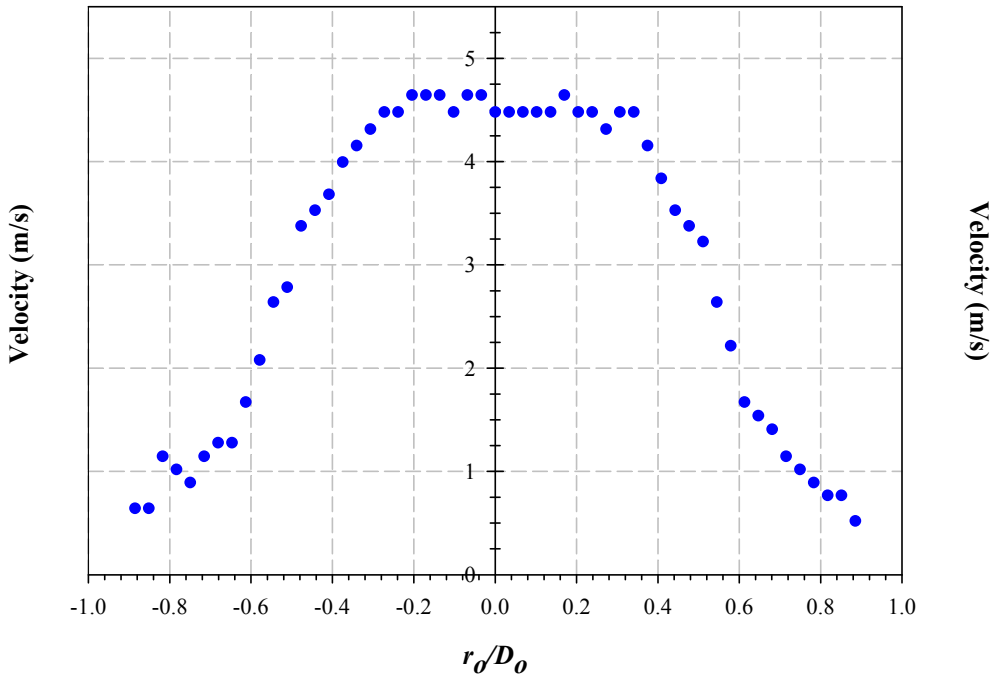

Figure B-22 Velocity Profile with Cavity IV using a Sine Driving Signal for a RFD Diaphragm at 32 Hz and 800 Vpp

Appendix C

Datasheet EH300/EH301 EPAD® Energy Harvesting™ Modules

ADVANCED
LINEAR
DEVICES, INC.

EH300/EH300A/EH301/EH301A

EH300/EH301 EPAD® ENERGY HARVESTING™ Modules

GENERAL DESCRIPTION

EH300/EH301 Series EPAD® ENERGY HARVESTING™ Modules can accept energy from many types of electrical energy sources and store this energy to power conventional 3.3V and 5.0V electrical circuits and systems. EH300/EH301 Series Modules are completely self-powered and always in the active mode. They are intended for low power intermittent duty cycle sampled data or condition-based monitoring/ extreme lifespan applications. These Modules can accept instantaneous input voltages ranging from 0.0V to +/-500V AC or DC, and input currents from 200nA to 400mA from energy harvesting sources that produce electrical energy in either a steady or an intermittent and irregular manner with varying source impedances. EH300/EH301 Series Modules condition the stored energy to provide power at output voltage and current levels that are within the limits of a particular electronic system power supply specifications. For example, 1.8V and 3.6V is a useful voltage range for many types of I.C. circuits such as microprocessors.

EH300/EH301 Series Modules are designed to continuously and actively operate to capture, accumulate and conserve energy from an external energy source. Each individual EH300/EH301 Series Module is set to operate between two supply voltage thresholds, +V_low DC and +V_high DC, corresponding to the minimum (VL) and maximum (VH) supply voltage values for the intended application. When an energy source starts to inject energy into the inputs of an EH300/ EH301 Series Module in the form of electrical charge impulses, these charge packets are collected, accumulated and stored onto an internal storage capacitor bank. For most common energy harvesting applications, the electrical energy charge packets arrives in the form of input voltage spikes that are uncontrolled and unpredictable. Often these cover a wide range of voltages, currents and timing waveforms. EH300/EH301 Series Modules are designed to accommodate such conditions with exceptional efficiency and effectiveness. As an example, EH300 Series Module can cycle within 4 minutes at an average input current of 10 µA and within 40 minutes at an average input current of just 1.0 µA.

SPECIFICATIONS

EH300/EH300A/EH301/EH301A
Input/Output Electrical Specifications @25° C

- Max. Instantaneous Input Voltage: +/- 500V
- Max. Instantaneous Input Current: 400mA
- Max. Input Power: 500mW
- Min. Operational Input: 0.0V@1nA
- Min. Charging Input (Max. Power Dissipation):

  - EH300 4.0V@200nA(800nW)
  - EH301 6.0V@300nA(1800nW)
  - EH300A 4.0V@500nA(2µW)
  - EH301A 6.0V@500nA(3µW)

- Internal Voltage Clamp: 7.0V@10mA
- Max. Output Current: 1 amp
- Operating Life Cycles: Virtually unlimited
- Logic Compatibility: CMOS

EH300
- VL=1.8V VH=3.6V
- Useful Energy Output@ 4.6mJ
- Output On-Time Rating: 68msec@25mA

EH300A
- VL=1.8V VH=3.6V
- Useful Energy Output@ 30mJ
- Output On-Time Rating: 75msec@150mA

EH301
- VL=3.1V VH=5.2V
- Useful Energy Output@ 8.3mJ
- Output On-Time Rating: 80msec@25mA

EH301A
- VL=3.1V VH=5.2V
- Useful Energy Output@ 55mJ
- Output On-Time Rating: 88msec@150mA

ORDERING INFORMATION

Part Number	Description
EH300 EH300A	4.6 mJ Module / 1.8V to 3.6V operation 30 mJ Module / 1.8V to 3.6V operation
EH301 EH301A	8.3 mJ Module / 3.1V to 5.2V operation 55 mJ Module / 3.1V to 5.2V operation
EHJ1C EHJ2C	6 inch cable / J1 connector (Input) 6 inch cable / J2 connector (Output)

Note: EH300A and EH301A are high energy output versions

FUNCTIONAL DESCRIPTION

EH300/EH301 Series Modules' voltage on the onboard storage capacitor bank is +V, which is also the positive supply voltage switched to power the output power load. Initially, +V voltage on an EH300/EH301 Series Module starts at 0.0V. During the initial charge period, +V starts charging from 0.0V. The internal circuit of the Module monitors and detects this +V voltage. When +V reaches V_H, the Module output (V_P) is enabled and turned to the ON state and is then able to supply power to a power load, such as a microprocessor and/or a sensor circuit. The amount of useful energy available is a function of the capacity of the storage capacitor bank. Meanwhile, an EH300/EH301 Series Module continue to accumulate any energy generated by external energy sources. If external energy input availability is high, output V_P remains in an ON state continuously, until such time that external energy availability is lower than the power demand required by the power load. As external energy input exceeds power loading, +V increases until internal voltage clamp circuits limit it to a maximum clamp voltage.

EH300/EH301 Waveforms

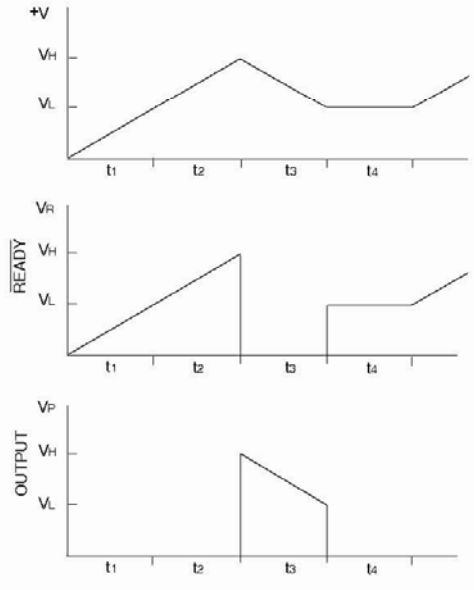

Mechanical Specifications

- Outline Dimensions:
  W x L x H : 0.55 in. x 2.00 in. x 0.70 in.
- 4 Mounting Holes: 0.085 in. diameter
- Weight: 0.5 ounce (14 grams) nominal

EH300/EH301 Top View

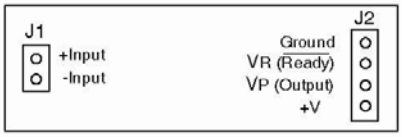

Socket Adapter Cable:
J1: Hirose Socket, 2 Position P/N : DF13-2S
J2: Hirose Socket, 4 Position P/N : DF13-4S

Module Dimensions

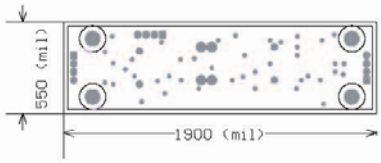

Environmental Specifications

- Leadfree (ROHS) compliant
- Operating Temperature Range: 0 to 70° C
- Max. Average Operating Temperature : 50° C
- Storage Temperature: -40 to +85° C
- Humidity: To 90% (no condensation)
- Protection: Conformal and Epoxy coated

During normal operation, as power is drawn from an EH300/EH301 Series Module, +V decreases in voltage. When +V reaches V_L, output V_P switches to an OFF state and stops supplying any further power to the power load. With built-in hysteresis circuits within the Module, V_P now remains in the OFF state even when the external energy source starts charging the capacitor bank again by importing fresh new impulses of electrical energy. Once V_H level is reached again, output V_P is then turned to the ON state again. Hence +V voltage cycles between V_H to V_L voltage levels and then to the OFF state. When in the ON state, V_P can supply up to 1A of current for a limited time period as determined by the stored useful energy and the energy demand by the power load. An optional input/ouput pin V_R functions as V_P on/off control (external input through 1KOhm) or as $\overline{\text{READY}}$ logical control (output) signal preceeding output V_P switching.

Input energy charging times t_1 and t_2 are limited by input energy available minus energy loss by an EH300/EH301 Series Module. The energy output time period t_3 is determined by the rate of energy used by the power load as a function of energy stored. Low input energy hold time t_4 is typically many orders of magnitude greater than the sum of t_1, t_2 and t_3.

Initial Setup & Calibration

EH300/EH301 Series Modules are setup and calibrated at the factory to standard specifications and settings. No user setup is required. Optional user control signal and connection to external capacitor or battery storage banks are available at the output port. All EH300/EH301 Series Modules are shipped Ready to Use.

EH300/EH301 Typical Application